Title
Urban greenhouse gas emissions as observed using a high-density sensor network

Author
Shusterman, Alexis

Publication Date
2018

Peer reviewed|Thesis/dissertation

Urban greenhouse gas emissions as observed using a high-density sensor network

By

Alexis A. Shusterman

A dissertation submitted in partial satisfaction of the

requirements for the degree of

Doctor of Philosophy

in

Chemistry

in the

Graduate Division

of the

University of California, Berkeley

Committee in charge:

Professor Ronald C. Cohen, Chair
Professor Kristie A. Boering
Professor Inez Y. Fung

Summer 2018

Urban greenhouse gas emissions as observed using a high-density sensor network

Abstract

Urban greenhouse gas emissions as observed using a high-density sensor network

by

Alexis A. Shusterman

Doctor of Philosophy in Chemistry

University of California, Berkeley

Professor Ronald C. Cohen, Chair

More than 70% of anthropogenic carbon dioxide emissions originate from cities, and that fraction is expected to grow with the increasing urbanization of the world population. Monitoring, reporting, and verification (MRV) of emission mitigation initiatives are complicated in urban areas by the combination of spatio-temporally heterogeneous landscapes of CO_2 sources and poorly constrained turbulent fluid dynamics near the rough and irregular surfaces of urban topography. In this dissertation, I present a novel approach to MRV of urban emissions using a distributed network of near-surface ambient CO_2 monitors stationed at 2 km intervals across an urban dome. The study area is the San Francisco Bay Area, a location characterized by a high density of disparate emission sources, irregular topography, as well as strong municipal and state level commitments to emission reductions. First, I describe the design, implementation, and evaluation of this unprecedented monitoring approach, hereafter the BErkeley Atmospheric CO_2 Observation Network ($BEACO_2N$). I demonstrate how the use of lower cost sensor technologies enables a high volume of monitors to be deployed at a cost competitive with conventional, non-spatially resolved monitoring approaches and find the lower cost monitors to be of sufficient accuracy and precision to capture typical urban CO_2 phenomena. Second, I leverage this validated framework to provide the first high-resolution characterization of the neighborhood-to-neighborhood variability in local CO_2 concentrations across the San Francisco Bay Area. I find significant differences even between nearby pairs of monitoring sites, leading to the derivation of a relatively short spatial correlation length scale for the study area and demonstrating a high degree of sensitivity to the unique emission sources local to each site. I determine these sensitivities to be capable of detecting changes in emission processes of policy-relevant magnitudes, providing a viable new constraint on regulations concerning, for example, fuel efficiency and vehicle electrification. Finally, I compare the CO_2 concentrations measured at nine $BEACO_2N$ sites to those predicted by an ensemble of atmospheric transport models. I find large disagreements between the observations and the simulations, only a small portion of which can be explained by known measurement errors or the spread in plausible transport and emissions scenarios, highlighting the utility of high-density observations for the validation and improvement of conventional modeling frameworks. Taken together, this body of work demonstrates the promise of atmospheric observation networks based on moderate quality sensor technologies as a practicable approach to the challenge of monitoring urban greenhouse gas emission patterns and trends.

Acknowledgements

My graduate education was funded by a UC Berkeley Chancellor's Fellowship as well as a Graduate Research Fellowship from the National Science Foundation, with additional support provided by the National Aeronautics and Aerospace Administration, the Bay Area Air Quality Management District, the Koret Institute for Personal Prevention, and the Environmental Defense Fund.

I also wish to acknowledge my advisor, Prof. Ronald Cohen, who once upon a time responded to an email from an unknown undergraduate chemistry major across the country looking for a summer research opportunity and six months later convinced her to apply to graduate school. Throughout the many ups and downs of my graduate career, Ron has always believed in me, even when I did not believe in myself, and I am where I am today because of his unwavering confidence.

I am also extremely thankful for the current and former members of the Cohen Group extended family, who were always generous with their scientific insight, good humor, and patience, especially Sally Pusede, my first mentor, and Jill Teige, the grandmother of the BEACO$_2$N project, without whom none of this work would have been possible.

Much gratitude is also due to the support staff of the Department of Chemistry, in particular Maria Rodriguez, Karla Rios, Carl Lamey, and Roy Washington, as well as the friendly faces at Al Lasher's Electronics.

I am furthermore profoundly grateful to the women of the Iota Sigma Pi Hydrogen Chapter, the Society of Women in the Physical Sciences, and the "ladies who lunch," for their inspiring example and enduring friendship. Many thanks to the various off campus communities that supported me throughout this process as well, including the UpSwing Aerial Dance Company, the crew at 2060 McGee, the Sunday night dinner club, and all of the Bay Area Brown University alumni.

Finally, I must sincerely thank my incredible family, who provided homework help, emotional support, and podcast recommendations in equal measure. Thank you especially to Isaac Goldberg, my coding guru, my cheerleader, and my partner through the good, the bad, and the ugly of this wild adventure.

Chapter 1

Introduction

1.1 Motivation and strategies for urban carbon dioxide monitoring

Carbon dioxide (CO_2) is a trace gas in the earth's atmosphere that contributes to the warming of the planet's surface via the greenhouse effect, or the absorption and bi-directional re-emission of longwave infrared radiation that would otherwise escape to space (Fourier, 1827; Foote, 1856). Natural variations in atmospheric CO_2 levels over geological timescales correspond to gradual, long-term oscillations between ice age and interglacial climate extrema (Lorius et al., 1990), but recent accelerations in the rate of increase in atmospheric CO_2 concentrations (Keeling, 1960) have led to concerns surrounding the ecological and sociological ramifications of more rapid alterations to global average temperatures and ocean chemistry. As a result, widespread efforts are underway on municipal to international scales (Rosenzweig et al., 2010) to identify and implement behavioral and technological interventions that will slow the release of additional carbon dioxide into the earth's atmosphere.

The vast majority of recent additions to the atmospheric carbon dioxide budget are anthropogenic in origin and attributable to combustion activities that oxidize hydrocarbons for the production of energy, e.g., the burning of fossil fuels for electricity generation, heating, and transportation (Stuiver and Quay, 1981). As such, reducing the volume of fossil fuel consumed by either abstaining from or increasing the energy efficiency of processes that rely on combustion are key targets for CO_2 emission reduction strategies. Such strategies are often costly and/or disruptive to execute, thus there exists a strong motivation to identify and ensure compliance with the most effective initiatives. These efforts to optimize the efficacy of emission reduction strategies are broadly referred to as monitoring, reporting, and verification (MRV) activities and can be divided into two major categories: (1) activity-based approaches that produce detailed accountings of known CO_2 emitting processes and scale their magnitude to estimate the resultant emissions, and (2) observation-based approaches that leverage ambient measurements of atmospheric species to infer underlying emission processes of known and unknown nature (Pacala et al., 2010).

Numerous activity-based CO_2 emission "inventories" have been produced at a myriad of spatio-temporal scales by various collaborations between academic and governmental agencies. Cities are of primary interest, given that more than 70% of anthropogenic greenhouse gas emissions originate from urban centers (United Nations, 2011). Previous analyses have determined an inventory spatial resolution of 100–1000 m to be required to sufficiently represent city-scale emission processes, for example the sharp gradients in CO_2 fluxes nearby major highways (McDonald et al., 2014; Liang et al., 2017). However, the necessary combustion activity data used to create these CO_2 inventories are typically reported as county-, state-, or even nation-wide aggregates (e.g., total vehicle miles traveled in a given country in a given year), and the downscaling of these total quantities to higher spatio-temporal resolutions is an extremely labor-intensive process. As a result, the production of highly resolved emission inventories for urban areas has thus far been a largely piecemeal effort, progressing one city at a time.

At the time of this writing, comprehensive, activity-based CO_2 emission inventories have been produced at resolutions $\leq$2.5 km^2 for the cities of Indianapolis, Indiana (Gurney et al., 2012), Paris, France (Bréon et al., 2015), Los Angeles, California (Newman et al., 2016), Salt Lake City, Utah (Patarasuk et al., 2016), San Francisco–San Jose, California, (Turner et al., 2016), Chennai, India (Kumar and Nagendra, 2016), Toronto, Canada (Pugliese et al., 2018), as well as the northeastern region of the United States (Gately and Hutyra, 2017). Additional high-resolution inventories that account only for CO_2 emissions from mobile sources exist for the cities of Norwich, United Kingdom (Nejadkoorki et al., 2008), New York City, New York, Houston and Dallas–Fort Worth, Texas (McDonald et al., 2014), and, most recently, the entire United States (Gately et al., 2015). However, even these extant local-level inventories are only intermittently updated and are known to possess significant uncertainties associated with the proxies and assumptions used to reallocate the primary activity data to the desired spatio-temporal specificity (Miller and Michalak, 2017). There is a broad consensus that corroboration of activity-based inventories against ambient atmospheric observations is necessary to improve confidence in said inventories if they are to be used in potentially legally binding MRV applications (Duren and Miller, 2012).

Historically, the observation-based field has been limited by the analytical challenge of providing quantitative measurements of an extremely dilute (<1000 ppm) trace gas in field conditions with variable meteorological parameters and interfering species (Fonselius et al., 1956). As such, most long-term ambient CO_2 monitoring networks are spatially sparse, consisting of fewer than 10 sites spread across entire nations or continents, such that the available resources can be focused on the proper maintenance and calibration of a smaller number of instruments. In this vein, the National Oceanic and Aerospace Administration coordinates a worldwide network of tower-based greenhouse gas observation sites as part of their Global Greenhouse Gas Reference Network (Andrews et al., 2014). Similar networks exist in China (Fu et al., 2010), Switzerland (Oney et al., 2015), and the United Kingdom (Stanley et al., 2018), and these mixing ratio measurements are supplemented by the Total Carbon Column Observing Network, a global web of 18 ground-based total column greenhouse gas observing sites founded in 2004 (Wunch et al., 2011).

In the interest of cost effectiveness, these networks are often purposefully sited in remote areas well suited for characterizing biogenic carbon exchange (e.g., Fang et al., 2014) and/or constraining national emissions (e.g., Kou et al., 2015; Yadav et al., 2016; Kou et al., 2017; Liu et al., 2014). This ensures their measurements are representative of the greatest possible domain but leaves little opportunity for direct observation of individual cities. Intensive field campaigns involving shorter term installations of a larger number of instruments have been used successfully in the past to constrain brief snapshots of CO_2 emissions without undue expense (e.g., Lauvaux et al., 2009; Miles et al., 2012; Lauvaux et al., 2013; Díaz-Isaac et al., 2018), but the limited duration of these studies precludes any understanding of the inter-annual trends most relevant to greenhouse gas emission mitigation. Space-based (e.g., Bovensmann, et al., 2010; Kort et al., 2012; Schneising et al., 2013; Kumar et al., 2014; Pillai et al., 2016; Nassar et al., 2017; Schwandner et al., 2017), aircraft-based (Lin et al., 2006; Lauvaux et al., 2009; Brioude et al., 2013; Cambaliza et al., 2014; O'Shea et al., 2014), and vehicle-based (e.g., Brondfield et al., 2012; Bush et al., 2015; Maness et al., 2015; Gately et al., 2017; Lee et al., 2017) monitoring techniques, although extreme opposites in terms of spatial scale, suffer from similarly limited temporal coverage. These "mobile" platforms revisit a given location very infrequently, inhibiting the analysis of temporal cycles and/or longitudinal trends without a much more substantial upfront data collection period.

The relatively recent introduction of commercially available cavity ring-down and other infrared spectroscopy equipment has significantly increased the feasibility of long-term ambient greenhouse gas monitoring within urban areas. Networks consisting of two or more CO_2 observing sites have been installed in Boston, Massachusetts, (2 sites; McKain et al., 2015), Rotterdam, the Netherlands (2 sites; Super et al., 2017a; Super et al., 2017b), Cape Town, South Africa (2 sites; Nickless et al., 2018), Montreal, Quebec (3 sites; Bergeron and Strachan, 2011), London, United Kingdom (4 sites; Boon et al., 2016), Xi'an, China (4 sites; Wang et al., 2018), Toronto, Canada (4 sites; Pugliese et al., 2018), Salt Lake City, Utah (5 sites; Pataki et al., 2003), Paris, France (5 sites; Bréon et al., 2015), Indianapolis, Indiana (12 sites; Richardson et al., 2017), Nagpur, India, (12 sites; Majumdar et al., 2017), and Los Angeles, California (16 sites; Verhulst et al., 2017).

A common application of these urban networks is to use their measurements as observational constraints in inversion analyses that couple computational atmospheric transport models with activity-based, a priori estimates of the CO_2 emissions in the surrounding domain (e.g., McKain et al., 2012; Bréon et al., 2015; Lauvaux et al., 2016; Staufer et al., 2016; Miles et al., 2017; Nickless et al., 2018). These models maximize the agreement between the simulated and observed CO_2 concentrations by systematically nudging the original emission estimate, either heterogeneously in space and time or with a single scale factor, thus arriving at an optimal posterior emission estimate for an urban area of interest (Ciais et al., 2010). With this approach, the aforementioned studies have reduced uncertainties in activity-based emission inventories by approximately 10–50%.

While it is generally thought that even greater error reductions might be achieved with higher density networks consisting of more urban monitoring sites (Staufer et al., 2016), the upfront price and ongoing maintenance costs associated with high-quality CO_2 monitoring equipment prohibits the arbitrary expansion of observation networks based on such technologies. Often, higher network density is only possible through a compromise in instrument quality. This tradeoff between the quality and quantity of observations has been investigated by numerous theoretical studies using synthetic data produced by hypothetical observing systems as inputs into inversion analyses (Michalak et al., 2017). By omitting a subset of the observations or artificially introducing additional measurement errors, these analyses are able to quantify the reductions in emission uncertainties possible with different network configurations. While the optimal network design depends on the specific topography, meteorology, and emission landscape of a given domain (Wu et al., 2018), most studies have concluded that the benefits of greater observational density easily outweigh the lower quality of said observations (e.g., Kort et al., 2013; Turner et al., 2016; Wu et al., 2016; Lopez-Coto et al., 2017).

High-resolution monitoring systems also offer the opportunity to directly observe individual CO_2 sources and sinks that are often otherwise compiled into sector- or citywide totals by atmospheric inversion analyses. While quantifying the integrated urban outflow is important to marking progress toward an overall mitigation goal, the majority of emission mitigation policies are typically comprised of dozens of rules and regulations targeting specific emission sources within the citywide total (e.g., Brown et al., 2014). These spatio-temporally heterogeneous phenomena are more faithfully captured by high density observing networks (Turner et al., 2016). Moreover, the resultant high-resolution record of CO_2 tracer transport through the urban domain has the

potential to increase understanding of near-surface dispersion dynamics in the complex, built environment (Nehrkorn et al., 2013; Deng et al., 2017). Neighborhood-level observations of CO_2 may also be individually relevant to air quality and public health concerns; Bares et al. (2018) found excess CO_2 above a given background concentration to be a reliable predictor of the presence of other, toxic gases.

Prior studies have identified several low-cost commercial CO_2 sensors as promising candidates for future high-density deployments (e.g., Rigby et al., 2008; Martin et al., 2017). However, despite demonstrated reliable in situ performance, subsequent applications of these technologies have involved only single monitoring sites (e.g., Sharma et al., 2011; Järvi et al., 2012).

Here I present the design, implementation, and analysis of a major innovation in the realm of observation-based approaches to MRV of CO_2 emission mitigation. The BErkeley Atmospheric CO_2 Observation Network ($BEACO_2N$) is a distributed web of moderate cost CO_2 and air quality sensing "nodes" originating in Oakland, California in 2012 that has since spread across the San Francisco Bay Area and been replicated in New York City and Houston, Texas. With more than 50 nodes in the Bay Area today, $BEACO_2N$ offers a unique tradeoff between sensor quantity and quality, enabling an unprecedented degree of spatial density that much more closely approaches the length scales of variability in urban CO_2 sources and sinks. It is hypothesized that increased sensitivity to individual sources increases the ability to specifically characterize and therefore inform mitigation of said sources. What follows is an evaluation of this novel CO_2 observation platform following its design, initial deployment, and subsequent iterations and expansions, including descriptions of its measurement capabilities as well as appropriate applications of the dataset to policy-relevant MRV tasks and opportunities to interface with computational atmospheric transport models.

1.2 Chapter 2: The BErkeley Atmospheric CO_2 Observation Network: initial evaluation

In Chapter 2, I describe the design of the BErkeley Atmospheric CO_2 Observation Network and offer an initial evaluation of its laboratory and in situ performance using a framework of four criteria: cost, reliability, precision, and bias. Via comparisons with high-quality reference instruments and case studies of well-documented atmospheric phenomena, I develop a calibration technique that produces unbiased observations of sufficient precision and reliability to capture CO_2 signals with magnitudes relevant to typical urban processes without exceeding the cost of a one to two site network utilizing conventional, higher cost technologies. Finally, I also present descriptive statistics and preliminary results from the first year of $BEACO_2N$'s pilot installation (28 sites) in Oakland, California.

1.3 Chapter 3: Observing local CO_2 sources using low-cost, near-surface urban monitors

In Chapter 3, I introduce a procedure for decomposing the $BEACO_2N$ data record into a network-wide, regional signal and site-specific local signals. I then characterize the degree of spatial heterogeneity represented in the local signals and illustrate the sensitivity of these local components to nearby emission activities using a case study of highway traffic flows. I also demonstrate a technique for isolating smaller signals from more distant processes using a multiple linear regression approach that is capable of removing the confounding effects of seasonality,

meteorology, and dynamics. I show that this technique allows for the detection of traffic-related emissions throughout the BEACO$_2$N network domain, and that these source-specific signatures are sufficiently sensitive to resolve emission trends on scale with those mandated by upcoming vehicle fuel efficiency regulations.

1.4 Chapter 4: High-resolution comparison of observed and simulated CO_2 mixing ratios

In Chapter 4, I present the results of a computational simulation based on a 1 km^2 atmospheric transport model and activity-based emission inventory developed for the San Francisco Bay Area. I compare the modeled CO_2 mixing ratios with those observed by nine BEACO$_2$N sites to illustrate the tendency of the model to underrepresent the spatio-temporal heterogeneity of the urban CO_2 landscape and offer an initial analysis of the factors that contribute to this model–data mismatch: instrument, transport, emissions, and representation error. I find that the former three error terms are unable to account for the entire difference between simulated and observed CO_2 concentrations, highlighting either the significance of representation error and/or large underestimations in the other error terms.

1.5 Chapter 5: Conclusions

In Chapter 5, I summarize the conclusions contained herein and recommend possible directions for future work.

Chapter 2

The BErkeley Atmospheric CO_2 Observation Network: initial evaluation

Adapted from Shusterman, A. A., Teige, V. E., Turner, A. J., Newman, C., Kim, J., and Cohen, R. C., Atmos. Chem. Phys., 16, 13449–13463, 2016.

2.1 Introduction

As two-thirds of the human population stand to inhabit cities by 2050 (United Nations, 2014), developing a thorough understanding of urban greenhouse gas emissions is of ever-growing importance. International and local law-making bodies around the world are agreeing to caps on total emissions and enacting multi-faceted regulations aimed at achieving these caps (e.g., A.B. 32, 2006; United Nations, 2015). As of yet there exists no mechanism for judging the efficacy of these individual rules or verifying compliance through direct observations of changes in CO_2 at the scale of cities (Duren and Miller, 2012).

Traditional strategies for assessing greenhouse gas emissions are limited to a small handful of monitoring instruments scattered sparsely across remote areas, mostly in developed nations (e.g., Worthy et al., 2003; Thompson et al., 2009; Andrews et al., 2014). These stations are capable of measuring regional average and some integrated urban concentrations with extreme accuracy and precision, but are purposefully distanced from and experience reduced sensitivity to urban signals, thus giving little to no spatially resolved information on emissions in the precise areas that the majority of greenhouse gas rules aim to regulate.

The increasing significance of urban emissions combined with the proliferation of commercial cavity ring-down spectroscopic instrumentation have resulted in a recent trend towards network sensing approaches for constraining greenhouse gas emissions in cities. For example, Ehleringer et al. (2008) maintain a CO_2 monitoring network in the Salt Lake City metropolitan area; the INFLUX network measures CO_2, $^{14}CO_2$, and total column CO_2 across the city of Indianapolis (Turnbull et al., 2015); and NASA's Megacities Carbon Project has established sensor networks in the pilot cities of Los Angeles (Kort et al., 2013) and Paris (Bréon et al., 2015). These ground-based monitoring efforts are complemented by space-based observations from SCIAMACHY (Burrows et al., 1995), GOSAT (Yokota et al., 2009), and most recently the Orbiting Carbon Observatory-2 (OCO-2) launched in July 2014, which provides total column CO_2 measurements over 1.29 by 2.25 km footprints once every 16 days (Eldering et al., 2012).

Thus far, the urban surface projects have relied on a relatively small number of instruments (between 5 and 15) distributed with sensor-to-sensor distances of 5 to 35 km. Initial efforts suggest this approach may be effective at characterizing average citywide emissions over monthly to annual timescales (McKain et al., 2012), however it has yet to be used to identify and quantify specific emission activities at neighborhood scales. To resolve individual emission sources, much finer spatial resolution is needed. Simple Gaussian dispersion models with total reflection at the surface predict >95% of the one-dimensional footprint of a sensor 10 m above ground level to be within 1.1 km of the sensor under typical conditions (Seinfeld and Pandis, 2006) and prior studies

(e.g., Zhu et al., 2006; Beckerman et al., 2008; Choi et al., 2014) have observed e-folding distances of ~100 to 1000 m for urban pollutant plumes mixing into the local background.

Here we propose an alternative approach that strikes a different balance between instrument quality and quantity than in previous CO_2 monitoring efforts. The BErkeley Atmospheric CO_2 Observation Network ($BEACO_2N$) is a large-scale network instrument that aims to leverage low-cost sensing techniques in order to enable a spatially dense network of CO_2 sensing "nodes" in and around the city of Oakland, California (Fig. 2.1 and 2.2). Using commercial CO_2 instrumentation of moderate quality and a suite of low-cost trace gas sensors for additional source attribution specificity, $BEACO_2N$ is able to achieve an unprecedented spatial resolution of approximately 2 km–to our knowledge the only sensor network to date that monitors CO_2 on scale with the heterogeneous patterns of urban sources and sinks (see Fig. 2.3 for examples of observed intracity CO_2 flux gradients). We present an initial description and characterization of the instrument, beginning with a description of the nodes, their locations, and the development of various laboratory and in situ calibration techniques. We then evaluate the network in terms of four factors–cost, reliability, precision, and systematic uncertainty; described below–and conclude by demonstrating $BEACO_2N$'s ability to resolve CO_2 signals of significance to the urban environment.

2.1.1 Cost

In order to remain cost-competitive with other, less dense networks employing higher grade instrumentation, a high-density network must utilize sensors with a price 1–2 orders of magnitude lower. However, as sensor price often scales with quality, low-cost instrumentation may carry associated penalties in other domains, such as diminished precision, persistent bias, or the need for frequent maintenance and/or re-calibration. Thus, we seek to optimize the trade-off between cost and the other considerations.

2.1.2 Reliability

Network reliability consists of sensor uptime and continuity of the data stream and is crucial to enabling comparison and averaging across sites as well as improving the statistics of temporal analyses. Poor reliability also has an indirect impact on cost via the resources expended on repeat maintenance visits and/or replacement part purchases.

2.1.3 Precision

The precision requirements at each individual site versus for a network instrument as a whole vary depending on the phenomena of interest. Metropolitan regions produce <10 ppm CO_2 enhancements in the boundary layer (Pacala et al., 2010), requiring sensitivity to changes orders of magnitude smaller for the characterization of citywide integrated inter-annual trends, for example. More specifically, according to the First Update to the Climate Change Scoping Plan, the state of California would have to reduce its overall CO_2 emissions by 4.7 million metric tons per year to achieve its goal of reaching 1990 emission levels by 2020 (Brown et al., 2014). Assuming a fraction of that total reduction is attributable to the San Francisco Bay Area in proportion to its population (~20% of the California total), this amounts to a change of -2.6×10^6 kg CO_2 day^{-1} for the San Francisco Bay Area. Given a residence time of air in the region of 1 day,

these emissions reductions spread evenly over the 22,681 km^2 domain and through a 1 km boundary layer would lead to a 65 ppb annual decrease in the daily CO_2 concentrations. If the goal is verification of regional inter-annual emission targets, we would therefore require N instruments of sufficient individual sensitivity and spatial representativeness such that their combined signals allow us to detect annual changes of ~65 ppb $year^{-1}$ with confidence.

However, the true strength of the high-density approach lies in the individual sensors' (or sub-group of sensors') sensitivity to intracity phenomena, which are orders of magnitude larger by virtue of their proximity to sources not yet diluted by advection. Larger signal sizes forgive poorer precision in the individual instruments, but demand sufficient temporal resolution to capture these anomalous, often unexpected, events of short duration on top of slowly varying domain-wide fluctuations in the background concentration. Because the $BEACO_2N$ instrument is unique in its sensitivity to these highly local processes, we will focus on this latter specification of the instrument precision in the characterization that follows.

2.1.4 Systematic uncertainty

Systematic uncertainties can be incurred somewhat abruptly during the initial field installation (bias) or accrued more gradually over time (drift). Systematic uncertainty in the sensor readings is of particular concern in a large-scale network deployment where onsite calibration materials such as reference gases are infeasible and frequent maintenance visits are undesirable. To ensure trustworthy observations, a given network sensing approach must demonstrate some combination of: (a) instrumentation that is reasonably robust against sudden or gradual introduction of systematic uncertainty, (b) a post hoc correction for systematic uncertainty in the data record, and/or (c) a procedure for identifying and replacing sensors whose systematic uncertainties cannot be remedied via the prior methods.

2.2 Node design, calibration, and deployment

Each $BEACO_2N$ node contains a non-dispersive infrared Vaisala CarboCap GMP343 sensor for CO_2 as well as SGX Sensortech MiCS-4514 and MiCS-2614 metal oxide-based micro-sensors used to detect CO/NO_2 and O_3, respectively. Following a large-scale node refurbishment and upgrading effort in mid-2014, these core elements are now supplemented with a Sensirion SHT15 and Bosch-Sensortec BMP180 sensor for measuring humidity (SHT15), pressure (BMP180), and temperature (both), a Shinyei PPD42NS nephelometric particulate matter sensor, and a suite of Alphasense B4 electrochemical trace gas sensors for O_3, CO, NO, and NO_2. A discussion of these latter, air quality-related technologies is presented in Kim et al. (2018).

All sensors are assembled into compact, weatherproof enclosures as seen in Fig. 2.4. A Raspberry Pi microprocessor automates data collection via a serial-to-USB converter (for CO_2, every ~2 seconds) and an Arduino Leonardo microcontroller (for everything else, every ~10 seconds), then transmits data to a central server using either: (a) a direct onsite Ethernet connection, (b) a Ubiquiti NanoStation locoM2 Wi-Fi antenna, or (c) an Adafruit FONA miniGSM cellular module. The latter has the unintended consequence of introducing a significant amount of electrical noise into the system. We reduce the impact of this noise by limiting data transmission to 2 hours per day, on a rotating schedule such that no periods are disproportionately afflicted by elevated noise levels.

Battery-powered real time clock modules are also included to ensure timestamp accuracy during planned and unexpected hiatuses in internet connectivity.

Airflow through the node is maintained by two 30 mm fans, one positioned in the "intake" orientation and the other in the "outflow" orientation. An additional, passive air outlet is located adjacent to the AC/DC power supply converter to prevent excessive heating inside the node. Node enclosures measure 90 mm by 160 mm by 360 mm and are made of corrosion-resistant die cast aluminum that minimizes meteorological and magnetic complications. Stainless steel fasteners and a weatherproof seal prevent water intrusion into the enclosure.

Laboratory calibrations are performed on each CarboCap sensor upon receipt of the instrument from the supplier and repeated whenever nodes are retrieved from the field for maintenance, resulting in a re-calibration every 12–18 months. Reference cylinders of 0 ppm, 1000 ppm, and either 320 ppm or 370 ppm CO_2 (±1%) are used for ~10-minute deliveries of each concentration to a chamber containing the sensor, which includes a built-in microprocessor that accepts the results of this multi-point calibration as input and automatically applies the appropriate corrections to the subsequent observations. The CarboCap microprocessor can also be configured to correct for the effects of oxygen, temperature, pressure, and humidity. The built-in oxygen compensation is utilized at a constant value of 20.95%, while the latter three compensations are turned off prior to sensor deployment. Instead, a post hoc correction is derived from the ideal gas law and Dalton's law of partial pressures:

$$[\mathrm{CO_2}]_{\mathrm{dry}} = [CO_2]_{raw} * \frac{1013.25\ \mathrm{hPa}}{P_{tot}} * \frac{T}{298.15\ \mathrm{K}} * \frac{1}{1-(\frac{P_{H_2O}}{P_{tot}})} \quad (2.1)$$

Here $[CO_2]_{dry}$ is the dry air mole fraction, or the amount of CO_2 that would be measured if the observed air parcel was dried and brought to standard temperature and pressure. $[CO_2]_{raw}$, T, P_{tot}, and P_{H_2O} are, respectively, the raw CO_2 concentration output by the CarboCap software in ppm, the temperature measured by the internal thermometer of the CarboCap in K, the atmospheric pressure in hPa, and the partial pressure of water in hPa, derived from the dew point temperature (T_{dew}, in ºC) using the August-Roche-Magnus approximation of the Clausius-Clapeyron relation as indicated below:

$$P_{H_2O} = 6.1094\ \mathrm{hPa} * exp\ (\frac{17.625\ T_{dew}}{243.04+T_{dew}}) \quad (2.2)$$

For post-2014 observations, we use the pressure and dew point temperature measured inside each node enclosure by the aforementioned BMP180 and SHT15 sensors, respectively. For data collected prior to 2014, Eq. (2.1) and (2.2) are calculated from the average sea level pressures (adjusted for altitude) and dew point temperatures measured within ~50 km of the BEACO$_2$N domain by weather stations in the NOAA Integrated Surface Database (https://www.ncdc.noaa.gov/isd/).

Figure 2.5 compares 1-minute mean CO_2 dry air mole fractions calculated as described above with readings from a custom cavity ring-down reference instrument based on the Picarro G2301 analyzer system co-located with an in-field CarboCap over the course of 2 weeks in January 2016.

The ratios between the CarboCap and Picarro observations are then shown in Fig. 2.6 as a function of temperature, total pressure, and the partial pressure of water. Although most of the impact of these environmental variables is removed by the ideal gas law-based correction in Eq. (2.1), slight dependencies on each variable remain, likely due to their influence on the vibrational spectra of CO_2 via pressure broadening, etc. Performing similar analyses on observations from in situ co-locations with other reference instruments (see LI-COR LI-820 in Sect. 2.3.4) reveals the temperature and water dependence to vary in sign and magnitude between individual sensors, while the pressure dependence is found to be quite robust. We therefore apply the following empirical correction to all CO_2 observations with coincident, onsite pressure measurements (i.e., post-2014 data sets):

$$[CO_2]_{corrected} = [CO_2]_{dry} * (-0.00055\, P_{tot} + 1.5) \quad (2.3)$$

The effect of this correction is shown in the histogram of CarboCap–Picarro differences in Fig. 2.5 (gray bars). The offset between the two instruments is reduced from -1 ppm to ~0 ppm and the standard deviation of their differences is tightened from ±1.5 ppm to ±1.4 ppm. This still exceeds the ±1.0 ppm precision one would expect under average conditions given the form of Eq. (2.1) and (2.2) and the manufacturer's specifications for the meteorological sensors (see Sect. 2.3.5), the CarboCap, and the Picarro (Sect. 2.3.3), suggesting that the combined effect of the lingering temperature and water biases with any unknown factors is ±0.4 ppm.

Calibrated nodes are installed on trailers and buildings 2–111 m above ground level (6–476 m above sea level), mounted to existing infrastructure or weighted industrial tripods. Rooftop position and intake orientation are chosen to optimize wireless connectivity (if applicable), maximize air exchange with the surrounding area, and minimize sampling of extremely local emission sources (e.g., rooftop ventilation ducts). BEACO$_2$N nodes are sited on an approximately 2 km square grid across the Oakland metropolitan area (see Fig. 2.1 and 2.2 and Table 2.1), often on top of schools and museums, which possess roughly the desired spatial density and also serve the educational and outreach goals of the project (see http://beacon.berkeley.edu). The 2 km spacing is chosen to ensure an approximately 1 km proximity to any significant CO_2 source or sink in the metropolitan area, maximizing coverage without undue overlap between neighboring footprints. Additional sites outside the 2 km grid are also included for sensitivity to potential emission sources of interest, for co-location with useful reference instruments, or as pilots for network expansion.

This largely opportunistic siting approach avoids the logistical and financial obstacles associated with tall tower sampling mechanisms, although it does present additional challenges for the quantification of network-wide phenomena in that no low-lying instrument can singlehandedly provide sensitivity to the entire domain. Installing sensors near the surface and/or built environment does ensure heightened sensitivity to individual, ground-level emission phenomena, but it is currently unknown whether a well-reasoned combination of these locally sensitive signals from a high volume of sensors could nonetheless yield reliable information about the integrated region. A full exploration of this possibility is beyond the scope of this study; the following analyses focus instead on establishing BEACO$_2$N as a viable platform for investigating such hypotheses.

2.3 Node Performance

2.3.1 Cost

The Vaisala CarboCap GMP343 CO_2 sensor in this study is used in its 0 to 1000 ppm measurement range and "diffusion sampling" mode, such that representative air samples passively diffuse into the path of the infrared light beam. With these specifications, each CarboCap costs approximately $2,800 USD. Although less expensive technologies are available, the CarboCap design has a clear advantage in that the unit contains a digitally controlled Fabry-Perot interferometer to switch on (4.26 μm) and off (3.9 μm) of the asymmetric stretching mode of CO_2, generating a baseline intensity measurement for each observation that compensates for variability in the light source.

Additional sensors, ancillary hardware, and labor then bring the total cost per node to ~$5,500 USD, or $154,000 USD for the entire 28 node BEACO$_2$N instrument. For comparison, a single commercial cavity ring-down analyzer is priced around $60,000 USD, and the total equipment cost can exceed $85,000 USD after accounting for pumps, data loggers, etc.

2.3.2 Reliability

Table 2.2 gives the percent uptime for nine representative BEACO$_2$N nodes over the course of 2013, calculated as the fraction of total minutes in the year during which a given node collected valid data. All nine nodes exhibit uptimes in excess of 50% via either hardwired Ethernet connections or Wi-Fi antennas, with six collecting data >80% of the time. Maintenance visits to these sites beginning in mid-2014 revealed little to no incidence of hardware failure. Instead, external issues, such as interruptions in the electricity or Wi-Fi connectivity, are found to be the limiting factors in determining sensor uptime. Transplanting nodes to sites with more dependable electricity supplies and increasing implementation of cellular modules (which are immune to interruptions in onsite Wi-Fi networks) continue to enhance network reliability over time. For example, the nine most reliable nodes during the January 2015–April 2016 period all exhibit uptimes >80%, with five collecting data and transmitting it within the next 48 hours ~100% of the time via either Ethernet or cellular data communication.

2.3.3 Precision

From a qualitative perspective, the Vaisala CarboCap GMP343 demonstrates exceptional sensitivity to CO_2 enhancements on scales typical of an urban environment. Figure 2.7 compares the 1-minute mean CO_2 dry air mole fractions measured at two nearby in-field BEACO$_2$N nodes (EXB and EXE in Fig. 2.1) during 1 week in early October 2015. As these sensors are not precisely co-located (one is stationed approximately 13 m above roadside in downtown San Francisco, while the other sits ~200 m back from the road, near the bay), an exact correlation is not expected. The two sensors nonetheless demonstrate remarkable agreement; while typical diurnal CO_2 variations during the same period are on the order of 20–60 ppm, the CarboCaps simultaneously detect CO_2 events as small as 8 ppm, providing preliminary evidence of the suitability of these sensors for high-density urban deployment.

More quantitatively, Vaisala advertises the CarboCap as possessing a response time of 75 seconds and a precision of ±3 ppm at 2-second measurement frequency. Here we present our own characterization of the sensors' precision via comparison to: (a) in-laboratory reference gases and (b) a co-located in situ reference instrument.

After exposing an ensemble of CarboCaps to a constant stream of reference gas, we find the 1-minute mean dry air mole fractions to exhibit 1σ precision between ±1.2 and ±2.0 ppm, roughly in keeping with the ±2 ppm precision observed by Rigby et al. (2008). Figure 2.5 shows the results from our aforementioned co-location with a Picarro G2301 reference instrument, demonstrating near perfect correlation (R^2 = 0.9999), slope ≅1, and an offset of approximately 0 ppm after meteorological corrections. In this case the 1σ precision of the 1-minute averages is ±1.4 ppm, given by the standard deviation of the differences between the minute-averaged CarboCap and Picarro observations and the Picarro's precision (±0.1 ppm at 5-second measurement frequency). This presents a slight improvement over the ±2.18 ppm in situ precision recorded by van Leeuwen et al. (2010), although still greater variability than would be expected given the manufacturer's 2-second specifications and a 1-minute averaging time ($3\ ppm/\sqrt{30} = 0.55\ ppm$). Nonetheless, the agreement between the time series of the Picarro and CarboCap measurements demonstrates this noise level to be effectively negligible on the scale of ambient urban CO_2 fluctuations.

Also presented in Fig. 2.5 is a time series of the running 1-hour means of the differences between the minute-averaged CarboCap and Picarro observations, demonstrating a short-term drift incurred on approximately hourly timescales found to range between 0.01 and 2.9 ppm during any given 6-hour period of the co-location. The upper bound exceeds the ±1 ppm manufacturer-specified 6-hour short-term stability as well as the 1.5 ppm maximum short-term drift observed by Rigby et al. (2008), but in many cases longer averaging times can be used to reduce the influence of short-term drift to well below 1 ppm. Some modeling studies, for example, utilize time steps of 6 hours or more (e.g., Bréon et al., 2015; Wu et al., 2016), and average diurnal cycles can often be assessed across several days. Although some applications require finer temporal resolution, these are typically plume-based analyses that rely on rapidly varying enhancements above recent background concentrations, essentially eliminating concerns about short-term drift.

2.3.4 Systematic uncertainty

Given the limited access to validation and calibration infrastructure, a major concern for a long-term field deployment is systematic uncertainty resulting from a combination of gradual temporal drift ($U_{temporal}$, in ppm day^{-1}) and constant biases or offsets from the "true" value ($U_{atemporal}$, in ppm), perhaps incurred abruptly upon installation. The measurement at a given site ($[CO_2]_{node}$, in ppm) is therefore the sum of the real regional and local influences at said site ($[CO_2]_{background}$ and $[CO_2]_{local}$, respectively), as well as these systematic uncertainties:

$$[CO_2]_{node} = [CO_2]_{background} + [CO_2]_{local} + U_{atemporal} + \left(U_{temporal} \times days\right) \qquad (2.4)$$

To derive post hoc corrections for $U_{atemporal}$ and $U_{temporal}$ at a given site, we first remove the $[CO_2]_{background}$ signal from the data record by subtracting off the weekly minimum CO_2 concentrations recorded at a reference site within the network domain. BEACO$_2$N's unique location near the Pacific coast results in a relatively consistent wind direction from largely

unpolluted over-ocean origins, such that the weekly minima can be assumed to reflect both the seasonal and synoptic variations in network-wide baseline CO_2 concentrations while avoiding the influence of shorter term variability in local sources and sinks. This assumption is supported by preliminary analyses comparing observations from a LI-COR LI-820 non-dispersive infrared CO_2 gas analyzer with a smoothed, three-dimensional "curtain" of surface CO_2 Pacific boundary conditions produced by NOAA's Global Greenhouse Gas Reference Network (Jeong et al., 2013). The LI-COR, positioned at sea level between the EXB and EXE nodes (see Fig. 2.1), is maintained by NOAA's Pacific Marine Environmental Laboratory and calibrated against compressed gas (400–500 ppm CO_2) prior to every hourly measurement and is assumed to have negligible bias. Despite a proximity to local surface-level emissions and complex boundary layer dynamics, the LI-COR's weekly minima are found to generally follow variations in the Pacific curtain, with an average residual of ~2 ppm.

Once the $[CO_2]_{background}$ term is removed, effectively de-seasonalizing the observations, we re-calculate the weekly minima of this new data record and fit the result as a (piecewise, if necessary) linear function of time, the slope of which gives the value of $U_{temporal}$. This linear fit is then itself subtracted from the de-seasonalized data record, yielding a remainder comprised of only the $[CO_2]_{local}$ and $U_{atemporal}$ terms. While the $[CO_2]_{local}$ component varies rapidly over several orders of magnitude, the contribution of $U_{atemporal}$ is, by definition, constant in time, so we once again compute the weekly minima of the new data record and define the mean weekly minimum as $U_{atemporal}$. Having obtained values for $U_{temporal}$ and $U_{atemporal}$, we simply subtract these components from the original data record to generate the unbiased observations at each site.

Table 2.3 gives the results from one iteration of the correction procedure outlined above executed using the ELC $BEACO_2N$ node (see Fig. 2.1) as the reference site needed to calculate $[CO_2]_{background}$. Only sites that enable at least 3 months of comparison to the ELC node are included; multiple values at a single site correspond to the piecewise linear fits employed when $U_{temporal}$ exhibits discontinuities over the data record. Because we universally define Day 1 to be 1 January 2013 and $U_{atemporal}$ is strongly influenced by the intercept of the linear fit used to characterize the temporal drift, it should be noted that the magnitude of $U_{atemporal}$ does not necessarily represent the actual bias present at a node on its deployment date (which may be before or after 1 January 2013), but rather an extrapolation of this initial bias forwards or backwards in time. Uncertainties in $U_{temporal}$ and $U_{atemporal}$ shown in Table 2.3 are calculated given ±1.4 ppm random error in the 1-minute averages, ±2.9 ppm short-term drift, and ±2 ppm agreement with the reference site's weekly minima, assumed to add in quadrature. Mapped onto the observations, these uncertainties result in a mean 1-minute error of ±4 ppm. This is the assumed cumulative error used in this study, although longer averaging times could be used to reduce this figure.

To evaluate the efficacy of this procedure, we compare the weekly minima of both the raw and corrected data records to the weekly minimum CO_2 concentrations measured by the aforementioned LI-COR LI-820. The results of said comparison are shown in Fig. 2.8, demonstrating significantly improved agreement (3.7 vs. 9.8 ppm mean residuals) with the LI-COR weekly minima after correction. This is likely a conservative estimate of the uncertainty reduction achievable with this method, as the ELC node we use to compute our $[CO_2]_{background}$ value is not itself an uncertainty-free reference. Although the raw ELC data record demonstrates

the least systematic uncertainty of all the BEACO$_2$N nodes in an initial comparison with the LI-COR, its observations are nonetheless afflicted by some unknown nonzero drift and/or atemporal bias. Direct in situ calibration of the reference instrument would allow us to constrain systematic uncertainties even further.

2.3.5 Performance of Ancillary Sensor Technology

According to manufacturer documentation, the Sensirion SHT15 provides relative humidity measurements to 0.05% resolution, with an advertised accuracy of ±2.0%, a repeatability of ±0.1%, an 8 second response time, and a long-term drift of <0.5% per year. Its temperature measurements are provided to 0.01 ºC resolution, with an advertised accuracy of ±0.3 ºC, a precision of ±0.1 ºC, a response time of 5 to 30 seconds, and a long-term drift of <0.04 ºC per year. The Bosch-Sensortec BMP180 provides pressure measurements to 0.01 hPa resolution, with an advertised accuracy of ±0.12 hPa, a precision of ±0.05 hPa, and a long-term drift of ±1.0 hPa per year. Its temperature measurements are provided to 0.1 ºC resolution, with an advertised accuracy of ±1.0 ºC. An independent verification of these performance specifications is not attempted here. However, the temperature observations from both sensors closely follow the structure of those detected by the internal temperature sensor of the CarboCap, although the CarboCap's readings are consistently slightly elevated, as expected given the heat produced by the instrument itself.

The BMP180 and SHT15 are not intended to reflect local meteorological conditions, but rather to provide a representative picture of conditions inside the node. These internal conditions are integral to various posterior corrections applied to the observations (see Sect. 2.2).

2.4 Initial Field Results

The BEACO$_2$N field campaign is a long-term, ongoing monitoring effort. Here we provide a time series of data collected from 16 BEACO$_2$N sites between January 2013 and April 2016 (Fig. 2.9) and some initial descriptive statistics of the bias-corrected dry air CO_2 mole fractions at nine representative sites in 2013 (Table 2.2).

Figure 2.9 demonstrates the volume and diversity of urban CO_2 concentrations sampled, exhibiting extreme short-term variability superimposed on a slower, seasonal fluctuation in the minimum values. For clarity, the bottom panels depicting month- and week-long samples of the overall time series show data from six representative sites. Network-wide, daytime (1100–1800 LT) means between 408 and 442 ppm are observed, with maximum values between 500 and 820 ppm and minima between 384 and 396 ppm. Standard deviations are seen to range from 9.57 to 22.4 ppm, all of which are lower than the corresponding nighttime (2200–0400 LT) standard deviations due to the reduced convective mixing in the shallow nocturnal boundary layer. Similarly, the majority of nighttime means and maxima exceed the daytime values at the same location, with the exception of three sites: FTK, LAU, and KAI. The dampened or inverted diurnal trends at these sites may be due to unique boundary layer dynamics at those locales or unusually large daytime CO_2 sources nearby. Daytime and nighttime minima do not differ as significantly.

Individual BEACO$_2$N nodes are observed to capture a number of patterns and cycles typical of ambient CO_2 monitoring. Figure 2.10 shows the monthly minimum CO_2 concentrations at six select sites in 2013, as the difference from their July value (defined as 0 ppm at each site). A

distinct seasonal cycle is observed, with wintertime minima exceeding summertime values by 7 to 24 ppm. For reference, the gray curve presents a similar treatment of the aforementioned Pacific boundary curtain. At many sites, the $BEACO_2N$ minima are seen to exhibit a seasonal variation of a magnitude roughly in keeping with that observed in the curtain, while other sites demonstrate a more exaggerated summer–winter contrast, as might be expected within an urban dome.

Figure 2.11 shows representative diurnal cycles in the bias-corrected CO_2 dry air mole fractions at three different $BEACO_2N$ nodes in September 2013. We observe elevated concentrations at night corresponding to a shallow nocturnal boundary layer, significant enhancements around the morning rush hour when emissions are increasing faster than boundary layer height, and midday minima reflecting mixing into the largest volume of air before the boundary layer collapses again at sunset. However, within this qualitatively well-understood average behavior remains a degree of intra-network variability that allows us to discover and probe local scale phenomena of unknown origin. At FTK, for example, concentrations are seen to decrease after an initial rush hour peak (~0800 LT) but remain somewhat elevated until sunset, never achieving the much more pronounced afternoon minimum observed at PAP, 13.5 km away.

Such intracity heterogeneities are difficult to capture accurately using atmospheric transport models alone. We simulate hourly CO_2 concentrations ($\widehat{\boldsymbol{y}}$) at each site in the network using the Stochastic Time-Inverted Lagrangian Transport model (STILT; Lin et al., 2003) coupled to the Weather Research and Forecasting model (WRF; Skamarock et al., 2008). The coupled model is known as "WRF-STILT" (Nehrkorn et al., 2010) and the setup used here follows that of Turner et al. (2016; see their Sect. S1 for details of the WRF setup). WRF-STILT advects an ensemble of 500 particles 3 days backwards in time, each with a small random perturbation, from the spatio-temporal locations of the $BEACO_2N$ observations using the meteorological fields from WRF. The trajectories of these 500 particles are then used to construct "footprints" for each observation that represent the sensitivity of the observation to a perturbation in emissions from a given location. The footprints can be represented in matrix form ($\boldsymbol{H}$) and multiplied by a set of gridded emissions ($\boldsymbol{x}$, from the high-resolution, bottom-up CO_2 inventory in Turner et al., 2016) to compute the CO_2 enhancement at each site ($\Delta\boldsymbol{y}$) due to local emissions:

$$\Delta\boldsymbol{y} = \boldsymbol{H}\boldsymbol{x} \tag{2.5}$$

We then add this local enhancement to a background concentration ($\boldsymbol{y_B}$, from the aforementioned Pacific boundary curtain) to obtain a model estimate of the $BEACO_2N$ observations shown as black squares in Fig. 2.11:

$$\widehat{\boldsymbol{y}} = \Delta\boldsymbol{y} + \boldsymbol{y_B} = \boldsymbol{H}\boldsymbol{x} + \boldsymbol{y_B} \tag{2.6}$$

While the model captures midday conditions at FTK and evening levels at PAP, the presence of both over- and under-estimations at other times suggests a need to re-examine the bottom-up emission inventory as well as the model's treatment of boundary layer dynamics. $BEACO_2N$ provides the ground truth necessary to identify such deficiencies and potentially improve upon them via inverse modeling, data assimilation, etc.

Comparison of diurnal cycles during noteworthy local scale emission events with averages such

as those seen in Fig. 2.11 gives further insight into the potential application of BEACO$_2$N observations to CO_2 source attribution. Figure 2.12 offers one such comparison using hourly averages collected from a BEACO$_2$N node positioned on top of Oakland High School (OHS in Fig. 2.1 and Table 2.1) during a weather-related school closure that occurred on 11 December 2014. Clear reductions in CO_2 concentrations are observed relative to what is typical at this site (and indeed network-wide, although to a lesser extent), as is expected in the absence of emissions related to students' commutes and presence on campus. The sensing technology implemented in the BEACO$_2$N nodes therefore proves adequate to resolve not only CO_2 patterns typical of an urban environment, but also short-term deviations during anomalous emission events, positioning BEACO$_2$N as an essential tool for the characterization of current urban conditions as well as the verification of subsequent emission reductions.

2.5 Discussion & Conclusion

We have described the design, implementation, and initial observations from a novel high-resolution CO_2 surface monitoring network instrument. We demonstrate that low-cost instrumentation enables an unprecedented level of spatial density, and describe a calibration protocol with post hoc bias corrections that permits the network to operate precisely and reliably enough to characterize variations in ambient concentrations with magnitudes relevant to metropolitan life.

Our preliminary analysis of the first ~3 years of CO_2 observations provides evidence of the expected diurnal and seasonal cycles as well as an encouraging sensitivity to short-term changes in local emission events. Furthermore, we show significant qualitative and quantitative differences among the diurnal cycles at individual nodes on spatial scales that cannot yet be accurately captured by atmospheric transport models, confirming the necessity of a high-density approach when attempting to faithfully represent the variability of a complex urban environment.

Although BEACO$_2$N demonstrates sensitivity to both highly local fluctuations as well as slowly varying hemispheric cycles, how best to bootstrap the network's measurements into the analysis of intermediary mesoscale phenomena remains to be determined. Future work will focus on constructing inferred emission patterns and trends at this scale from the body of observations. In an initial effort in this regard, Turner et al. (2016) constructed and applied a WRF-STILT inverse model to synthetic observations with density similar to BEACO$_2$N. For an area source the size of the Oakland metropolitan area, emissions were estimated to within 18% accuracy; for a freeway-sized line source to within 36%; and to within 60% for the sum of six industrial point sources–consistently outperforming a smaller hypothetical network (three sites) with significantly better precision. Using week-long averages, the BEACO$_2$N-like network was able to further reduce the uncertainty in the integrated urban area source to <2%, a significant improvement over the citywide emission estimates provided by real and proposed ~10 site sensor networks described by Lauvaux et al. (2016) (25% uncertainty in 5-day averages), Kort et al. (2013) (>10% uncertainty in monthly averages), and Wu et al. (2016) (11% uncertainty in monthly totals). These other studies use more conservative estimates of the combined instrument, model, and representativeness error (≥3 ppm, as opposed to ±1 ppm). These combined error budgets are typically dominated by transport (model) error, which potentially explains why models based on BEACO$_2$N-like networks perform comparably to or better than those based on sparser networks of higher quality sensors,

for which instrument error may be reduced but accurately representing transport between observation sites is of greater importance. Further work is needed to fully assess the efficacy of inverse methods based on the BEACO$_2$N approach.

In addition, further characterization of the trace gas and particulate matter sensors will allow for more specific source attribution via the exploitation of emission factors unique to various combustion activities (e.g., Ban-Weiss et al., 2008; Harley et al., 2015), while providing public health-relevant air quality information as well. There is also potential for fine-grained verification of space-based observations or even of personal sensors when their inherent mobility brings them within the geographical area well represented by the fixed BEACO$_2$N network.

This work constitutes a promising initial infrastructure upon which further advances in high-density atmospheric monitoring can be built, capable of providing research, regulatory, and layperson communities with greenhouse gas and air toxics information on the scale at which emissions and personal exposure actually occur. Expansion of the validated pilot network into the neighboring locales of San Francisco and Richmond, California will allow for the characterization of other emissions sources, such as oil refining facilities. These efforts will be complemented by modeling studies comparing different sampling resolutions (i.e., 2 km vs. 4 km sensor spacing) and spatial configurations, yielding general network optimization principles that will facilitate future implementations of high-resolution CO_2 monitoring networks in diverse locations.

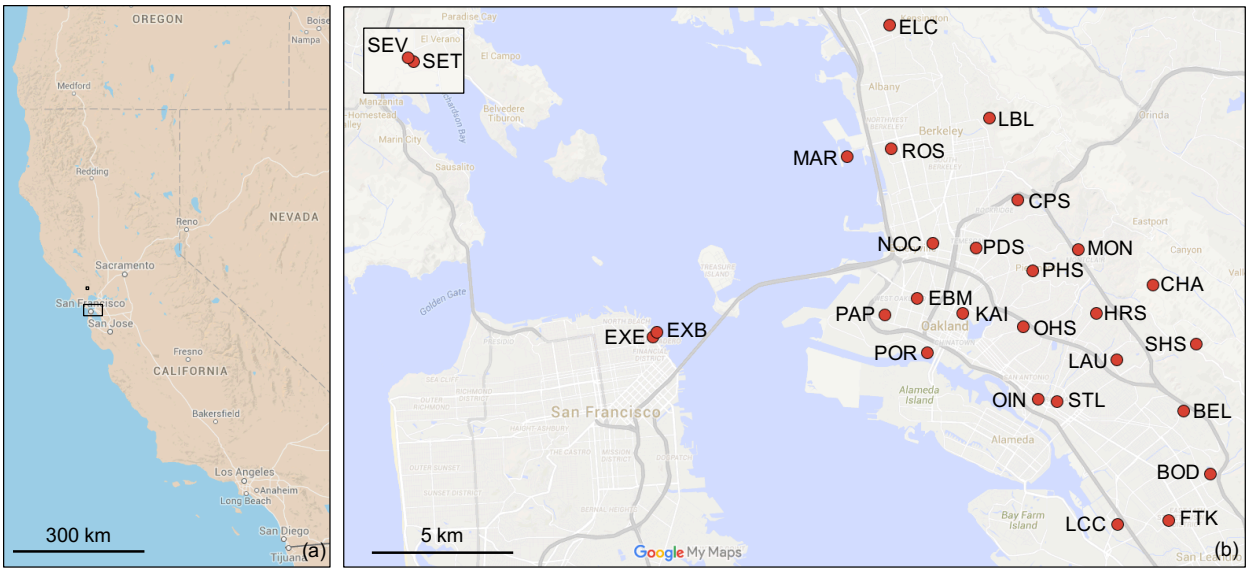

Figure 2.1. Map of the BEACO$_2$N domain **(a)** in the context of the western United States and (b) showing individual node locations. Inset in panel **(b)** shows the pair of nodes stationed in Sonoma County. Map data © 2016 Google.

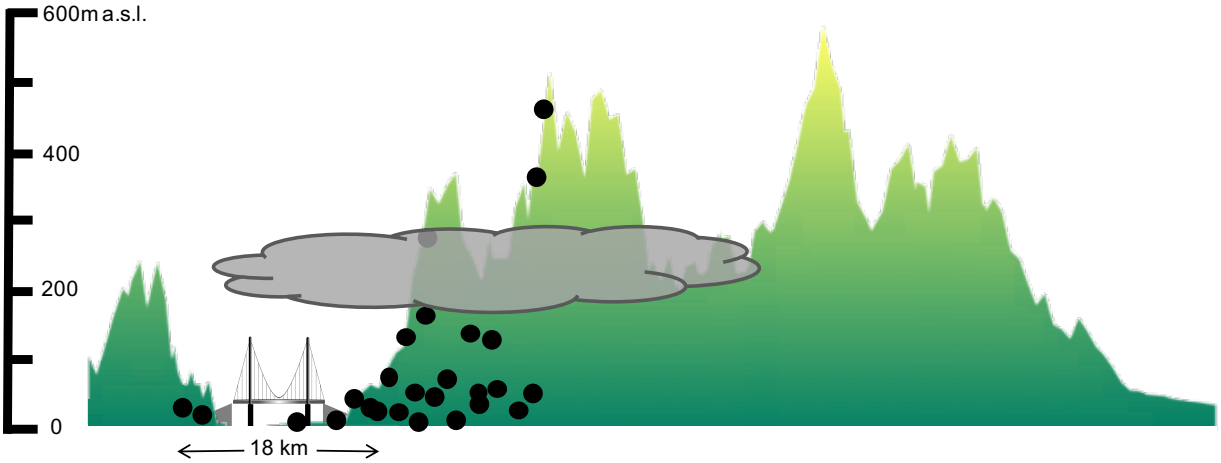

Figure 2.2. North-facing schematic of Fig. 2.1 indicating a representative vertical distribution of BEACO$_2$N node sites (circles) over the topography of Oakland, CA. Cloud marks the altitude and thickness of a typical marine fog layer; bridge delineates the height of the San Francisco-Oakland Bay Bridge. Horizontal placement of nodes has been skewed for visual clarity.

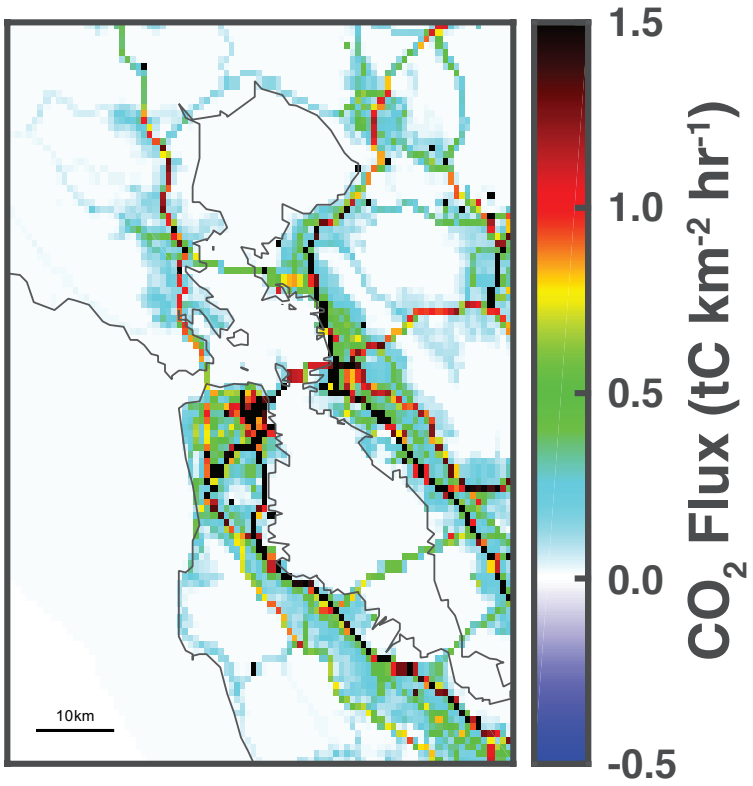

Figure 2.3. A sample high-resolution, bottom-up emission inventory for the Bay Area adapted from Turner et al. (2016).

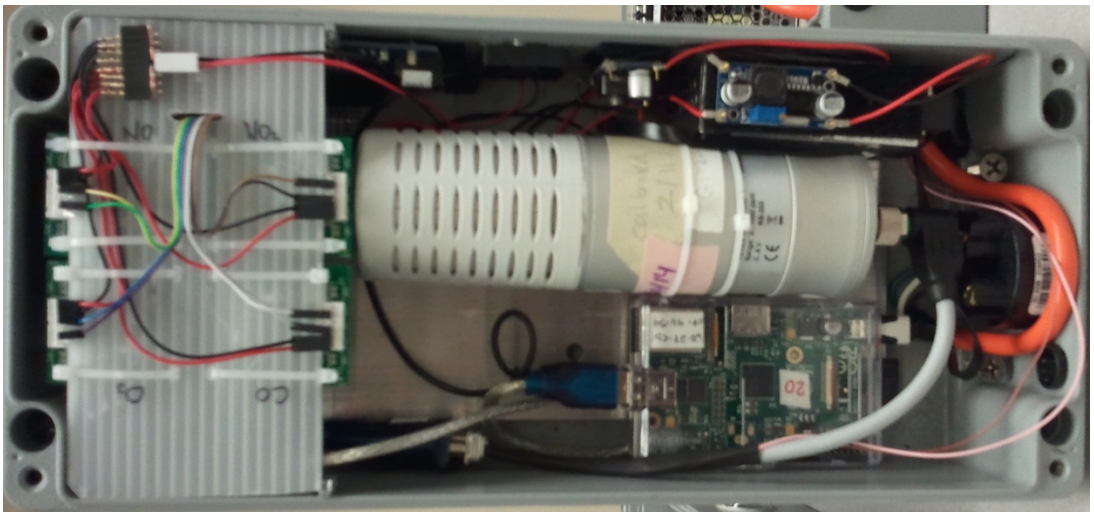

Figure 2.4. BEACO$_2$N node design used in this study.

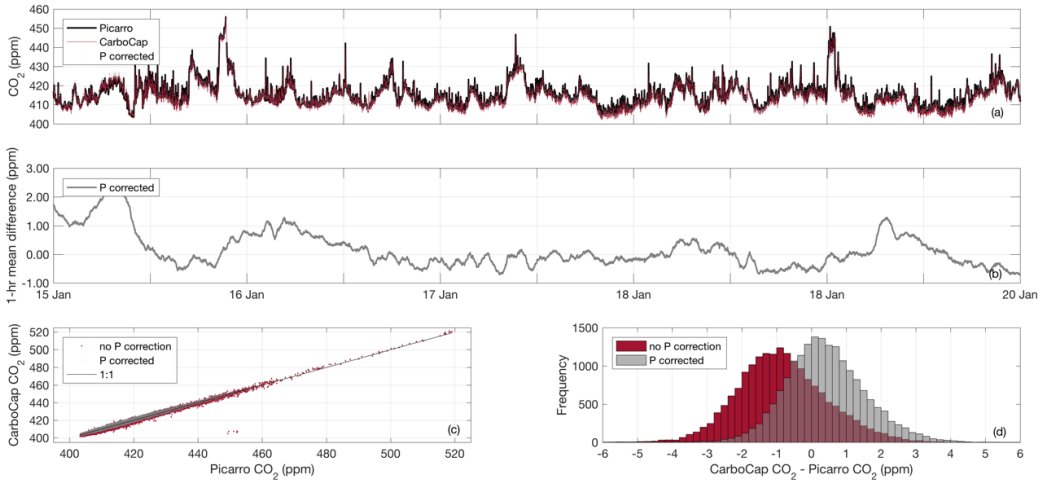

Figure 2.5. One-minute mean results from a 2-week co-location of a Vaisala CarboCap GMP343 and a custom cavity ring-down reference instrument based on the Picarro G2301 system: **(a)** representative 5-day time series, **(b)** 1-hr running mean of the differences over the same 5-day period, **(c)** direct comparison, **(d)** histogram of the differences. CarboCap observations are dry air mole fractions calculated using Eq. (2.1) and subsequently pressure corrected with Eq. (2.3).

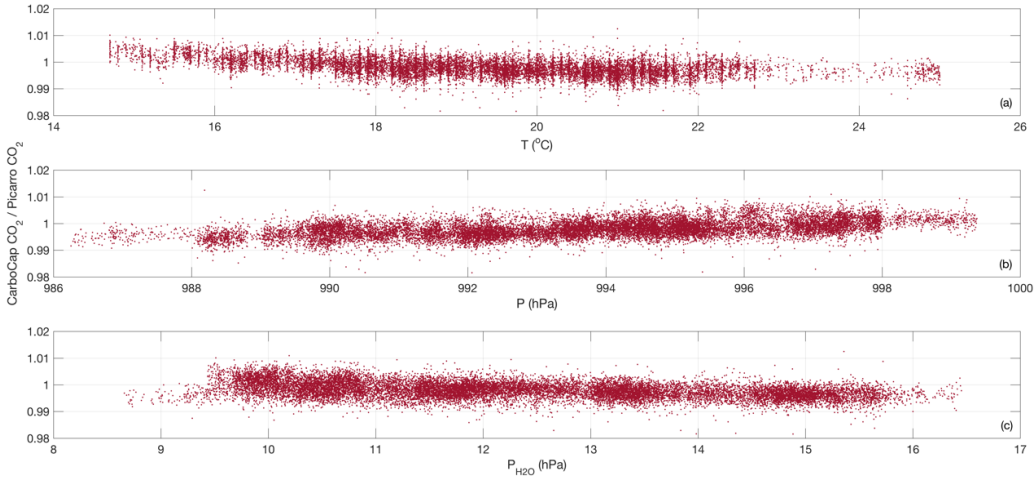

Figure 2.6. Ratio of 1-minute mean CO_2 dry air mole fractions presented in Fig. 2.5, shown as a function of temperature **(a)**, pressure **(b)**, and the partial pressure of water **(c)**.

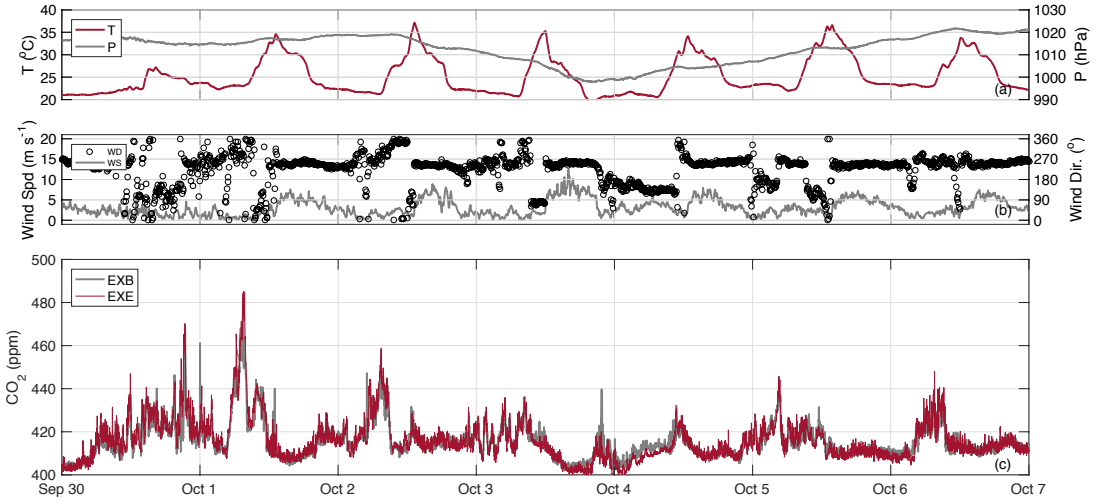

Figure 2.7. Representative weeklong time series of observations collected at or near two nearby in-field BEACO$_2$N nodes (EXB and EXE in Fig. 2.1; ~200 m apart) in October 2015: **(a)** temperature and pressure averaged to 1 minute, **(b)** wind speed and direction collected once every 6 minutes, **(c)** drift- and bias-corrected CO_2 dry air mole fractions averaged to 1 minute.

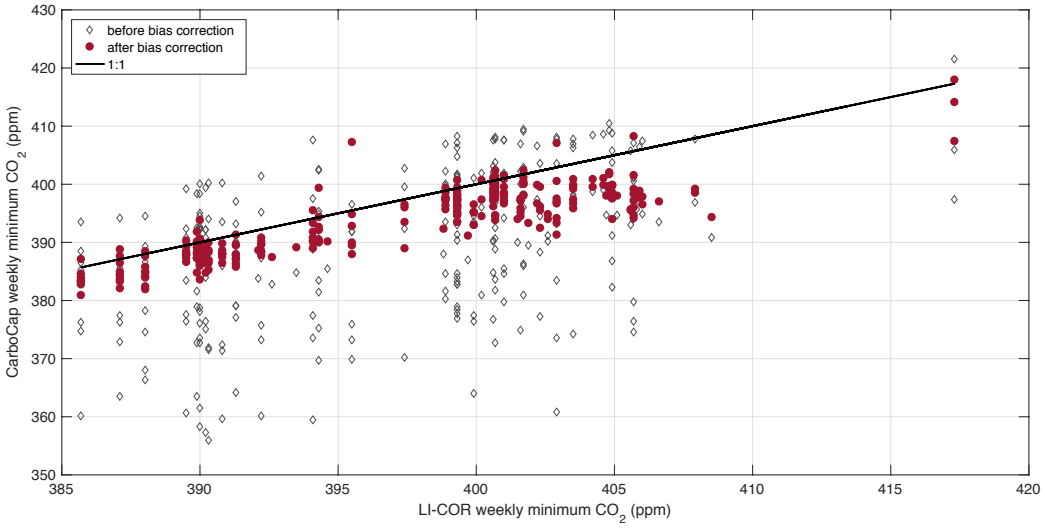

Figure 2.8. Weekly minimum CO_2 concentrations measured by a LI-COR LI-820 reference instrument compared with weekly minima calculated from the BEACO_2N data record before and after correction for systematic uncertainties.

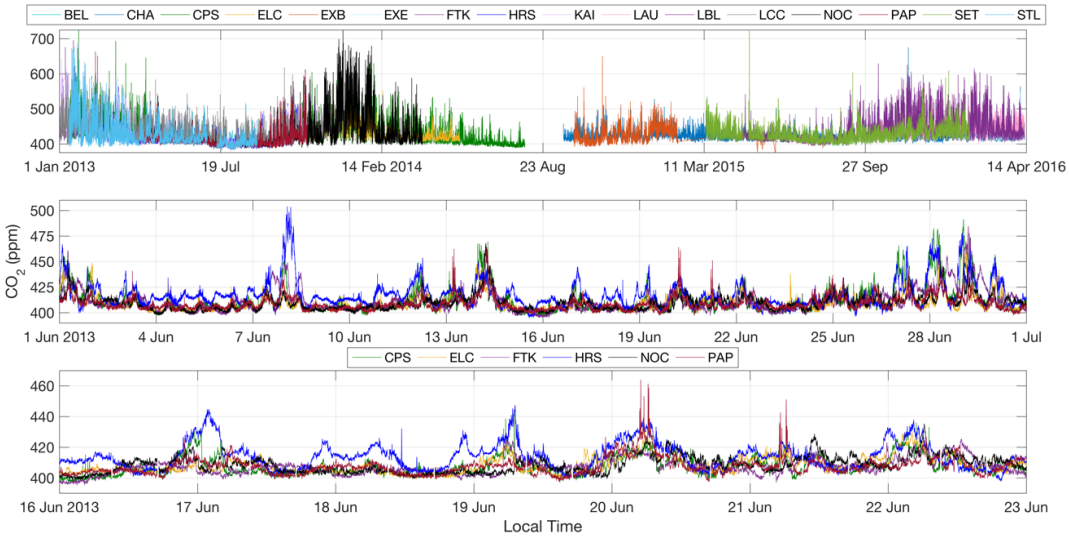

Figure 2.9. Time series of drift- and bias-corrected CO_2 dry air mole fractions collected over the course of ~2.5 years at 16 BEACO_2N sites (top), 1 month at six representative sites (middle), and 1 week at the same six sites (bottom). The hiatus around 23 August corresponds to a largescale hardware refurbishment effort that began in mid-2014.

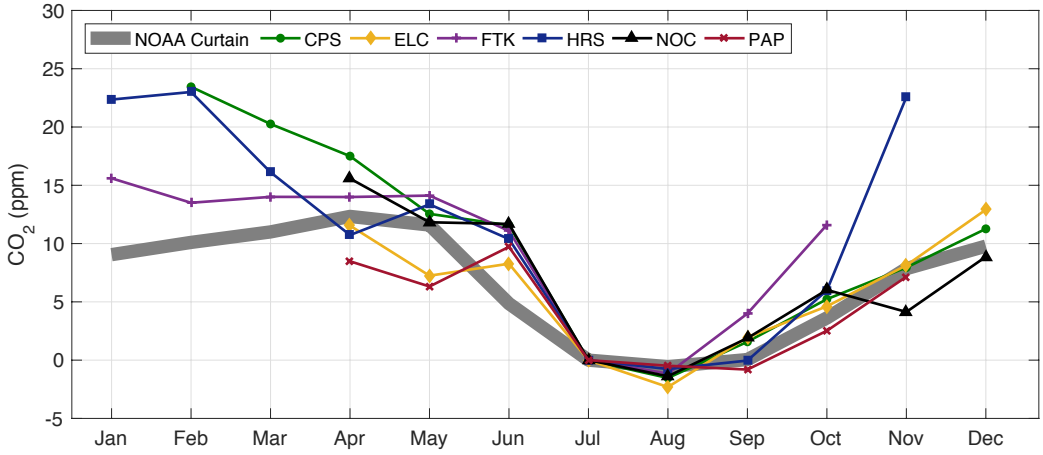

Figure 2.10. Monthly minimum drift- and bias-corrected CO_2 dry air mole fractions observed during 2013 at the same six BEACO_2N sites shown in the bottom panels of Fig. 2.9, plotted as the enhancement above the July value. Bold gray curve shows a similar treatment of the surface level Pacific Ocean empirical boundary curtain values for 38° N.

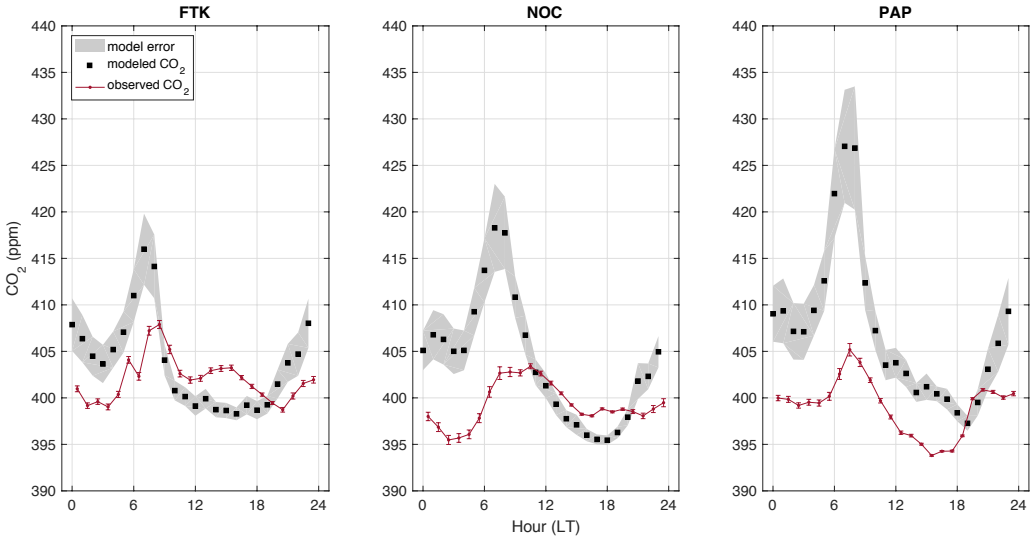

Figure 2.11. Diurnal variation in drift- and bias-corrected CO_2 dry air mole fractions observed and modeled at three representative BEACO$_2$N sites during September 2013. Error bars indicate the standard error of the mean (instrument error is negligible at this timescale); thick shaded curves indicate standard deviation.

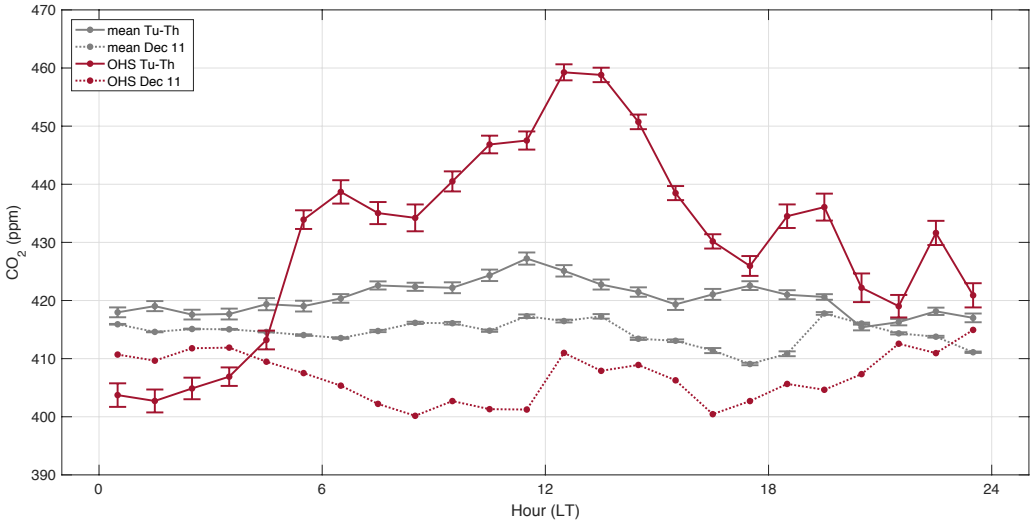

Figure 2.12. Comparison of diurnal variation in drift- and bias-corrected CO_2 dry air mole fractions observed at Oakland High School (OHS in Fig. 2.1) during a rain-related school closure on 11 December 2014 vs. the mean variation observed on other Tuesdays, Wednesdays, and Thursdays during December 2014 when the school was operating normally. Mean values from five other BEACO_2N sites operational during these time periods are also shown for reference. Error bars indicate standard error (instrument error is negligible at this timescale).

CODE	FULL SITE NAME	LAT	LON	ELEV (m asl)	ELEV (m agl)
BEL	Burckhalter Elementary School	37.775	-122.167	97	8
BOD	Bishop O'Dowd High School	37.753	-122.155	82	8
CHA	Chabot Space & Science Center	37.819	-122.181	476	11
CPS	College Preparatory School	37.849	-122.241	102	4
EBM	W. Oakland EBMUD Monitoring Stn.	37.814	-122.282	6	2
ELC	El Cerrito High School	37.907	-122.294	49	13
EXB	Exploratorium (Bay)	37.802	-122.397	13	9
EXE	Exploratorium (Embarcadero)	37.801	-122.399	13	5
FTK	Fred T. Korematsu Discovery Acad.	37.737	-122.173	16	6
HRS	Head Royce School	37.809	-122.204	114	5
KAI	Kaiser Center	37.809	-122.264	115	111
LAU	Laurel Elementary School	37.792	-122.196	74	6
LBL	Lawrence Berkeley Nat'l Lab, Bldg. 70	37.876	-122.252	246	11
LCC	Lighthouse Community Charter School	37.736	-122.196	9	5
MAR	Berkeley Marina	37.863	-122.314	6	2
MON	Montclair Elementary School	37.830	-122.211	193	4
NOC	N. Oakland Community Charter School	37.833	-122.277	24	6
OHS	Oakland High School	37.805	-122.236	49	7
OIN	International Community School	37.779	-122.231	19	6
PAP	PLACE at Prescott Elementary	37.809	-122.298	12	6
PDS	Park Day School	37.832	-122.257	39	7
PHS	Piedmont Middle & High School	37.824	-122.233	86	10
POR	Port of Oakland Headquarters	37.796	-122.279	35	32
ROS	Rosa Parks Elementary School	37.865	-122.295	22	10
SET	Stone Edge Farms (near turbine)	38.289	-122.503	54	2
SEV	Stone Edge Farms (in vineyard)	38.291	-122.506	61	3
SHS	Skyline High School	37.798	-122.161	359	3
STL	St. Elizabeth High School	37.779	-122.222	28	11

Table 2.1. List of site names, abbreviated codes, geo-coordinates, and elevations used in this study.

SITE CODE	UPTIME (%)	MEAN (ppm)	STD (ppm)	MAX (ppm)	MIN (ppm)
CPS	94.6	416	21.6	589	385
		423	24.3	730	384
ELC	90.1	411	18.5	581	387
		415	21.3	567	388
FTK	91.2	415	17.7	609	387
		418	26.4	567	383
HRS	69.1	410	14.7	506	384
		428	18.4	514	398
LAU	91.2	429	22.4	687	392
		421	26.4	603	381
KAI	83.1	442	21.8	820	396
		418	24.7	604	382
NOC	87.3	411	18.4	560	387
		428	50.5	724	384
PAP	55.5	403	9.57	500	387
		411	19.1	548	388
STL	59.1	417	17.5	586	389
		421	36.9	616	383

Table 2.2. Descriptive statistics for the drift- and bias-corrected CO_2 dry air mole fraction measured at nine representative sites during 2013. Upper row for each site gives the daytime (1100–1800 LT) statistics; lower row gives the nighttime (2200–0400 LT). The ELC node is used as the reference site in Sect. 2.3.4 and so is presented here without correction for systematic uncertainties.

SITE CODE	$U_{temporal}$ day^{-1} (ppm day^{-1})	$U_{atemporal}$ (ppm)
BEL	0.03 ± 0.02	-3 ± 1
CPS	-0.014 ± 0.002	3.1 ± 0.5
FTK	0.02 ± 0.01	6.1 ± 0.8
HRS	-0.12 ± 0.01	1.2 ± 0.8
LAU	0.10 ± 0.01	-26.9 ± 0.8
KAI	0.04 ± 0.01; -0.08 ± 0.05	-23 ± 1; 6 ± 4
NOC	-0.11 ± 0.02; 0.030 ± 0.006	22 ± 1; -2.7 ± 0.7
PAP	-0.092 ± 0.005	8.7 ± 0.7
STL	-0.03 ± 0.01	9 ± 1

Table 2.3. Results from drift- and bias-correction analysis at sites for which at least 3 months of observations are available for comparison with the ELC BEACO$_2$N node.

Chapter 3

Observing local CO_2 sources using low-cost, near-surface urban monitors

Adapted from Shusterman, A. A., Kim, J., Lieschke, K. J., Newman, C., Wooldridge, P. J., and Cohen, R. C., Atmos. Chem. Phys. Discuss., 2018.

3.1 Introduction

Initiatives to curb greenhouse gas emissions and thereby reduce the extent of climate change-related damages are gaining momentum from city to global scales (United Nations, 2015). To support this effort, there is a clear need for monitoring, reporting, and verification (MRV) strategies capable of describing emission changes and attributing those changes to the relevant policy measures (Pacala et al., 2010). Currently, an estimated 70% of global CO_2 emissions are urban in origin and this fraction is expected to grow as migration to urban areas continues and intensifies with the industrialization of developing nations (United Nations, 2011). However, cities also present the largest MRV challenge in that many disparate emission sources combine with complex topography.

A considerable amount of MRV-related work has been invested in the development of activity-based emission inventories for selected metropolitan areas, such as Indianapolis (Gurney et al., 2012), Paris (Bréon et al., 2015), Los Angeles (Newman et al., 2016), Salt Lake City (Patarasuk et al., 2016), and Toronto (Pugliese et al., 2018), as well as other inventories constructed and maintained by individual air management agencies for internal use. These inventories, when updated regularly, offer the possibility of direct source attribution without the use of computationally intense and/or heavily parameterized atmospheric transport models; they do, however, typically rely on interpolations, generalizations, or proxies to generate the necessary input activity data. The Fuel-based Inventory for Vehicle Emissions (FIVE) developed by McDonald et al. (2014), for example, uses a representative 7 days of highway traffic flow measurements to drive the weekly cycle of CO_2 emissions from mobile sources on roads of all sizes year round. While traffic patterns as well as residential and commercial energy usage are known to vary by day of week (Harley et al., 2005), the specific timing and magnitude of these variations are likely to be heterogeneous in space and time. Mobile emission estimates constructed using an average week of highway observations therefore neglect the impact of anomalous events as well as the variety of vehicle fleets, commute practices, and congestion patterns that occur at the neighborhood level. As knowledge of emission factors and fuel efficiency grows, activity data will become one of the largest sources of uncertainty in bottom-up inventory products.

Ambient atmospheric measurements offer the opportunity to observe nuanced variations in CO_2 emission activities directly without generalizing across space and time. In order to document baseline conditions in and upcoming changes to urban greenhouse gas emissions, surface-level monitoring campaigns in cities using varied approaches are being pursued (e.g., Bréon et al., 2015; Chen et al., 2016; McKain et al., 2012; McKain et al., 2015; Shusterman et al., 2016; Turnbull et al., 2015; and Verhulst et al., 2017). These networks, typically consisting of 2–15 instruments, attempt to constrain and supplement activity-based emission inventories with observation-based estimates. Most previous work on observation-based emission estimates has focused on domain-

wide emission totals over monthly to annual timescales (e.g., Kort et al., 2013). This emphasis on integrated signals has led to site selection and data analysis techniques that minimize sensitivity to local emissions, thus discarding a large portion of the information contained in the datasets collected at individual measurement sites and the differences between them (Shusterman et al., 2016; Turner et al., 2016).

We hypothesize that, if trends in the specific, small-scale CO_2 sources implicated in most mitigation strategies are to be resolved from atmospheric monitoring datasets, site-to-site heterogeneity must be sought out and retained. Here we present an initial characterization of the degree of spatial heterogeneity present in an urban monitoring dataset and offer these direct observations of intracity heterogeneities as a possible strategy for providing direct constraints on CO_2 emissions from individual sectors. We provide an initial approach to quantifying changes in the mobile sector and separating the influence of that sector from other emissions.

3.2 Measurements

3.2.1 The BErkeley Atmospheric CO_2 Observation Network

The BErkeley Atmospheric CO_2 Observation Network ($BEACO_2N$; see Shusterman et al., 2016) is an ongoing greenhouse gas and air quality monitoring campaign operating in the San Francisco Bay Area since late 2012. The current network is comprised of ~50 "nodes" stationed on top of schools and museums at approximate 2 km intervals (Fig. 3.1). The nodes contain a variety of commercially available, low-cost sensor technologies: a Vaisala CarboCap GMP343 for CO_2, a Shinyei PPD42NS for particulate matter, a suite of Alphasense B4 electrochemical devices for O_3, CO, NO, and NO_2, as well as meteorological sensors for pressure, temperature, and relative humidity. Data is collected every 2–10 s and transmitted wirelessly or via an onsite Ethernet connection to a central server, where it is made publicly available in near real time. The distributed low-cost dataset is supplemented by a "supersite" at the RFS location featuring a Picarro G2401 cavity ring-down spectroscopy analyzer for CO_2, CO, and H_2O, a TSI Optical Particle Sizer 3330 for particulate matter, a ThermoFisher Scientific 42i-TL NO_x analyzer for NO and NO_2, a Teledyne 703E photometric calibrator for O_3, a Pandora spectrometer system for total column O_3 and NO_2, a Lufft CHM 15k ceilometer for cloud and aerosol layer height, as well as various instruments for meteorological measurements (i.e., a Vaisala WXT520 weather transmitter, a Campbell Scientific CS500 temperature and relative humidity probe, and a Davis Vantage Pro2 system with a Davis 6410 anemometer and Davis 6450 solar radiation sensor). This high-cost, reference-grade instrumentation is calibrated using gas standards calibrated relative to World Meteorological Organization (WMO) scales (Zhao and Tans, 2006) and therefore serves as a high-accuracy anchor point within the network domain. Atmospheric boundary conditions are monitored by the Bay Area Air Quality Management District's Greenhouse Gas Measurement Program, which maintains its own reference instruments at four background sites to the northwest, east, southeast, and south. A description of the design, deployment, and evaluation of the $BEACO_2N$ approach can be found in Shusterman et al. (2016) and Kim et al. (2018).

Here we utilize CO_2 observations from the 20 $BEACO_2N$ sites operating most consistently during the summer and/or winter of 2017 (Table 3.1), defined as 1 June 2017 through 30 September 2017 and 1 November 2017 through 31 January 2018, respectively. The raw 2-second CO_2

concentrations are averaged to 1-minute means, which are subsequently converted to bias-corrected dry air mole fractions using site-specific meteorological observations and in-network reference measurements (see Shusterman et al., 2016). The processed 1-minute averages are assumed to have an uncertainty of less than ±4 ppm, or ±0.5 ppm at the hourly temporal resolution discussed most often hereafter.

3.2.2 Traffic counts

Traffic count data is collected by the California Department of Transportation as part of the Caltrans Performance Measurement System (PeMS; http://pems.dot.ca.gov/). Hourly passenger vehicle flow data (in vehicles per hour) are obtained from the road monitors nearest to the relevant BEACO$_2$N site with >50% directly observed (as opposed to modeled) data and are summed across all lanes and directions. Due to limited data coverage, in some cases it is necessary to sample road monitors upstream or downstream of the desired roadway segment; here we assume the sampled traffic conditions to be reasonable approximations of those on the desired segment. The specific monitor IDs used in each analysis are given in Table 3.1.

3.3 Results & Discussion

To quantify the spatial heterogeneity present across the network, we examine the degree of correlation between every possible pairing of sites in a given season as a function of the distance between them (Figs. 3.2 and 3.3), borrowing from a similar analysis used by McKain et al. (2012). For straightforward comparison with the McKain et al. results, we first average to 5-minute resolution and allow for up to a ±3 h lag between the two time series before performing a linear regression and choosing the optimal r^2 value.

In the summer months, there appears to be some relationship between the proximity of the sites and the correlation of their observations at all hours, with higher correlations between neighboring sites decaying into more modest, but still significant, correlations at longer inter-site distances. The characteristic length scale of this correlation is 2.9 km (defined as the e-folding distance of the exponential fits in Fig. 3.2; 3.6 km during the day and 2.2 km at night). The winter months meanwhile exhibit lower pairwise correlations overall and shorter correlation lengths (2.4 km; 2.6 km during the day and 2.1 km at night). Some portion of the summer–winter differences may be attributable to seasonal differences in dominant wind patterns, although this effect is difficult to disentangle from the slightly different collection of sites sampled during the two seasons; the winter sample, for example, contains fewer pairs with separation lengths less than 5 km, which affects the perceived overall trend. In either season, the correlation lengths are considerably longer than the ~100 to 1000 m e-folding distances of urban pollutants derived by previous studies (e.g., Zhu et al., 2006; Beckerman et al., 2008; Choi et al., 2014), however, the correlation length observed here does validate the original choice of 2 km as the desirable inter-site separation in the design of the BEACO$_2$N instrument.

The 24-hour findings (top panels of Figs. 3.2 and 3.3) compare well to those presented by McKain et al., who also documented a decaying but nevertheless persistent correlation with increasing site separation. However, whereas McKain et al. saw very little correlation after restricting their analysis to daytime hours, even at very short (<5 km) inter-site distances, we observe moderate to

high correlations during the day. This suggests that the data record at a particular BEACO$_2$N site contains information about both local and regional emissions and transport phenomena. Figure 3.4 demonstrates these dual scales of influence by providing a spatial visualization of the correlation coefficients at four representative sites. PER, for example, is well correlated with its neighbors only, suggesting the presence of local phenomena that do not affect other parts of the network. LCC, however, also exhibits relationships with more distant sites, indicating a sensitivity to more regional-scale influence(s). Meanwhile, HRS and OHS each possess a few near neighbors with whom they are poorly correlated, perhaps due to hyperlocal events specific to those sites. While the region-wide phenomena can be characterized using sparser networks of high-cost, conventional monitoring equipment, the ability to capture these local processes is unique to the high-density approach.

We posit that the true strength of a high-density, surface-level monitoring network lies in its characterization of hyperlocal phenomena unique to a given site or subset of sites. In order to directly examine signals attributable to these specific, local CO_2 emission processes, we separate each site's observations into a "regional" and "local" component. The regional component is, by definition, the same at all sites network-wide, calculated from the bottom 10th percentile of all BEACO$_2$N readings collected during the surrounding 1-hour window. The bottom 10th percentile is chosen (rather than the absolute minimum) to account for measurement error (see Shusterman et al., 2016) as well as any near-field draw down from the local biosphere; negative values in the local signals are likely attributable to some combination of these effects. While many different sites contribute to this bottom 10th percentile over the course of the data record, some sites located in close proximity to emission sources are never represented in the bottom 10th percentile and always exhibit some enhancement (i.e., a non-zero local component) over the regional background signal. The regional component is allowed to vary throughout the data record and will therefore reflect domain-wide changes in response to day of week, synoptic weather events, etc.

The diel profiles of the regional signal measured in summer and winter 2017 are shown in Fig. 3.5, reflecting the typical convolution of background concentrations, emission processes, and dynamics experienced across the entire BEACO$_2$N domain. In both seasons, we see an increase in the regional signal beginning around 0400 local time (LT), followed by a decrease in concentrations at 0800 LT in the winter months and 1100 LT in the summer, and another increase in early to late afternoon depending on the season. This diurnal profile corresponds well with known patterns in traffic emissions–which are largely consistent across seasons–superimposed on diel fluctuations in boundary layer height that vary in timing and magnitude according to the season. Namely, the nighttime boundary layer in the BEACO$_2$N domain appears to be shallower during the winter months, producing a larger regional increase in response to rush hour traffic. The wintertime layer also expands and re-contracts earlier in the day than the summertime layer, resulting in both an earlier minimum and an earlier rise in afternoon–evening concentrations. An analysis of the regional signals calculated for similar periods in 2013 revealed qualitatively similar results (Fig. 3.6), although it should be noted that the 2013 analysis uses observations from a significantly different subset of sites in the BEACO$_2$N network.

We isolate the local signals by subtracting the network-wide regional component from the data record at each site. Median 1-minute local CO_2 signals range from 0.3 to 40.2 ppm during the day (1100–1800 LT) and 1.1 to 38.5 ppm at night (2100–0400 LT) during the summer months,

although the distributions are skewed, with the 10th to 90th percentile ranges stretching from -2.4 to 69.0 ppm during the day and -2.0 to 45.0 ppm at night. During the winter months, the daytime medians range from 3.6 ppm to 34.8 ppm (-7.0 to 90.8 ppm 10th to 90th percentile range) and -0.8 ppm to 58.7 ppm (-15.0 to 90.6 ppm 10th to 90th percentile range) at night. A full picture of the overall distributions is shown in Figs. 3.7 and 3.8, confirming a much greater frequency of high CO_2 concentrations during the winter months. In both seasons, the distribution of the local enhancements is typically unimodal with a heavy right-hand tail, although some sites exhibit more complex bi- or multi-modal distributions.

By definition, we expect these local signals to represent a unique combination of emission sources and atmospheric dynamics specific to a given site. Mobile sources are estimated to comprise approximately 40% of the San Francisco Bay Area's annual CO_2 emissions (Claire et al., 2015) and are likely to represent an even larger fraction within the urban core, where electricity and co-generation sources are less abundant. However, as noted in the discussion of the regional signals above, direct observation of the magnitude and variation of traffic emissions via ambient CO_2 concentrations is complicated by the coincident variation in turbulent mixing and boundary layer height as the earth's surface warms and cools at sunrise and sunset (Fig. 3.9).

In order to more directly examine the relationship between highway traffic flow and urban CO_2 concentrations, we begin by analyzing the subset of observations collected between 0400 and 0800 LT at the LAN site, located less than 40 m from Interstate 880. During this period, traffic emissions are high, but the boundary layer is relatively shallow, thus increasing the sensitivity of the surface-level monitor to the traffic signal. The resultant strong positive correlation between rush hour traffic flow and local CO_2 concentrations is shown in Fig. 3.10, along with the median CO_2 concentrations observed in each 500 veh h^{-1} traffic flow increment and the linear regressions through these binned medians. (An alternative analysis using traffic density–obtained by dividing the traffic flow by the average vehicle speed–yields almost identical results.) We observe a factor of 2 difference in local CO_2 between congested vs. free-flowing conditions, similar to that observed by a previous on-road mobile monitoring study by Maness et al. (2015). The uncertainty in the slope of the linear regression is 17%, indicating that this analysis of a single site could be used to detect 17% changes in average emissions per vehicle. For reference, under the Corporate Average Fuel Economy standards, the state of California aims to achieve a fleet-wide average fuel economy of 54.5 miles per gallon by the year 2025 (US EPA, 2012), corresponding to a 35% decrease in emissions relative to the 35.5 miles per gallon economy of 2012–2016 model year vehicles.

In addition to this first-order sensitivity to vehicle emissions at the near-roadway LAN site, we find that policy-relevant emission changes can also be detected using nodes stationed greater distances from the highway by controlling for the impacts of dispersion. To do so, we decompose the CO_2 signals into terms that represent the influence of meteorology and emissions separately via a multiple linear regression approach analogous to that described by de Foy (2018). Briefly, linear coefficients describing the relationship of a site's CO_2 signal to temperature, specific humidity, wind, boundary layer height, time of day, day of week, and time of year are derived in an iterative, compounding fashion, with the variable leading to the greatest increase in the square of the Pearson correlation coefficient being added to the regression until the addition of a new variable no longer increases the r^2 value by at least 0.005. Temperature, specific humidity, wind

speed, and wind direction are taken from the Port of Oakland International Airport weather station maintained by the NOAA Integrated Surface Database (https://www.ncdc.noaa.gov/isd/) and boundary layer heights are provided by the ECMWF's ERA-Interim model (Dee et al., 2011; http://apps.ecmwf.int/datasets/). The nonlinear relationship between CO_2 concentrations and wind or boundary layer height is captured by dividing these meteorological datasets into quartiles and deriving a linear coefficient for each subset. The wind speed quartiles are further subdivided by wind direction before fitting.

For this analysis, we use hourly total CO_2 concentrations (the sum of the local and regional components) measured at five sites between 15 February 2017 and 15 February 2018; a representative comparison of the observed and modeled results at the LCC site is shown in Fig. 3.11. The intercept of the multiple linear regression provides an estimate of the average background CO_2 concentration observed at a given site over the entire analysis period; here we find a mean intercept of 426 ppm across the five sites. This is considerably higher than the average 407 ppm regional signal calculated for the summer months using the bottom 10th percentile method described above, but in good agreement with the average wintertime regional signal (425 ppm).

Multiple linear regression coefficients are derived for each hour of the day during five types of days of the week (Mondays, Tuesdays through Thursdays, Fridays, Saturdays, and Sundays); for clarity, Fig. 3.12 shows the regression coefficients for Tuesdays through Thursdays and Sundays. These MLR "factors" signify the average CO_2 enhancement or depletion (in ppm) uniquely associated with a particular hour of a particular day of the week. The dependencies on time of day and day of week derived via this method primarily reflect the changes in emissions, as the influence of the coincident changes in atmospheric dynamics has been at least partially controlled for. Indeed, we do observe some intuitive patterns in the linear regression coefficients, such as higher coefficients on weekday mornings corresponding to higher rush hour traffic emissions on those days. As expected, the weekday enhancement is larger at the sites located close to a freeway (e.g., 520% at FTK) but is less pronounced at LBL (70%), which is farther away from major mobile sources. For reference, the 1 km by 1 km FIVE mobile emission inventory developed for the San Francisco Bay Area by McDonald et al. (2014) predicts a ~210% weekday enhancement on average, peaking around 0500 LT, much earlier in the day than is observed here. When we examine the relationship between these multiple linear regression coefficients and morning traffic flow as we did at LAN (Fig. 3.13), we find positive correlations enabling the detection of 11–30% changes in emissions. This is sufficient sensitivity to detect and monitor future increases in the fuel efficiency of the California passenger vehicle fleet with a record as short as 2–3 years.

It is likely that even greater sensitivity could be achieved with more accurate meteorological datasets. While the single weather station and relatively coarse (0.125^o by 0.125^o) reanalysis product we use here may be adequate to represent the meteorological conditions across some domains, the San Francisco Bay Area is at the high end of complexity in terms of terrain and microclimatology. Higher resolution boundary layer heights and neighborhood-specific wind observations may improve the results of our multiple linear regression, but these types of measurements are rarely available on the spatial scale of the $BEACO_2N$ instrument and are difficult to simulate with accuracy (Jiménez et al., 2013; Banks et al., 2016). In future work, high-density

networks like BEACO$_2$N may therefore be useful not just in source attribution but also in providing a much needed observational constraint on our understanding of near-surface transport.

Future work will also make use of the ancillary datasets provided by the BEACO$_2$N platform, such as the concurrent NO_x and CO concentrations. The ratio of these species to CO_2 provides a unique signature for each different CO_2 source (e.g., Ban-Weiss et al., 2008; Harley et al., 2005), allowing "plumes" or other subsets of the data record to be directly attributed to specific (e.g., mobile) source types and allowing the relationship between these specific activities and CO_2 mixing ratios to be derived more precisely. With such a precise methodology for converting between emissions and concentrations, subtler inter-annual trends in emissions could be detected, for example changes in vehicle emissions following construction of new housing.

3.4 Conclusions

We have described the heterogeneity measured at the individual sites of a high-density, surface-level urban CO_2 monitoring network. Networkwide, correlation length scales are found to be slightly longer during daytime during the summer, and generally shorter during winter months, but falling in the range of values reported previously based on other stationary observation networks and mobile monitoring campaigns. High near-field correlations are thought to be driven by shared sensitivity to local emission events, while moderate far-field correlations reflect regional episodes, suggesting that a given site's data record is likely a convolution of both phenomena. We therefore present a methodology for separating the observed CO_2 concentrations into local and regional components and observe distinct distributions (i.e., unimodal vs. bimodal) of local CO_2 enhancements within single neighborhoods. A clear relationship is seen between morning rush hour traffic counts and local CO_2 concentrations, allowing for the detection of changes in vehicle emissions within 2–3 years, if those changes proceed at a rate consistent with policy objectives.

Prior publications (e.g., McKain et al., 2012; Kort et al., 2013; Wu et al., 2018) have favored sparser networks of high-quality instruments, criticizing high-density, low-cost approaches as either: (a) providing redundant constraints on total urban emissions, (b) offering information on CO_2 sources in their immediate surroundings only, or (c) possessing insufficient accuracy to resolve small emission trends. The ideal trade-off between measurement quality and instrument quantity has been investigated previously using an ensemble of observing system simulations by Turner et al. (2016), who found BEACO$_2$N-like observing systems to outperform smaller, higher quality networks in estimating regional as well as more localized emission phenomena. While Turner et al. saw significant benefits to achieving an instrument precision of 1 ppm, further increases in measurement quality offered little advantage in constraining emissions, especially those from line and point sources.

This work thus provides an important data-based verification of the conclusions of Turner et al.'s theoretical analysis. Not only do we demonstrate the ability of low-cost sensors to sufficiently constrain policy-relevant trends in line source (i.e., highway traffic) emissions, but we do so without the use of computationally intense and heavily parameterized atmospheric transport models. Furthermore, we show that a multiple linear regression analysis allows the signature of highway traffic to be extracted from sites located throughout the network, enabling trends in mobile emissions to be quantified without specially situated, roadside monitors. This is an

important result, as deriving and implementing a particular, a priori network layout is a non-trivial task. Domain-specific transport patterns prevent the development of general principles of optimal sensor placement, and, even if ideal locations can be identified, cooperation from facilities in the area cannot be guaranteed. By establishing for the first time that an ad hoc, opportunistic sensor siting approach can nonetheless provide sensitivity to emission sources of interest, we thus improve the prospects for widespread adoption of distributed monitoring systems in the future.

Progress toward evaluating the capabilities and proper use of low-cost sensors has particular relevance for nations with rapidly developing economies, where CO_2 emissions are increasing much faster than the resources needed to monitor them by conventional means. Domestically, citizen science and environmental justice groups are also adopting these technologies (Snyder et al., 2013) as an economically accessible means of advocating for greater public health and ecological wellbeing. While the specific correlation lengths and emission estimates we derive here are unique to the San Francisco Bay Area domain, the sensor performance capabilities and data analysis techniques we outline provide guidance more generally to any future studies attempting to interpret similar datasets around the world. High-resolution surface networks enabled by low-cost technologies offer a unique opportunity to provide ground truth constraints on difficult-to-model near-surface dynamics as well as on the individual CO_2 sources and sinks that comprise the strategic backbone of greenhouse gas mitigation regulation.

Figure 3.1. Map of $BEACO_2N$ node locations (black dots). Nodes used in this study are labeled. Map data © 2017 Google.

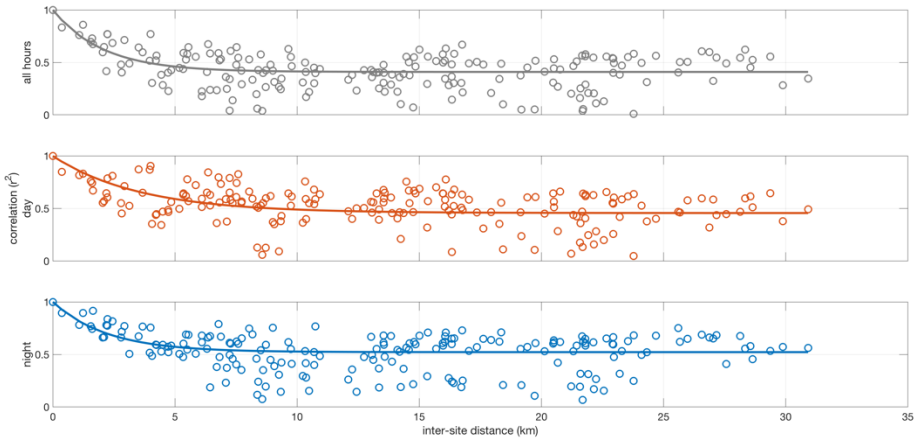

Figure 3.2. Optimal correlation coefficients for every possible pairing of summer 2017 sites as a function of their separation distance during all hours (top), daytime hours (1100–1800 LT, middle), and nighttime hours (2100–0400 LT, bottom). Solid lines show exponential decay of the correlation coefficients.

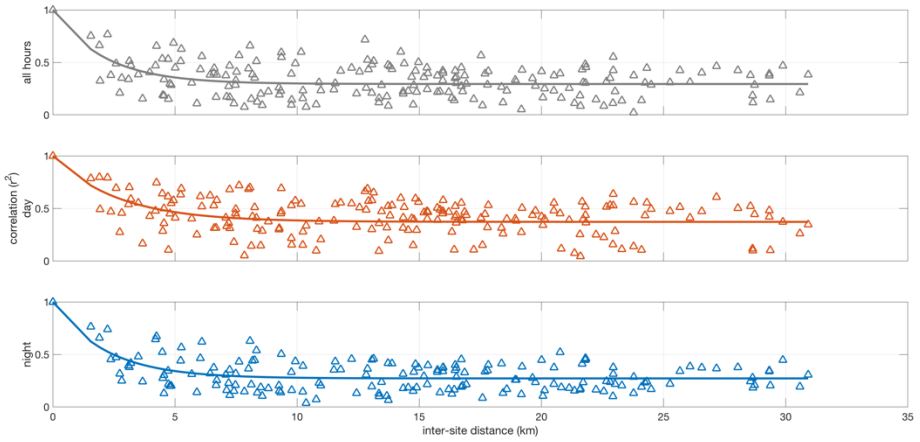

Figure 3.3. Optimal correlation coefficients for every possible pairing of winter 2017 sites as a function of their separation distance during all hours (top), daytime hours (1100–1800 LT, middle), and nighttime hours (2100–0400 LT, bottom). Solid lines show exponential decay of the correlation coefficients.

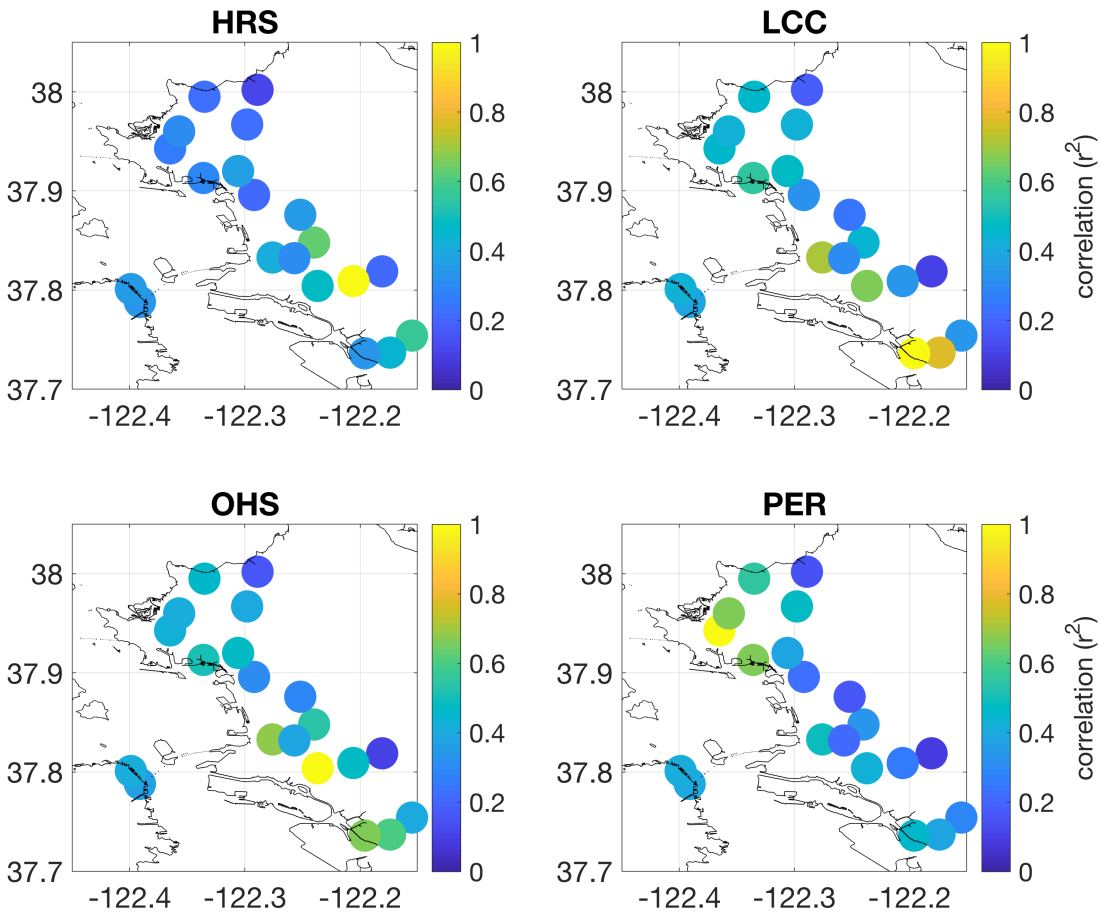

Figure 3.4. Optimal correlation coefficients representing network-wide correlation with 5-minute mean total CO_2 concentrations measured at four representative sites during all hours of winter 2017. Yellow spot ($r^2 = 1$) on each subplot shows the location of the site with which the correlation is examined.

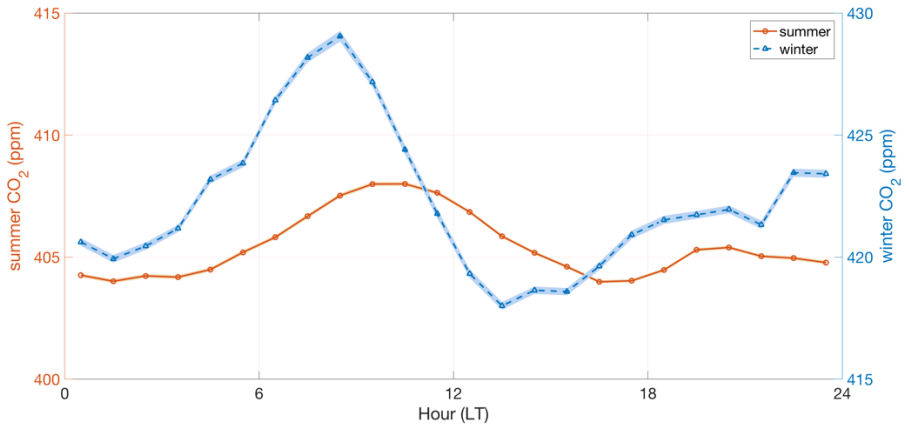

Figure 3.5. Hourly median values of the network-wide, regional CO_2 signals calculated for summer (orange) and winter (blue) periods in 2017. Lighter colored curves indicate the standard error; note the difference in y-scale.

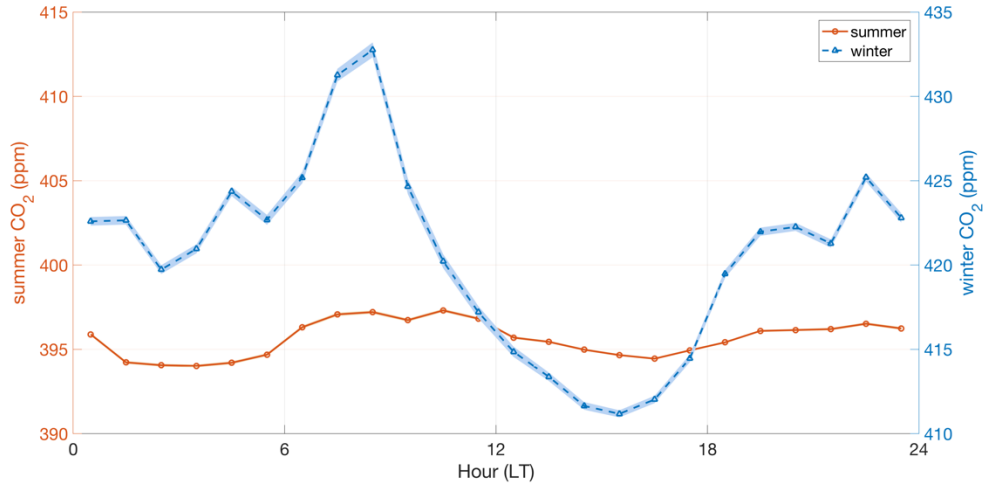

Figure 3.6. Hourly median values of the network-wide, regional CO_2 signals calculated for summer (orange) and winter (blue) periods in 2013. Lighter colored curves indicate the standard error; note the difference in y-scale.

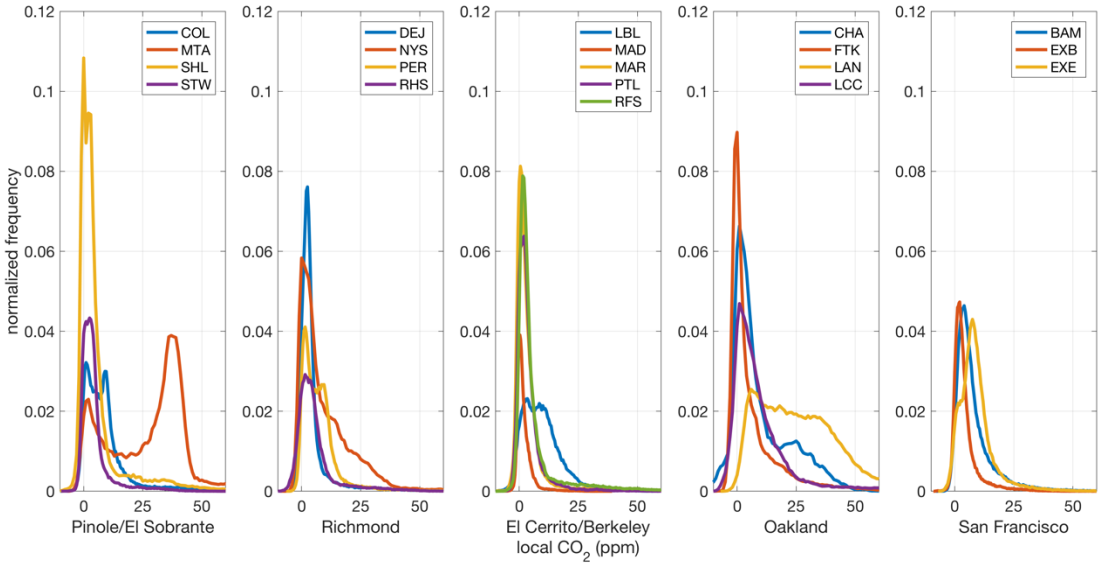

Figure 3.7. Normalized distributions of local CO_2 concentrations observed during summer 2017.

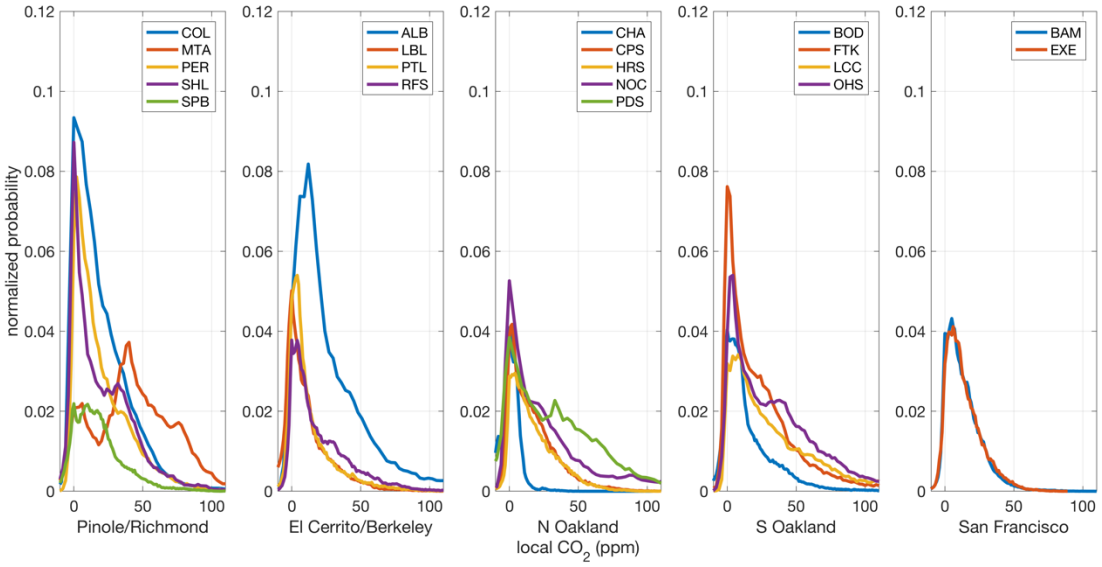

Figure 3.8. Normalized distributions of local CO_2 concentrations observed during winter 2017.

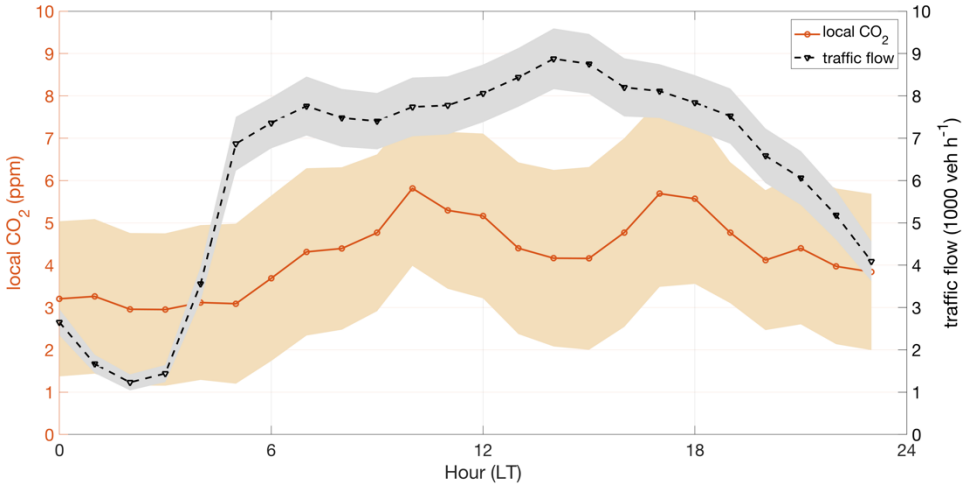

Figure 3.9. Hourly network-wide median local CO_2 and traffic flows observed during summer 2017. Lighter colored curves indicate standard error.

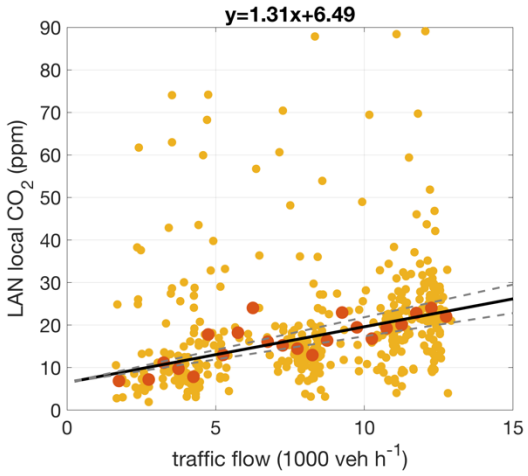

Figure 3.10. Morning (0400–0800 LT) local summertime CO_2 concentrations at LAN shown as a function of nearby highway traffic flow. Darker points indicate the median CO_2 concentration observed in each 500 veh h^{-1} traffic flow increment; black solid line indicates the linear regression through the binned medians (equation given above plot) and gray dashed lines show the uncertainty in the regression slope.

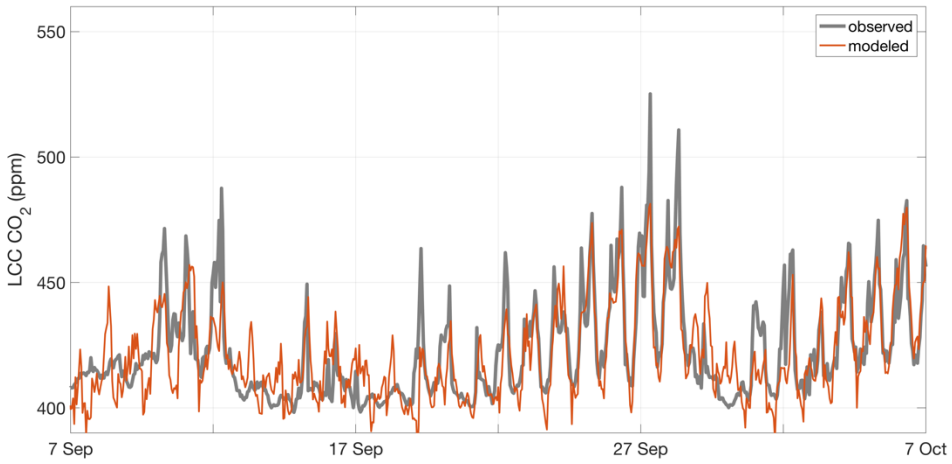

Figure 3.11. Representative month of total CO_2 concentrations observed (thick gray curve) and modeled (thin orange curve) at LCC site using a multiple linear regression approach based on de Foy (2018).

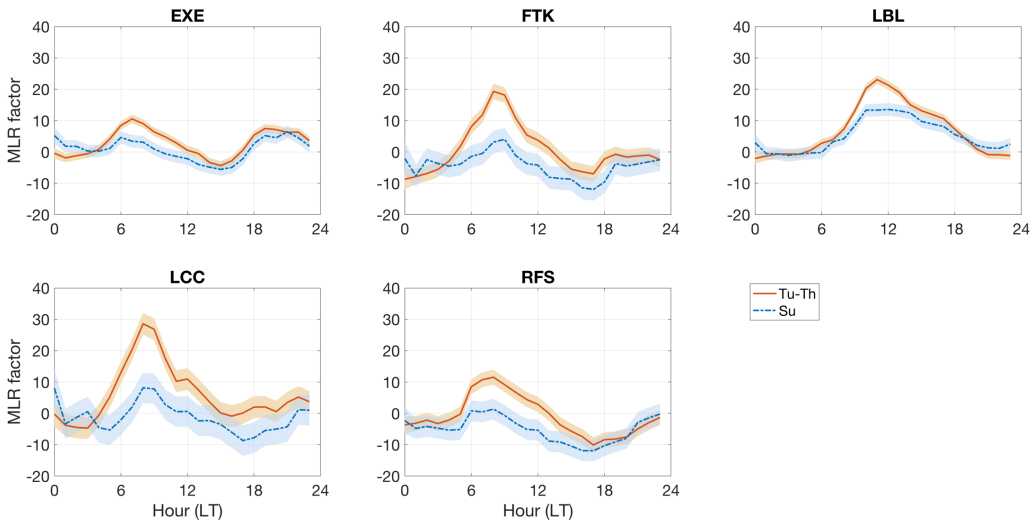

Figure 3.12. Multiple linear regression coefficients for five sites derived for each hour of the day on Tuesdays through Thursdays (orange solid line) and Sundays (blue dashed line) between 15 February 2017 and 15 February 2018.

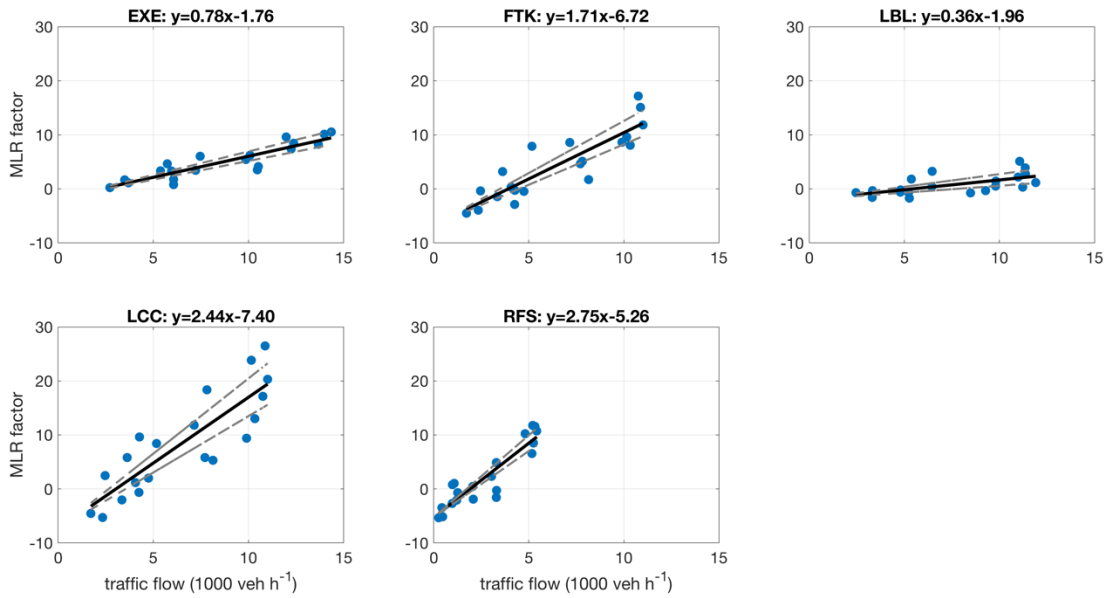

Figure 3.13. Morning (0400–0800 LT) multiple linear regression coefficients shown as a function of summertime traffic flow; black solid lines indicate the linear regression through the MLR factors (equations given above each subplot) and gray dashed lines show the uncertainty in the regression slope.

SITE CODE	LAT (° N)	LON (° E)	TRAFFIC MONITOR ID	DISTANCE FROM HIGHWAY (m)
ALB*	37.896	-122.292	401052, 402062	1390
BAM	37.788	-122.391	402815, 404920	170
BOD*	37.754	-122.156	401857, 401858	300
CHA	37.819	-122.181	400302, 400308	1720
COL	38.002	-122.289	401230, 401269	510
CPS*	37.848	-122.240	402201, 402202	220
DEJ†	37.933	-122.338	400361, 400445	950
EXB†	37.802	-122.397	402815, 404920	1570
EXE	37.801	-122.399	402815, 404920	1580
FTK	37.737	-122.173	JJAS: 400442, 400955 NDJ: 400608, 400793	1350
HRS*	37.809	-122.205	400302, 400308	700
LAN†	37.794	-122.263	400835, 408138	40
LBL	37.876	-122.252	400176, 400728	3090
LCC	37.736	-122.196	JJAS: 400442, 400955 NDJ: 400608, 400793	220
MAD†	37.928	-122.299	400819, 401558	1850
MAR†	37.863	-122.314	400176, 400728	950
MTA	37.995	-122.335	400538, 400976	2040
NOC*	37.833	-122.276	401211, 401513	750
NYS†	37.928	-122.359	400359, 400734	380
OHS*	37.804	-122.236	400261, 401017	160
PDS*	37.831	-122.257	400224, 401381	800
PER	37.943	-122.365	400639, 400738	1790
PTL	37.920	-122.306	400819, 401588	970
RFS	37.913	-122.336	400202, 400675	760
RHS†	37.953	-122.347	401228, 406660	1530
SHL	37.967	-122.298	416774, 416790	2030
SPB*	37.960	-122.357	401894, 401895	2280
STW†	37.990	-122.291	400313, 400902	500

Table 3.1. List of site geo-coordinates, relevant traffic monitor IDs, and approximate distances from a highway. Asterisks indicate sites with data available in winter 2017 only; daggers indicate sites with data available in summer 2017 only.

Chapter 4

High-resolution comparison of observed and simulated CO_2 mixing ratios

4.1 Introduction

In 2011, it was estimated that more than 70% of the world's fossil fuel CO_2 emissions originated in cities (United Nations, 2011). With the urban population expected to continue to grow in the coming decades, so does the importance of constraining and mitigating these associated urban greenhouse gas emissions. However, urban areas present a unique challenge with respect to protocols for monitoring, reporting, and verifying (MRV) emissions reductions in that a variety of disparate emitters covered under disparate regulations reside in close proximity to one another, complicating the attribution of observed trends to any particular policy or action.

Much recent work to this end has centered on the construction of high-resolution, bottom-up emission inventories for several major metropolitan areas (e.g., Bréon et al., 2015; Gurney et al., 2012; Newman et al., 2016; Patarasuk et al., 2016; and Pugliese et al., 2018). However, concerns surrounding the accuracy of these inventories remain, given the uncertainties associated with downscaling national inventories (Gately et al., 2013; Gately et al., 2015) and their reliance on non-representative chassis dynamometer studies (Yanowitz et al., 2000) as well as self-reporting by possibly disingenuous stakeholders (US EPA, 2015). Forward and time-inverted atmospheric models have been implemented in an effort to constrain and supplement these inventories using top-down observations (e.g., Bréon et al., 2015; Kort et al., 2013), but these techniques are strongly influenced by assumptions regarding the magnitude and covariance of the various sources of error involved (Lauvaux et al., 2016).

Turner et al. (2016) identify three types of error contributing to the "total mismatch" between observed mixing ratios and those simulated using atmospheric transport models: instrument error, model error, and representation error. Instrument error is unique to the particular measurement and calibration technique, ranging in order of magnitude from 0.15 ppm (Newman et al., 2013) to 4 ppm (Shusterman et al., 2016). The error associated with a given type of instrumentation and the calibration thereof is inversely correlated with cost, such that there exists for every application an optimal trade-off between instrument quality and quantity that must be considered. Model (i.e., transport) error is known to be significant when modeling the dynamics of urban boundary layers, where variable topography, street canyons, and heterogeneous surface roughness combine to create complex, turbulent flows. Many modeling studies therefore limit their analyses to afternoon hours (e.g., 1100–1700 LT; see Kort et al., 2014), when the planetary boundary layer is thought to be well-mixed and therefore more likely to be captured accurately by transport models. Even so, the magnitude of most models' transport error and the structure of its spatial correlation across a given urban domain are not entirely understood (Wu et al., 2018). Representation error refers to the inaccuracies that result from using averages across regularly shaped and spaced model grid cells to simulate conditions observed at discrete locations, which may or may not be well-represented by said averages (Turner and Jacob, 2015). While it is generally thought that the representativeness of a model is enhanced by the use of smaller grid cells (e.g., Valin et al., 2011), modeling atmospheric conditions at arbitrarily high spatio-temporal resolution requires significant computation time and power.

Prior studies have focused primarily on reducing the instrument and transport error terms (e.g., Deng et al., 2017; Wu et al., 2018), likely because these are the most straightforward to address, not necessarily because they are known to be the most important. Indeed, little is known about the magnitudes of each of these error terms relative to the error present in a given activity-based emission inventory. Here we present a comparison of CO_2 mixing ratios observed using a high-density sensor network ($BEACO_2N$; see Shusterman et al., 2016) in the San Francisco Bay Area over 2 weeks in August and September 2013 with those simulated using a high-resolution emission inventory for the region developed by McDonald et al. (2014) and Turner et al. (2016). By systematically varying the emission estimates as well as the boundary layer parameterization of the transport model, we assess the relative magnitudes of the instrument, transport, representation, and emission error terms.

4.2 Methods

4.2.1 Emission inventory

A detailed description of the CO_2 emission inventory utilized in this study is given in Turner et al. (2016). Briefly, we construct an hourly, 1 km^2 bottom-up inventory for the San Francisco Bay Area by combining point source and residential fuel usage data from the Bay Area Air Quality Management District (Mangat et al., 2010) with representative hourly traffic emissions from the 1 km^2 Fuel-based Inventory for Vehicle Emissions (FIVE) developed by McDonald et al. (2014). The result is believed to account for 95.8% of the anthropogenic CO_2 emissions in the domain and is further supplemented with 3 hourly, 1^o x 1^o biogenic, ocean, and fire emissions from the CarbonTracker CT2013B product (Peters et al., 2007), interpolated to hourly, 1 km^2 intervals. A representative time step from the inventory is shown in Fig. 4.1.

In addition to this best estimate (hereafter referred to as the "baseline" inventory), we also construct two alternate emission inventories with all traffic emissions scaled by 50% (i.e., the "minus-50" inventory) or 150% ("plus-50"). These adjusted inventories provide a conservative upper and lower bound on sources of error present in current inventory estimation techniques related to factors like real-world engine performance (Yanowitz et al., 2000), congestion (Barth and Boriboonsomsin, 2008), and the availability and representativeness of traffic flow data (McDonald et al., 2014). These scalings also allow for the exploration of possible future changes to the baseline emission inventory resulting from upcoming tighter fuel efficiency standards (US EPA, 2012) and/or increased electrification of the passenger vehicle fleet (Brown, 2016).

4.2.2 Model simulations

We use the aforementioned emission inventories as inputs for a custom version of the Weather Research and Forecasting/Chemistry (WRF-Chem) mesoscale model (Grell et al., 2005) with 1 km^2 and 6 s resolution, outputting every hour. WRF-Chem is not by default configured to treat CO_2 specifically, so for our purposes the CO_2 emission rates and mixing ratios are intentionally mislabeled "CO," an acceptable substitution given that the atmospheric lifetime of CO assumed by the model chemistry (2 months) is much longer than the lifetime of air in the model domain (<1 day). Boundary conditions are given by the three-dimensional Pacific "curtain" produced by

NOAA's Global Greenhouse Gas Reference Network (Jeong et al., 2013), interpolated to the native MOZART resolution and also temporarily labeled "CO."

We repeat each simulation with five different combinations of boundary and surface layer parameterizations to create an ensemble of model predictions representing the variety of plausible transport schemes:

- Model A: Mellor-Yamada-Janjic boundary layer, 5-layer surface diffusion land surface
- Model B: Mellor-Yamada-Janjic boundary layer, Noah land surface
- Model C: Yonsei University boundary layer, 5-layer surface diffusion land surface
- Model D: Yonsei University boundary layer, Noah land surface
- Model E. Pleim-Xiu boundary layer, Pleim-Xiu land surface

These configurations are summarized in Table 4.1. The result is a continuous field of CO_2 concentrations across the San Francisco Bay Area that allows us to examine domain-wide trends, although for direct comparison with the surface monitoring sites, we examine only the modeled concentrations in the corresponding individual grid cells.

4.2.3 The BErkeley Atmospheric CO_2 Observation Network

The BErkeley Atmospheric CO_2 Observation Network ($BEACO_2N$) is an ensemble of more than 50 CO_2 and air quality monitoring "nodes" distributed at roughly 2 km intervals throughout the San Francisco Bay Area. A full description and characterization of the instrument is given in Shusterman et al. (2016) and Kim et al. (2018). Briefly, each $BEACO_2N$ node is equipped with a suite of moderate cost, commercially available sensor technologies: a Vaisala CarboCap GMP343 non-dispersive infrared sensor for CO_2, a Shinyei PPD42NS nephelometric particulate matter sensor, a suite of four Alphasense B4 electrochemical sensors for O_3, CO, NO, and NO_2, and a meteorological sensor (Bosch Sensortec BME280) for temperature, pressure, and humidity. Data is transmitted to a central repository and made publicly available online (http://beacon.berkeley.edu/) in near real time.

Here we use 1 min mean dry air mole fractions collected at 9 sites (Fig. 4.1) between 25 August and 8 September 2013 for comparison with the CO_2 concentrations simulated using the various emission inventories and boundary layer schemes described in Sect. 4.2.1 and 4.2.2. The observations are corrected for meteorological dependencies, temporal drift, and systematic uncertainty as described in Shusterman et al. (2016) and subsequently averaged to 5-minute windows centered at each model output time. This averaging approach accounts for the fact that the model output represents instantaneous conditions, while also providing some allowance for random error in the $BEACO_2N$ measurements or slight offsets in timing of events.

4.3 Results & Discussion

Observed and simulated median diel cycles generated over the 2-week study period using the baseline emission estimates are shown in Fig. 4.2. We see that at least one of the model simulations captures the diel cycles observed at some sites (e.g., CPS, ELC, and PAP) remarkably well. However, even when using five different model configurations, the ensemble of simulations consistently underestimates the magnitude of both the inter-site variability as well as the intra-site variability over the course of the 24-hour cycle. Specifically, while all of the models predict

generally low concentrations interrupted by a modest morning rush hour peak (and sometimes an even smaller evening peak), in the observations we find a much greater diversity of diel patterns, with some sites exhibiting midday or afternoon maximum CO_2 concentrations (e.g., LAU, KAI, FTK, and STL) and others exhibiting significantly elevated nighttime concentrations (HRS).

Díaz-Isaac et al. (2018) previously analyzed the accuracy of the meteorologies simulated by an ensemble of different WRF parameterization permutations and found the specific land surface and boundary layer schemes used in each model run to have a considerable impact on CO_2 concentration estimates. They were unable, however, to identify a single land surface or boundary layer scheme that would result in consistently superior performance across all meteorological variables investigated and/or across the entire modeling domain (the US Midwest). Here we find our results to be relatively insensitive to the choice of land surface parameterization (e.g., compare the CO_2 levels in Fig. 4.2 predicted by Models A and B, which share a boundary layer scheme and differ in land surface model only), likely due to the lack of soil moisture in our predominantly urban domain. However, we are similarly unable to recommend a particular boundary layer parameterization that appears to reduce the model–data mismatch at all sites. A previous investigation into the relative merits of various boundary layer dynamics schemes for simulating the meteorology of the San Francisco Bay Area in particular found the Pleim-Xiu parameterization (Model E) to produce the most accurate results (BAAQMD, 2017), although it should be noted that the Mellor-Yamada-Janjic scheme used in Models A and B was not included in that analysis. In Fig. 4.3 we see that Models A and B yield better agreement with afternoon boundary layer heights derived from radiosondes released at the Oakland International Airport. (We do not compare morning boundary layer heights, as the negligible surface heating and mixing observed at those hours complicates the calculation of a boundary layer height; see Fig. 4.4.) We cannot, however, characterize domain-wide model performance from comparison with sparse observations made at a single location.

In the absence of a clearly superior strategy for sub-grid cell parameterization, we endeavor to quantify the probable magnitude of the modeled transport error and its relative contribution to the total model–data mismatch observed here. For this purpose, we define transport error as the standard deviation across the CO_2 concentrations predicted by the five model configurations at a given location and model time step. Meanwhile, the instrument error is known to be ±1.8 ppm at 5 min resolution, given by the combination of the random error, short-term drift, and systematic uncertainty corrections derived by Shusterman et al. (2016). Finally, an upper bound on the emissions error is derived from the mean difference between the CO_2 concentrations predicted using the minus-50 and plus-50 emission inventories under each of the various meteorological schemes. We calculate the fractional contribution of a given error term X to the total model–data mismatch (σ_{total}) according to the equation below:

$$frac_X = \frac{\sigma_X^2}{\sigma_{total}^2} \tag{4.1}$$

The mean contributions of the three error terms described above to the total model–data mismatch at each site are shown in Fig. 4.5. We see that, at all sites, the instrument error makes the smallest or nearly the smallest contribution to the overall error budget, while the transport error typically comprises the second largest fraction. While the relative importance of transport error has been documented previously (e.g., Lauvaux et al., 2016; Deng et al., 2017), the relative unimportance

of instrument error is noteworthy, given the lower quality monitoring equipment in use in this study. These results support the conclusion of Turner et al. (2016) that use of moderate cost sensor technologies does not significantly compromise the integration of ambient observations with model simulations. They also highlight, however, the importance of improving simulated transport–whether via advances in model parameterizations, data assimilation, or hyperparameter estimation–in order to best take advantage of these measurements.

Figure 4.5 also demonstrates that the quality of the prior emission inventory makes the most significant contribution to the overall error in the simulated CO_2 concentrations at all sites. This is a somewhat unsurprising result, given that many urban modeling studies are conducted with the express purpose of improving greenhouse gas emission estimates. It is possible that the dominance of the emissions error term is partially attributable to the magnitude of perturbation introduced to the emission inventory; indeed, error sums exceeding 100% at NOC, PAP, and STL indicate that ±50% error may be an overestimation of the true uncertainty in the prior mobile emission estimate. However, previous studies of urban greenhouse gas inventories have indicated that scale factors of up to 1.5 to 1.8 may be necessary to bring prior emission estimates into agreement with observations (e.g., McKain et al., 2012). Furthermore, the remaining six sites (LAU, KAI, CPS, FTK, HRS, and ELC) possess error sums far below 100% of the total model–data mismatch, suggesting either an underestimation of one of the error terms included in said sum or the presence of a significant contribution from representation error. If we define the representation error as the remainder of the model–data mismatch after instrument, transport, and emissions error have been accounted for, we calculate that representation error contributes an average of 67% of the total mismatch at these six sites.

It should also be noted that estimation of emissions error via a uniform scale factor assumes that all uncertainty in the emission inventory is contained in the magnitude of the emissions, rather than their spatio-temporal distribution. Indeed, the FIVE inventory on which our mobile emission estimates are based (McDonald et al., 2014) imposes the same diel cycle on highway emissions throughout the domain, which does not reflect the heterogeneity in traffic flows observed across the highway system (see Fig. 4.6). Thus the true value of the emissions error contains contributions from errors in magnitude as well as timing.

The uncertainty in our emissions error estimate means that our derived representation error value should not be overinterpreted as a precise quantification, as this would require a negative representation error at NOC, PAP, and STL. Rather than implying a nonphysical representation scenario, this result likely indicates that either: (a) the CO_2 simulations for these three sites are particularly sensitive to changes in mobile emissions, and/or (b) the emissions from highway segments in their footprint of influence are already accurate to within much better than ±50% in the prior inventory. In order to investigate these two possibilities, we decompose the modeled change in CO_2 concentrations ($\partial C/\partial t$, in μmol m^{-3} s^{-1}) into four contributing terms:

$$\frac{\partial C}{\partial t} = \frac{Q}{h} + H\frac{\partial h}{\partial t}\frac{C_h - C}{h} - \frac{\partial}{\partial x}u \cdot C - \frac{\partial}{\partial y}v \cdot C \qquad (4.2)$$

Here, Q is the CO_2 flux (in μmol m^{-2} s^{-1}) in the emission inventory grid cell that contains a given BEACO$_2$N site, h is the height of the planetary boundary layer (in m) in said cell calculated by the transport model, C_h is the CO_2 mixing ratio in the first model layer above said boundary layer

height (in μmol m^{-3}), u is the east–west component of the modeled wind speed (in m s^{-1}) in the site's grid cell, and v is the north–south component. We assume constant wind speeds across a grid cell, which simplifies the spatial derivatives to gradients in CO_2 concentration alone. These are calculated by subtracting the surface CO_2 concentration in the upwind grid cell from that in the cell of interest and dividing that difference by the grid size (1000 m). Finally, H is the Heaviside function with the argument $\partial h/\partial t$ that sets the entrainment term to zero whenever the boundary layer height is decreasing.

Reading the righthand side of Eq. (4.2) from left to right, we refer to each addend as the emissions, entrainment, u-advection, and v-advection contributions to the total modeled CO_2, respectively. The mean fractional contribution of each of these terms to $\partial C/\partial t$ calculated using a separate 3-day (18–20 May 2013) simulation run at 10-minute time resolution is shown in Fig. 4.7. Even when a different time period is used, we see that the sites that depend significantly on the emissions term (NOC, PAP, and STL) are the same sites with especially large emissions errors in Fig. 4.5. At the remaining six sites, more than half of the simulated CO_2 concentration changes are dictated by the u-advection term, uncertainties in which may contribute to both transport and representation error. Previous studies have thoroughly documented the Weather Research and Forecasting model's inability to accurately simulate horizontal wind speeds (e.g., Díaz-Isaac et al., 2018); sites whose modeled concentrations are particularly dependent on advection may be especially vulnerable to such inaccuracies. Equation (4.2) therefore provides a useful first-order indication of which sites (or proposed sites) in a given observation network are best positioned to constrain urban emissions (i.e., those with dominant emissions terms) vs. urban dynamics (those with dominant advection terms). Depending on the intent of the analysis, an optimal network or data subset could then be designed or selected appropriately.

4.4 Conclusion

Here we present one of the first validations of simulated urban CO_2 concentrations against a high-resolution, surface-level greenhouse gas monitoring network. We discover a much higher degree of diel and inter-site variability to be present in the observations than is predicted by the mesoscale atmospheric transport model and present an initial analysis of the error terms that contribute to this model–data mismatch, namely: instrument error, transport error, emissions error, and representation error. We find the error budget to be dominated by emissions error, while instrument error is seen to be a small contributor to the overall error budget, indicating that future work could potentially use less precise instruments with negligible impacts on the overall error budget. Transport error is on average more significant, although not substantial enough to account for the magnitude of model–data mismatch observed here. At some sites, introducing a ±50% mobile emissions error is more than enough to close the error budget, but this finding is limited to sites whose simulated CO_2 concentrations are dominated by the emissions in their local model grid cell. The remaining majority of sites possess yet unexplained portions of their model–data mismatch, pointing to significant contributions from representation error and/or some underestimation of the other error terms.

This finding has important implications for future analyses pairing surface-level observing systems with transport models to constrain emission estimates. In the past, these analyses have typically attempted to resolve the entirety of the model–data mismatch through changes to the emission

estimate alone, assuming other error terms to be negligible and/or relegating these uncertainties to poorly understood error covariance matrices (Lauvaux et al., 2016). However, we see here that even significant perturbations of the emission inventory cannot account for even half of the model–data mismatch at some sites, suggesting that other sources of error must also be carefully considered.

Inversion analyses used to constrain emissions under fixed meteorological conditions would therefore benefit greatly from an initial evaluation of modeled meteorology (which influences transport as well as representation error) to ensure the best possible simulation of near-surface dynamics. Unfortunately, many of the relevant meteorological variables are monitored only infrequently, if at all, and virtually never at the spatial resolution implemented in these mesoscale inversion studies. Dilution and dynamics can vary across very short spatial scales, as evidenced here by the anti-correlated diel profiles observed at LAU and HRS, located only 2 km apart. In addition to increased frequency and density of meteorological observations and improved modeling techniques, CO_2 records from difficult-to-model, near-surface sites present extremely valuable sources of information for constraining these sub-grid cell atmospheric dynamics. Future work will leverage BEACO_2N CO_2 observations more rigorously as passive tracers of urban surface layer dynamics and as potential candidates for data assimilation techniques that allow meteorological fields to be updated in tandem with emission estimates.

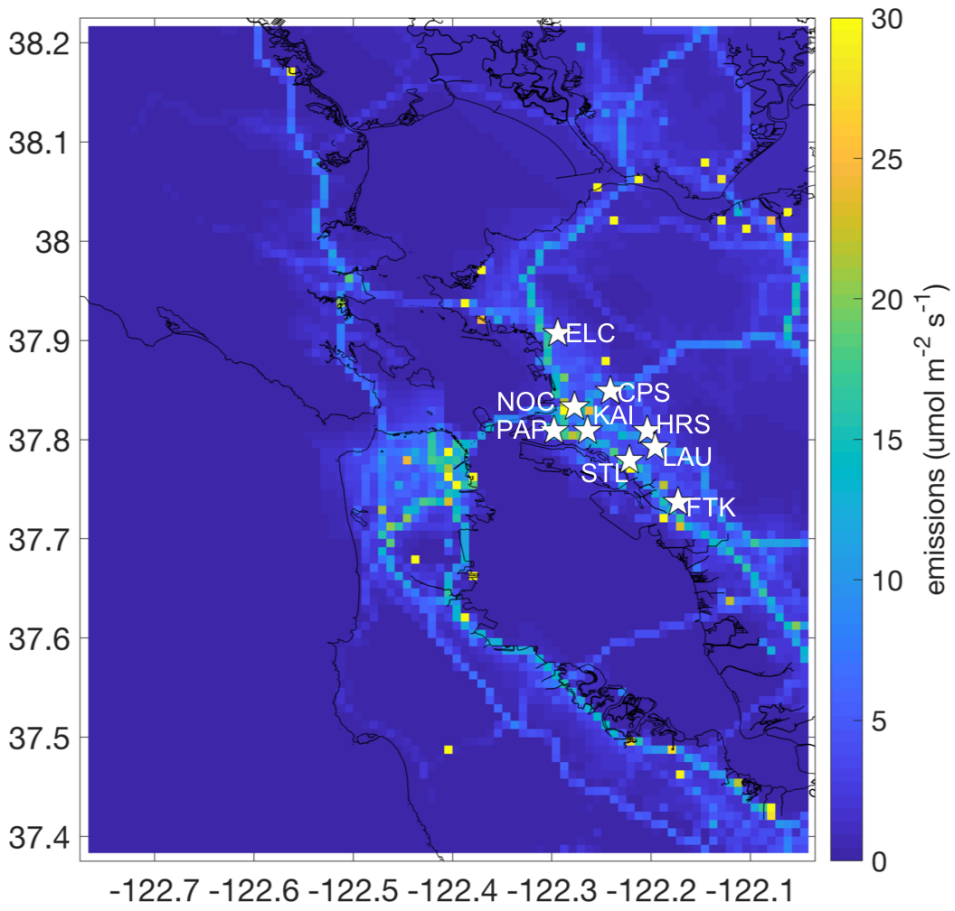

Figure 4.1. Sample time step of baseline emission inventory with locations of BEACO$_2$N sites used in this study labeled as white stars.

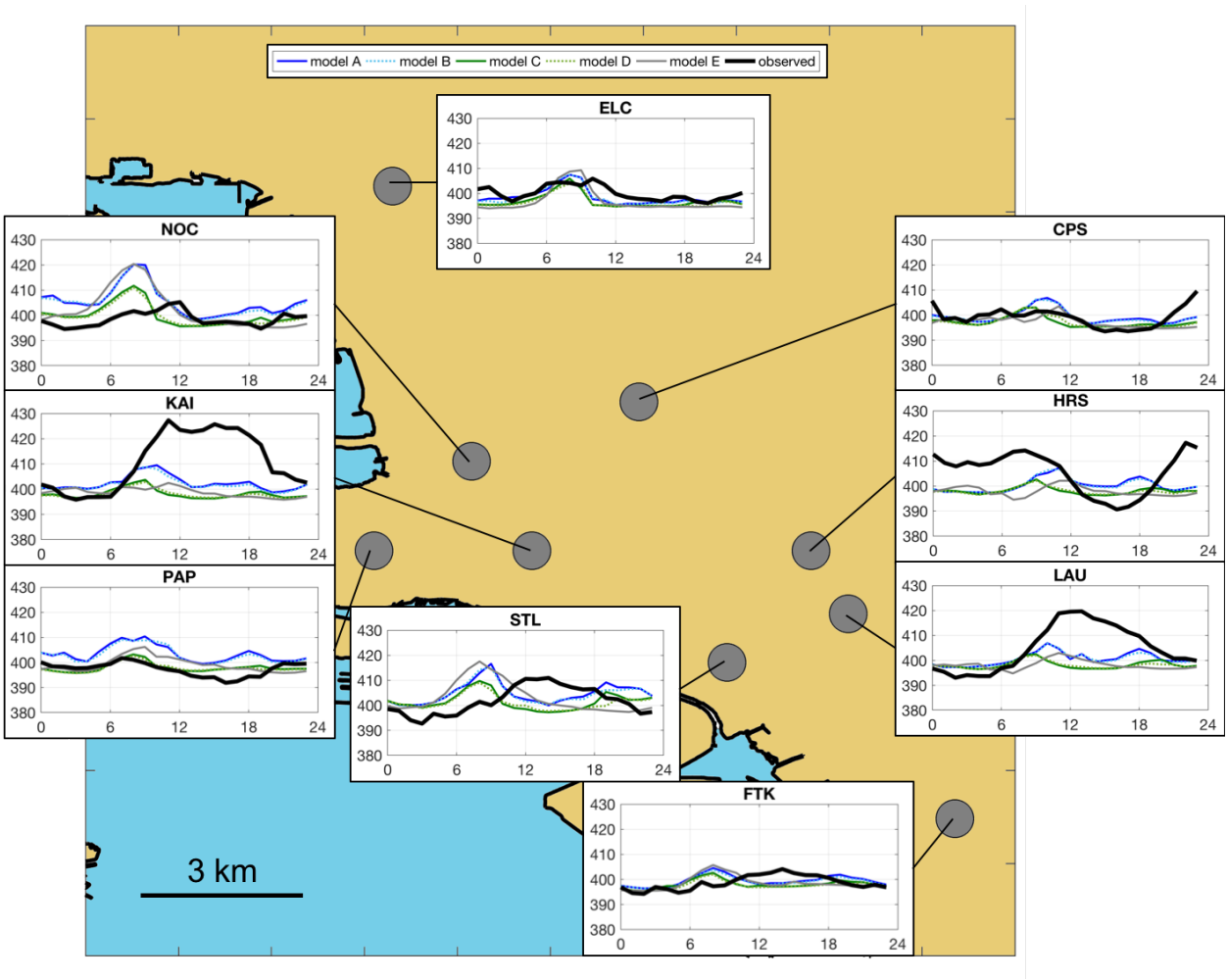

Figure 4.2. Median diel cycles in CO_2 concentrations observed and simulated using baseline emission estimates.

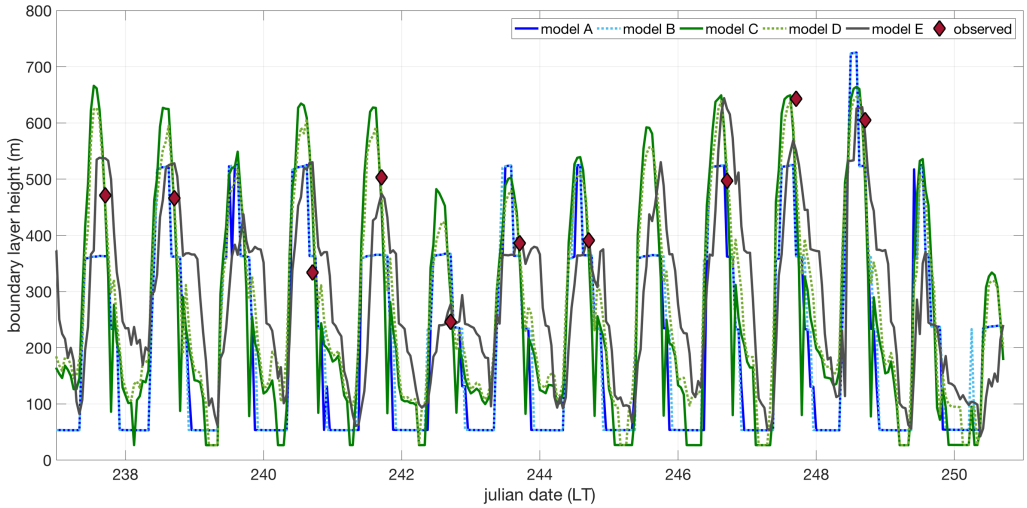

Figure 4.3. Boundary layer heights observed at the Oakland International Airport and simulated at the nearby FTK site.

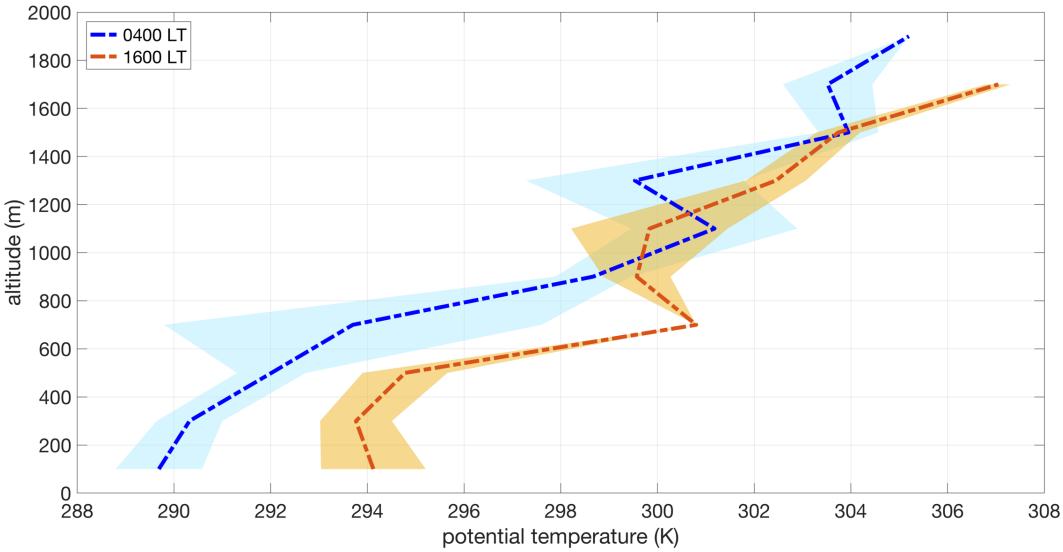

Figure 4.4. Mean vertical profiles in potential temperature measured by radiosondes released at Oakland International Airport at 0400 and 1600 LT during the study period.

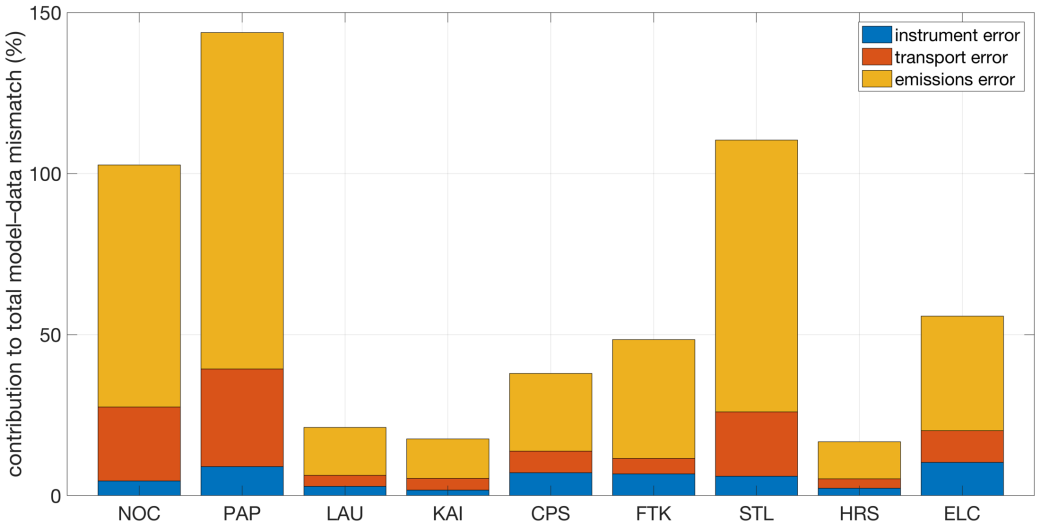

Figure 4.5. Mean fractional contribution of error terms to the total model–data mismatch.

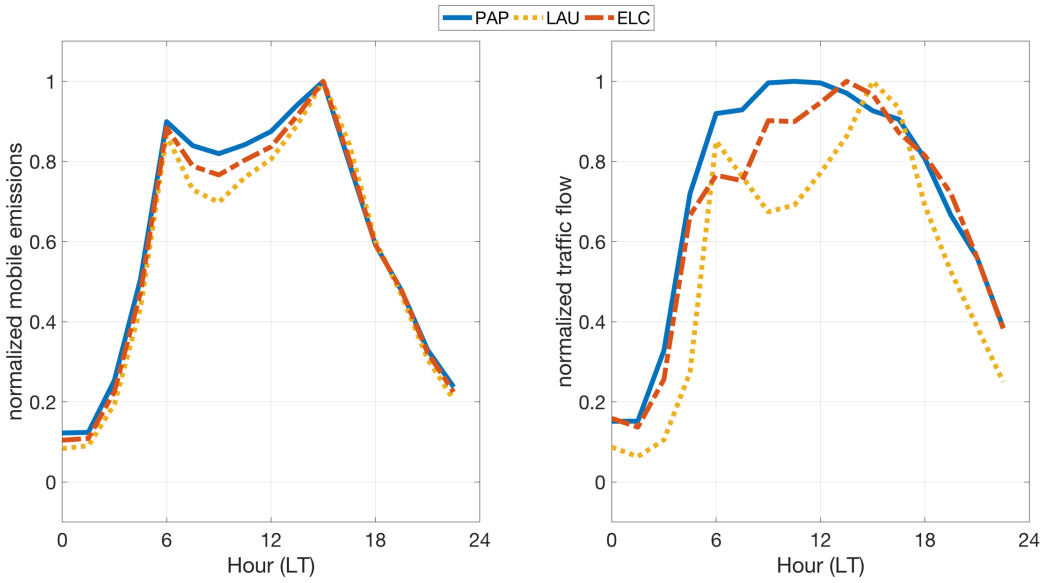

Figure 4.6. Median diel cycles in estimated mobile emissions (left) and observed traffic flow (right; courtesy of the Caltrans Performance Measurement System, http://pems.dot.ca.gov/) at or near three representative sites during the study period.

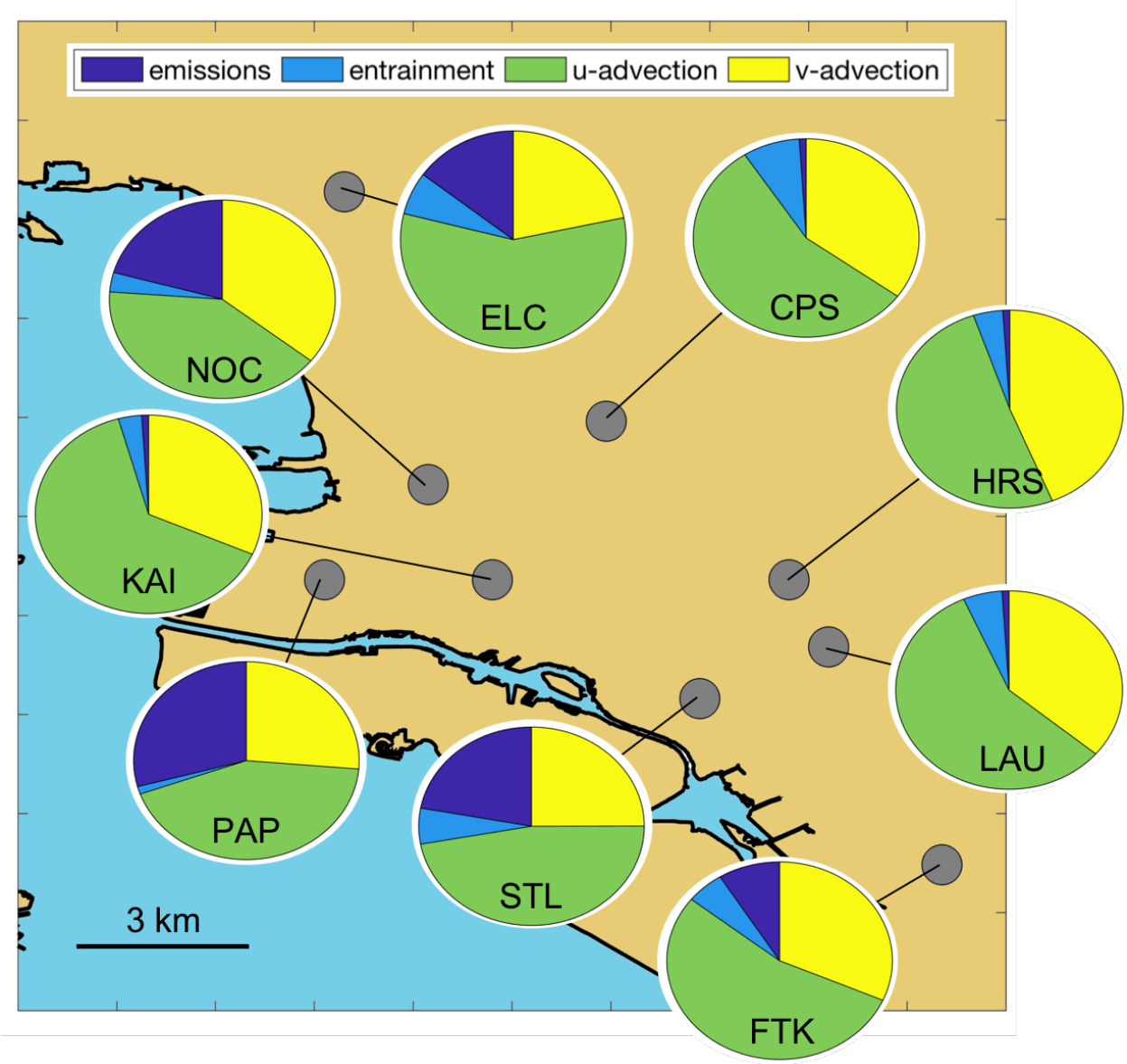

Figure 4.7. Fractional contribution of emissions, entrainment, and advection terms to the time derivative of the simulated CO_2 concentrations.

MODEL	BOUNDARY LAYER	LAND SURFACE
A	MYJ	MM5
B	MYJ	Noah
C	YSU	MM5
D	YSU	Noah
E	PX	PX

Table 4.1. Boundary layer and land surface parameterization combinations used to create the five transport model configurations considered in this study.

Chapter 5

Conclusions

5.1 Summary

In this dissertation, I presented the first high-resolution urban CO_2 observing system based on low-cost sensor technology: the BErkeley Atmospheric CO_2 Observation Network ($BEACO_2N$). In the previous three chapters, I rigorously characterized the in situ performance of the $BEACO_2N$ platform, established its sensitivity to policy-relevant trends in CO_2 emissions from specific roadways, and demonstrated its potential as a tool for validating simulations based on state-of-the-art atmospheric transport models and activity-based emission inventories. By constructing this novel network and thoroughly characterizing the first 5 years of $BEACO_2N$'s operation, I have introduced an important proof of concept for low-cost, high-density observation techniques and established a rigorous body of baseline observations against which ongoing developments can be compared, thus demonstrating that we are well on the way towards the continuous monitoring of CO_2 emissions at high spatio-temporal resolution within an urban domain.

5.2 Future directions

As the longitudinal strength of the $BEACO_2N$ data record continues to grow, future analyses should take advantage of this long-term continuity to characterize inter-annual trends in CO_2 emissions and concentrations. These are the timescales on which regulatory and sociological change take place, and low-cost platforms that are economically feasible to maintain over long time periods are uniquely situated to document these changes. The San Francisco Bay Area in particular has been the site of many significant emission reduction initiatives since $BEACO_2N$'s foundation in 2012 (e.g., the electrification of the Port of Oakland), and the network will be crucial in evaluating the outcomes of those initiatives in the long term.

Moreover, once a significant observational record has been established in $BEACO_2N$'s secondary locations (New York City and Houston), an inter-city analysis should be conducted to compare the suitability of the $BEACO_2N$ approach to differently configured urban areas. It is highly possible that the different topographies, dominant meteorologies, and emission profiles of the three cities each require a unique observing system design. For example, it has been hypothesized that emissions from Indianapolis, Indiana are sufficiently constrained by fewer, higher quality monitoring sites because: (1) Indianapolis is a relatively small city that produces correspondingly subtle enhancements in CO_2 concentrations, perhaps requiring high-quality instrumentation to detect, and (2) the topography is mostly flat and surrounded on all sides by rural areas, perhaps necessitating fewer observation sites to characterize the entire urban footprint (Wu et al., 2018). Houston is similar to Indianapolis in the simplicity of its topography but features more complex boundary conditions, with the Gulf of Mexico and an accompanying shipping port to the southeast and other significant urban centers to the west and north. New York City, meanwhile, is even more heavily urbanized than the San Francisco Bay Area, with skyscrapers introducing a variety of emission heights and dramatic street canyon dynamics. Understanding the ability of low-cost sensors to characterize emission activities in these two cities is crucial to the potential future expansion of the $BEACO_2N$ framework to other urban centers.

In this vein, a more thorough investigation of the representativeness of a given near-surface monitoring site should be performed. The work I have presented here suggests a significant discontinuity between the resolution at which most atmospheric transport models are run and the spatial footprint represented by a single $BEACO_2N$ measurement. Recent mobile monitoring campaigns in the San Francisco Bay Area (e.g., Apte et al., 2017) provide a unique opportunity to probe the spatial extent captured by each stationary observing site in extremely high resolution. A rigorous understanding of the irregular localities encoded in the $BEACO_2N$ dataset would not only improve the accounting of representation error in ongoing modeling studies but also inform the ideal siting of new monitoring stations.

Finally, future analyses of the $BEACO_2N$ data record should leverage the wealth of other available observations not touched upon here. Since 2014, some subset of the network has also possessed equipment for the measurement of ancillary trace gases (CO, NO, NO_2, and O_3) as well as particulate matter. Highly relevant to air quality and therefore public health interests in their own right, these species are also co-emitted with CO_2 in ratios indicative of the precise fuel and combustion processes involved. These instruments have recently been validated for in-field use (Kim et al., 2018), and their analysis alongside the primary CO_2 instrumentation offers the opportunity for greater specificity of source attribution and quantification.

The meteorological sensors included in the $BEACO_2N$ sensor package might also be repurposed for analyses beyond the calibration applications described here. The measurements could allow for the high-density validation of near-surface temperature, humidity, and pressure predicted by atmospheric transport models. These meteorological constraints, in combination with a treatment of CO_2 as a passive tracer species, could aid in the selection of optimal model parameterizations for a given urban area and further improve understanding of boundary layer dynamics.

The development of MRV strategies that inform effective mitigation of greenhouse gas emissions is a task of great societal as well as scientific importance. Successful efforts will require an unprecedented degree of synergy between activity-based and observation-based initiatives across all spatial scales and geopolitical boundaries. The continued study of low-cost, high-density monitoring approaches constitutes an important piece of this multifaceted endeavor and will be crucial to confronting the challenges presented in this dissertation and beyond.

References

A.B. 32: California Global Warming Solutions Act, Assemb. Reg. Sess. 2005–2006, (CA 2006).

Andrews, A. E., Kofler, J. D., Trudeau, M. E., Williams, J. C., Neff, D. H., Masarie, K. A., Chao, D. Y., Kitzis, D. R., Novelli, P. C., Zhao, C. L., Dlugokencky, E. J., Lang, P. M., Crotwell, M. J., Fischer, M. L., Parker, M. J., Lee, J. T., Baumann, D. D., Desai, A. R., Stanier, C. O., De Wekker, S. F. J., Wolfe, D. E., Munger, J. W., and Tans, P. P.: CO_2, CO, and CH_4 measurements from tall towers in the NOAA Earth System Research Laboratory's Global Greenhouse Gas Reference Network: instrumentation, uncertainty analysis, and recommendations for future high-accuracy greenhouse gas monitoring efforts, Atmos. Meas. Tech., 7, 647–687, doi:10.5194/amt-7-647-2014, 2014.

Apte, J. S., Messier, K. P., Gani, S., Brauer, M., Kirchstetter, T. W., Lunden, M. M., Marshall, J. D., Portier, C. J., Vermeulen, R. C. H., and Hamburg, S. P.: High-resolution air pollution mapping with Google Street View cars: exploiting big data, Environ. Sci. Technol., 51, 6999–7008, doi:10.1021/acs.est.7b00891, 2017.

Banks, R. F., Tiana-Alsina, J., Baldasano, J. M., Rocadenbosch, F., Papayannis, A., Solomos, S., and Tzanis, C. G.: Sensitivity of boundary-layer variables to PBL schemes in the WRF model based on surface meteorological observations, lidar, and radiosondes during the HygrA-CD campaign, Atmos. Res., 176, 185–201, doi:10.1016/j.atmosres.2016.02.024, 2016.

Ban-Weiss, G. A., McLaughlin, J. P., Harley, R. A., Lunden, M. M., Kirchstetter, T. W., Kean, A. J., Strawa, A. W., Stevenson, E. D., and Kendall, G. R.: Long-term changes in emissions of nitrogen oxides and particulate matter from on-road gasoline and diesel vehicles, Atmos. Environ., 42, 220–232, doi:10.1016/j.atmosenv.2007.09.049, 2008.

Barth, M., and Boriboonsomsin, K.: Real-world carbon dioxide impacts of traffic congestion, Transp. Res. Rec., 2058, 163–171, doi:10.3141/2058-20, 2008.

Bay Area Air Quality Management District, Spare the Air: Cool the Climate, A blueprint for clean air and climate protection in the Bay Area: San Francisco, CA, 2017.

Beckerman, B., Jerrett, M., Brook, J. R., Verma, D. K., Arain, M. A., and Finkelstein, M. M.: Correlation of nitrogen dioxide with other traffic pollutants near a major expressway, Atmos. Environ., 42, 275–290, doi:10.1016/j.atmosenv.2007.09.042, 2008.

Bergeron, O. and Strachan, I. B.: CO_2 sources and sinks in urban and suburban areas of a northern mid-latitude city, Atmos. Environ., 45, 1564–1573, doi:10.1016/j.atmosenv.2010.12.043, 2011.

Boon, A., Broquet, G., Clifford, D. J., Chevallier, F., Butterfield, D. M., Pison, I., Ramonet, M., Paris, J.-D., and Ciais, P.: Analysis of the potential of near-ground measurements of CO_2 and CH_4 in London, UK for the monitoring of city-scale emissions using an atmospheric transport model, Atmos. Chem. Phys., 16, 6735–6756, doi:10.5194/acp-16-6735-2016, 2016.

Bovensmann, H., Buchwitz, M., Burrows, J. P., Reuter, M., Krings, T., Gerilowski, K., Schneising, O., Heymann, J., Tretner, A., and Erzinger, J.: A remote sensing technique for global monitoring of power plant CO_2 emissions from space and related applications, Atmos. Meas. Tech., 3, 781–811, doi:10.5194/amt-3-781-2010, 2010.

Bréon, F. M., Broquet, G., Puygrenier, V., Chevallier, F., Xueref-Rémy, I., Ramonet, M., Dieudonné, E., Lopez, M., Schmidt, M., Perrussel, O., and Ciais, P.: An attempt at estimating Paris area CO_2 emissions from atmospheric concentration measurements, Atmos. Chem. Phys., 15, 1707–1724, doi:10.5194/acp-15-1707-2015, 2015.

Brioude, J., Angevine, W. M., Ahmadov, R., Kim, S.-W., Evan, S., McKeen, S. A., Hsie, E.-Y., Frost, G. J., Neuman, J. A., Pollack, I. B., Peischl, J., Ryerson, T. B., Holloway, J., Brown, S. S., Nowak, J. B., Roberts, J. M., Wofsy, S. C., Santoni, G. W., Oda, T., and Trainer, M.: Top-down estimate of surface flux in the Los Angeles Basin using a mesoscale inverse modeling technique: assessing anthropogenic emissions of CO, NO_x and CO_2 and their impacts, Atmos. Chem. Phys., 13, 3661–3677, doi:10.5194/acp-13-3661-2013, 2013.

Brondfield, M. N., Hutyra, L. R., Gately, C. K., Raciti, S. M., and Peterson, S. A.: Modeling and validation of on-road CO_2 emissions inventories at the urban regional scale, Environ. Pollut., 170, 113–123, doi:10.1016/j.envpol.2012.06.003, 2012.

Brown Jr., E. G., Rodriquez, M., Nichols, M. D., and Corey, R. W.: First Update to the Climate Change Scoping Plan: Building on the Framework, California Air Resources Board, Sacramento, CA, 2014.

Brown Jr., E. G.: 2016 ZEV action plan: an updated roadmap toward 1.5 million zero-emission vehicles on California roadways by 2025, Governor's Interagency Working Group on Zero-Emission Vehicles, Sacramento, CA, USA, 2016.

Burrows, J. P., Hölze, E., Goede, A. P. H., Visser, H., and Fricke, W.: SCIAMACHY–scanning imaging absorption spectrometer for atmospheric chartography, Acta Astronaut., 35, 445–451, doi:10.1016/0094-5765(94)00278-T, 1995.

Bush, S. E., Hopkins, F. M., Randerson, J. T., Lai, C.-T., and Ehleringer, J. R.: Design and application of a mobile ground-based observatory for continuous measurements of atmospheric trace gas and criteria pollutant species, Atmos. Meas. Tech., 8, 3481–3492, doi:10.5194/amt-8-3481-2015, 2015.

Cambaliza, M. O. L., Shepson, P. B., Caulton, D. R., Stirm, B., Samarov, D., Gurney, K. R., Turnbull, J., Davis, K. J., Possolo, A., Karion, A., Sweeney, C., Moser, B., Hendricks, A., Lauvaux, T., Mays, K., Whetstone, J., Huang, J., Razlivanov, I., Miles, N. L., and Richardson, S. J.: Assessment of uncertainties of an aircraft-based mass balance approach for quantifying urban greenhouse gas emissions, Atmos. Chem. Phys., 14, 9029–9050, doi:10.5194/acp-14-9029-2014, 2014.

Chen, J., Viatte, C., Hedelius, J. K., Jones, T., Franklin, J. E., Parker, H., Gottlieb, E. W., Wennberg, P. O., Dubey, M. K., and Wofsy, S. C.: Differential column measurements using compact solar-tracking spectrometers, Atmos. Chem. Phys., 16, 8479–8498, doi:10.5194/acp-16-8479-2016, 2016.

Choi, W., Winer, A. M., and Paulson, S. E.: Factors controlling pollutant plume length downwind of major roadways in nocturnal surface inversions, Atmos. Chem. Phys., 14, 6925–6940, doi:10.5194/acp-14-6925-2014, 2014.

Ciais, P., Rayner, P., Chevallier, F., Bousquet, P., Logan, M., Peylin, P., and Ramonet, M.: Atmospheric inversions for estimating CO_2 fluxes: methods and perspectives, Climatic Change, 103, 69–92, doi:10.1007/s10584-010-9909-3, 2010.

Claire, S. J., Dinh, T. M., Fanai, A. K., Nguyen, M. H., and Schultz, S. A.: Bay Area emissions inventory summary report: greenhouse gases, Tech. rep., Bay Area Air Quality Management District, San Francisco, CA, USA, 2015.

Dee, D. P., Uppala, S. M., Simmons, A. J., Berrisford, P., Poli, P., Kobayashi, S., Andrae, U., Balmaseda, M. A., Balsamo, G., Bauer, P., Bechtold, P., Beljaars, A. C. M., van de Berg, L., Bidlot, J., Bormann, N., Delsol, C., Dragani, R., Fuentes, M., Geer, A. J., Haimberger, L., Healy, S. B., Hersbach, H., Hólm, E. V., Isaksen, L., Kållberg, P., Köhler, M., Matricardi, M., McNally, A. P., Monge-Sanz, B. M., Morcrette, J.-J., Park, B.-K., Peubey, C., de Rosnay, P., Tavolato, C., Thépaut, J.-N., and Vitart, F.: The ERA-Interim reanalysis: configuration and performance of the data assimilation system, Q. J. Royal Meteorol. Soc., 137, 553–597, doi:10.1002/qj.828, 2011.

de Foy, B.: City-level variations in NO_x emissions derived from hourly monitoring data in Chicago, Atmos. Environ., 176, 128–139, doi:10.1016/j.atmosenv.2017.12.028, 2018.

Deng, A., Lauvaux, T., Davis, K. J., Gaudet, B. J., Miles, N., Richardson, S. J., Wu, K., Sarmiento, D. P., Hardesty, R. M., Bonin, T. A., Brewer, W. A., and Gurney, K. R.: Toward reduced transport errors in a high resolution urban CO_2 inversion system, Elem. Sci. Anth., 5, 20, doi:10.1525/elementa.133, 2017.

Díaz-Isaac, L. I., Lauvaux, T., and Davis, K. J.: Impact of physical parameterizations and initial conditions on simulated atmospheric transport and CO_2 mole fractions in the US Midwest, Atmos. Chem. Phys. Discuss., in review, 2018.

Duren, R. M. and Miller, C. E.: Measuring the carbon emissions of megacities, Nature Clim. Change, 2, 560–562, doi:10.1038/nclimate1629, 2012.

Ehleringer, J., Schauer, A. J., Lai, C.-T., Bowling, D. R., Pataki, D. E., and Stephens, B. B.: Long-term carbon dioxide monitoring in Salt Lake City, AGU Fall Meeting, San Francisco, CA, 15–19 December 2008, B43D-0466, 2008.

Eldering, A., Solish, B., Kahn, P., Boland, S., Crisp, D., and Gunson, M.: High precision atmospheric CO_2 measurements from space: The design and implementation of OCO-2, in:

Aerospace Conference, 2012 IEEE, Big Sky, MT, 3–10 March 2012, 1–10, doi:10.1109/AERO.2012.6187176, 2012.

Fang, Y., Michalak, A. M., Shiga, Y. P., and Yadav, V.: Using atmospheric observations to evaluate the spatiotemporal variability of CO_2 fluxes simulated by terrestrial biospheric models, Biogeosciences, 11, 6985–6997, doi:10.5194/bg-11-6985-2014, 2014.

Fonselius, S., Koroleff, F., and Wärme, K.-E.: Carbon dioxide variations in the atmosphere, Tellus, 8, 176–183, doi:10.1111/j.2153-3490.1956.tb01208.x, 1956.

Foote, E.: Circumstances affecting the heat of the sun's rays: Am. J. Sci. Arts., 22, 382–383, 1856.

Fourier, J.-B. J.: Mémoire sur les Températures du Globe Terrestre et des Espaces Planétaires, Mémoires de l'Académie Royale des Sciences, 7, 569–604, 1827.

Fu, B., Li, S., Yu, X., Yang, P., Yu, G., Feng, R., and Zhuang, X.: Chinese ecosystem research network: progress and perspectives, Ecol. Complex., 7, 225–233, doi:10.1016/j.ecocom.2010.02.007, 2010.

Gately, C. K., Hutyra, L. C., Wing, I. S., and Brondfield, M. N.: A bottom up approach to on-road CO_2 emissions estimates: Improved spatial accuracy and applications for regional planning, Environ. Sci. Technol., 47, 2423–2430, doi:10.1021/es304238v, 2013.

Gately, C. K., Hutyra, L. R., and Wing, I. S.: Cities, traffic, and CO_2: a multidecadal assessment of trends, drivers, and scaling relationships, Proc. Natl. Acad. Sci. USA, 16, 4999–5004, doi:10.1073/pnas.1421723112, 2015.

Gately, C. K., Hutyra, L. R., Peterson, S., and Wing, I. S.: Urban emissions hotspots: quantifying vehicle congestion and air pollution using mobile phone GPS data, Environ. Poll., 229, 496–504, doi:10.1016/j.envpol.2017.05.091, 2017.

Gately, C. K. and Hutyra, L. R.: Large uncertainties in urban-scale carbon emissions, J. Geophys. Res.–Atmos., 122, 11242–11260, doi:10.1002/2017JD027359, 2017.

Grell, G. A., Peckham, S. E., Schmitz, R., McKeen, S. A., Frost, G., Skamarock, W. C., and Eder, B.: Fully coupled "online" chemistry within the WRF model, Atmos. Environ., 39, 6957–6975, doi:10.1016/j.atmosenv.2005.04.027, 2005.

Gurney, K. R., Razlivanov, I., Song, Y., Zhou, Y., Benes, B., and Abdul-Massih, M.: Quantification of fossil fuel CO_2 emissions on the building/street scale for a large U.S. city, Environ. Sci. Technol., 46, 12194–12202, doi:10.1021/es3011282, 2012.

Harley, R. A., Marr, L. C., Lehner, J. K., and Giddings, S. N.: Changes in motor vehicle emissions on diurnal to decadal time scales and effects on atmospheric composition, Environ. Sci. Technol., 39, 5356–5362, doi:10.1021/es048172+, 2005.

Järvi, L., Nordbo, A., Junninen, H., Riikonen, A., Moilanen, J., Nikinmaa, E., and Vesala, T.: Seasonal and annual variation of carbon dioxide surface fluxes in Helsinki, Finland, in 2006–2010, Atmos. Chem. Phys., 12, 8475–8489, doi:10.5194/acp-12-8475-2012, 2012.

Jeong, S., Hsu, Y.-K., Andrews, A. E., Bianco, L., Vaca, P., Wilczak, J. M., and Fischer, M. L.: A multitower measurement network estimate of California's methane emissions, J. Geophys. Res.–Atmos., 118, 11339–11351, doi:10.1002/jgrd.50854, 2013.

Jiménez, P. A., Dudhia, J., González-Rouco, J. F., Montávez, J. P., García-Bustamante, E., Navarro, J., Vilà-Guerau de Arellano, J., and Muñoz-Roldán, A.: An evaluation of WRF's ability to reproduce the surface wind over complex terrain based on typical circulation patterns, J. Geophys. Res.–Atmos., 118, 7651–7669, doi:10.1002/jgrd.50585, 2013.

Keeling, C. D.: The concentration and isotopic abundances of carbon dioxide in the atmosphere, Tellus, 12, 200–203, doi:10.1111/j.2153-3490.1960.tb01300.x, 1960.

Kim, J., Shusterman, A. A., Lieschke, K. J., Newman, C., and Cohen, R. C.: The BErkeley Atmospheric CO_2 Observation Network: field calibration and evaluation of low-cost air quality sensors, Atmos. Meas. Tech., 11, 1937–1946, doi:10.5194/amt-11-1937-2018, 2018.

Kort, E. A., Frankenberg, C., Miller, C. E., and Oda, T.: Space-based observations of megacity carbon dioxide, Geophys. Res. Lett., 39, L17806, doi:10.1029/2012GL052738, 2012.

Kort, E. A., Angevine, W. M., Duren, R., and Miller, C. E.: Surface observations for monitoring urban fossil fuel CO_2 emissions: minimum site location requirements for the Los Angeles megacity, J. Geophys. Res.–Atmos., 118, 1577–1584, doi:10.1002/jgrd.50135, 2013.

Kort, E. A., Frankenberg, C., Costigan, K. R., Lindenmaier, R., Dubey, M. K., and Wunch, D.: Four corners: the largest US methane anomaly viewed from space, Geophys. Res. Lett., 41, 6898–6903, doi:10.1002/2014GL061503, 2014.

Kou, X., Zhang, M., Peng, Z., and Wang, Y.: Assessment of the biospheric contribution to surface atmospheric CO_2 concentrations over East Asia with a regional chemical transport model, Adv. Atmos. Sci., 32, 287–300, doi:10.1007/s00376-014-4059-6, 2015.

Kou, X., Tian, X., Zhang, M., Peng, Z., and Zhang, X.: Accounting for CO_2 variability over East Asia with a regional joint inversion system and its preliminary evaluation, J. Meteor. Res., 31, 834–851, doi:10.1007/s13351-017-6149-8, 2017.

Kumar, K. R., Revadekar, J. V., and Tiwari, Y. K.: AIRS retrieved CO_2 and its association with climatic parameters over India during 2004–2011, Sci. Total Environ., 476–477, 79–89, doi:10.1016/j.scitotenv.2013.12.118, 2014.

Kumar, M. K. and Nagendra, S. M. S.: Quantification of anthropogenic CO_2 emissions in a tropical urban environment, Atmos. Environ., 125, 272–282, doi:10.1016/j.atmosenv.2015.11.024, 2016.

Lauvaux, T., Gioli, B., Sarrat, C., Rayner, P. J., Ciais, P., Chevallier, F., Noilhan, J., Miglietta, F., Brunet, Y., Ceschia, E., Dolman, H., Elbers, J. A., Gerbig, C., Hutjes, R., Jarosz, N., Legain, D., and Uliasz, M.: Bridging the gap between atmospheric concentrations and local ecosystem measurements, Geophys. Res. Lett., 36, L19809, doi:10.1029/2009GL039574, 2009.

Lauvaux, T., Miles, N. L., Richardson, S. J., Deng, A., Stauffer, D. R., Davis, K. J., Jacobson, G., Rella, C., Calonder, G.-P., and DeCola, P. L.: Urban emissions of CO_2 from Davos, Switzerland: the first real-time monitoring system using an atmospheric inversion technique, J. Appl. Meteorol. Clim., 52, 2654–2668, doi:10.1175/JAMC-D-13-038.1, 2013.

Lauvaux, T., Miles, N. T., Deng, A., Richardson, S. J., Cambaliza, M. O., Davis, K. J., Gaudet, B., Gurney, K. R., Huang, J., O'Keefe, D., Song, Y., Karion, A., Oda, T., Patarasuk, R., Razlivanov, I., Sarmiento, D., Shepson, P., Sweeney, C., Turnbull, J., and Wu, K.: High-resolution atmospheric inversion of urban CO_2 emissions during the dormant season of the Indianapolis Flux Experiment (INFLUX), J. Geophys. Res.–Atmos., 121, 5213–5236, doi:10.1002/2015JD024473, 2016.

Lee, J. K., Christen, A., Ketler, R., and Nesic, Z.: A mobile sensor network to map carbon dioxide emissions in urban environments, Atmos. Meas. Tech., 10, 645–665, doi:10.5194/amt-10-645-2017, 2017.

Liang, J., Gurney, K. R., O'Keeffe, D., Hutchins, M., Patarasuk, R., Huang, J., Song, Y., and Rao, P.: Optimizing the spatial resolution for urban CO_2 flux studies using the Shannon entropy, Atmos., 8, 90, doi:10.3390/atmos8050090, 2017.

Lin, J. C., Gerbig, C., Wofsy, S. C., Andrews, A. E., Daube, B. C., Davis, K. J., and Grainger, C. A.: A near-field tool for simulating the upstream influence of atmospheric observations: the Stochastic Time-Inverted Lagrangian Transport (STILT) model, J. Geophys. Res.–Atmos., 108, 4493, doi:10.1029/2002JD003161, 2003.

Lin, J. C., Gerbig, C., Wofsy, S. C., Daube, B. C., Matross, D. M., Chow, V. Y., Gottlieb, E., Andrews, A. E., Pathmathevan, M., and Munger, J. W.: What have we learned from intensive atmospheric sampling field programmes of CO_2?, Tellus B, 58, 331–343, doi:10.1111/j.1600-0889.2006.00202.x, 2006.

Liu, Z., Bambha, R. P., Pinto, J. P., Zeng, T., Boylan, J., Huang, M., Lei, H., Zhao, C., Liu, S., Mao, J., Schwalm, C. R., Shi, X., Wei, Y., and Michelsen, H. A.: Toward verifying fossil fuel CO_2 emissions with the CMAQ model: motivation, model description and initial simulation, J. Air. Waste Manage., 64, 419–435, doi:10.1080/10962247.2013.816642, 2014.

Lopez-Coto, I., Ghosh, S., Prasad, K., and Whetstone, J.: Tower-based greenhouse gas measurement network design–the National Institute of Standards and Technology North East Corridor Testbed, Adv. Atmos. Sci., 34, 1095–1105, doi:10.1007/s00376-017-6094-6, 2017.

Lorius, C., Jouzel, J., Raynaud, D., Hansen, J., and Le Treut, H.: The ice-core record: climate sensitivity and future greenhouse warming, Nature, 347, 139–145, doi:10.1038/347139a0, 1990.

Majumdar, D., Rao, P., and Maske, N.: Inter-seasonal and spatial distribution of ground-level greenhouse gases (CO_2, CH_4, N_2O) over Nagpur in India and their management roadmap, Environ. Monit. Assess., 189, 121, doi:10.1007/s10661-017-5829-2, 2017.

Maness, H. L., Thurlow, M. E., McDonald, B. C., and Harley, R. A.: Estimates of CO_2 traffic emissions from mobile concentration estimates, J. Geophys. Res.–Atmos., 120, 2087–2102, doi:10.1002/2014jd022876, 2015.

Mangat, T. S., Claire, S. J., Dinh, T. M., Fanai, A. K., Nguyen, M. H., and Schulz, S. A.: Source inventory of Bay Area greenhouse gas emissions, Tech. rep., Bay Area Air Quality Management District, 2010.

Martin, C. R., Zeng, N., Karion, A., Dickerson, R. R., Ren, X., Turpie, B. N., and Weber, K. J.: Evaluation and environmental correction of ambient CO_2 measurements from a low-cost NDIR sensor, Atmos. Meas. Tech., 10, 2383–2395, doi:10.5194/amt-10-2383-2017, 2017.

McDonald, B. C., McBride, Z. C., Martin, E. W., and Harley, R. A.: High-resolution mapping of motor vehicle carbon dioxide emissions, J. Geophys. Res.–Atmos., 119, 5283–5298, doi:10.1002/2013JD021219, 2014.

McKain, K., Wofsy, S. C., Nehrkorn, T., Eluszkiewicz, J., Ehleringer, J. R., and Stephens, B. B.: Assessment of ground-based atmospheric observations for verification of greenhouse gas emissions from an urban region, P. Natl. Acad. Sci. USA, 109, 8423–8428, doi:10.1073/pnas.1116645109, 2012.

McKain, K., Down, A., Raciti, S. M., Budney, J., Hutyra, L. R., Floerchinger, C., Herndon, S. C., Nehrkorn, T., Zahniser, M. S., Jackson, R. B., Phillips, N., and Wofsy, S. C.: Methane emissions from natural gas infrastructure and use in the urban region of Boston, Massachusetts, P. Natl. Acad. Sci. USA, 112, 1941–1946, doi:10.1073/pnas.1416261112, 2015.

Michalak, A. M., Randazzo, N. A., Chevallier, F.: Diagnostic methods for atmospheric inversions of long-lived greenhouse gases, Atmos. Chem. Phys., 17, 7405–7421, doi:10.5194/acp-17-7405-2017, 2017.

Miles, N. L., Richardson, S. J., Davis, K. J., Lauvaux, T., Andrews, A. E., West, T. O., Bandaru, V., and Crosson, E. R.: Large amplitude spatial and temporal gradients in atmospheric boundary layer CO_2 mole fractions detected with a tower-based network in the U.S. upper Midwest, J. Geophys. Res., 117, G01019, doi:10.1029/2011JG001781, 2012.

Miles, N. L., Richardson, S. J., Lauvaux, T., Davis, K. J, Balashov, N. V., Deng, A., Turnbull, J. C., Sweeney, C., Gurney, K. R., Patarasuk, R., Razlivanov, I., Cambaliza, M. O. L., and Shepson, P. B.: Quantification of urban atmospheric boundary layer greenhouse gas dry air mole fraction enhancements in the dormant season: results from the Indianapolis Flux Experiment (INFLUX), Elem. Sci. Anth., 5, 27, doi:10.1525/elementa.127, 2017.

Miller, S. M. and Michalak, A. M.: Constraining sector-specific CO_2 and CH_4 emissions in the US, Atmos. Chem. Phys., 17, 3963–3985, doi:10.5194/acp-17-3963-2017, 2017.

Nassar, R., Hill, T. G., McLinden, C. A., Wunch, D., Jones, D. B. A., and Crisp, D.: Quantifying CO_2 emissions from individual power plants from space, Geophys. Res. Lett., 44, 10045–10053, doi:10.1002/2017GL074702, 2017.

Nehrkorn, T., Eluszkiewicz, J., Wofsy, S. C., Lin, J. C., Gerbig, C., Longo, M., and Freitas, S.: Coupled weather research and forecasting–stochastic time-inverted lagrangian transport (WRF–STILT) model, Meteorol. Atmos. Phys., 107, 51–64, doi:10.1007/s00703-010-0068-x, 2010.

Nehrkorn, T., Henderson, J., Leidner, M., Mountain, M., Eluszkiewicz, J., McKain, K., and Wofsy, S.: WRF simulations of the urban circulation in the Salt Lake City Area for CO_2 modeling, J. Appl. Meteorol. Clim., 52, 323–340, doi:10.1175/JAMC-D-12-061.1, 2013.

Nejadkoorki, F., Nicholson, K., Lake, I., and Davies, T.: An approach for modelling CO_2 emissions from road traffic in urban areas, Sci. Total Environ., 406, 269–278, doi:10.1016/j.scitotenv.2008.07.055, 2008.

Newman, S., Jeong, S., Fischer, M. L., Xu, X., Haman, C. L., Lefer, B., Alvarez, S., Rappenglueck, B., Kort, E. A., Andrews, A. E., Peischl, J., Gurney, K. R., Miller, C. E., and Yung, Y. L.: Diurnal tracking of anthropogenic CO_2 emissions in the Los Angeles basin megacity during spring 2010, Atmos. Chem. Phys., 13, 4359–4372, doi:10.5194/acp-13-4359-2013, 2013.

Newman, S., Xu, X., Gurney, K. R., Hsu, Y. K., Li, K. F., Jiang, X., Keeling, R., Feng, S., O'Keefe, D., Patarasuk, R., Wong, K. W., Rao, P., Fischer, M. L., and Yung, Y. L.: Toward consistency between trends in bottom-up CO_2 emissions and top-down atmospheric measurements in the Los Angeles megacity, Atmos. Chem. Phys., 16, 3843–3863, doi:10.5194/acp-16-3843-2016, 2016.

Nickless, A., Rayner, P. J., Engelbrecht, F., Brunke, E.-G., Erni, B., and Scholes, R. J.: Estimates of CO_2 fluxes over the city of Cape Town, South Africa, through Bayesian inversion modelling, Atmos. Chem. Phys., 18, 4765–4801, doi:10.5194/acp-18-4765-2018, 2018.

Oney, B., Henne, S., Gruber, N., Leuenberger, M., Bamberger, I., Eugster, W., and Brunner, D.: The CarboCount CH sites: characterization of a dense greenhouse gas observation network, Atmos. Chem. Phys., 15, 11147–11164, doi:10.5194/acp-15-11147-2015, 2015.

O'Shea, S. J., Allen, G., Fleming, Z. L., Bauguitte, S. J.-B., Percival, C. J., Gallagher, M. L., Lee, J., Helfter, C., and Nemitz, E.: Area fluxes of carbon dioxide, methane, and carbon monoxide derived from airborne measurements around Greater London: a case study during summer 2012, J. Geophys. Res.–Atmos., 119, 4940–4952, doi:10.1002/2013JD021269, 2014.

Pacala, S. W., Breidenich, C., Brewer, P. G., Fung, I., Gunson, M. R., Heddle, G., Law, B., Marland, G., Paustian, K., Prather, M., Randerson, J. T., Tans, P., and Wofsy, S. C.: Verifying Greenhouse Gas Emissions: Methods to Support International Climate Agreements, The National Academies Press, Washington, D. C., 2010.

Pataki, D. E., Bowling, D. R., and Ehleringer, J. R.: Seasonal cycle of carbon dioxide and its isotopic composition in an urban atmosphere: anthropogenic and biogenic effects, J. Geophys. Res.–Atmos., 108, 4735, doi:10.1029/2003JD003865, 2003.

Patarasuk, R., Gurney, K. R., O'Keeffe, D., Song, Y., Huang, J., Preeti, R., Buchert, M., Lin, J. C., Mendoza, D., and Ehleringer, J. R.: Urban high-resolution fossil fuel CO_2 emissions quantification and exploration of emission drivers for potential policy applications, Urban Ecosyst., 19, 1013–1039, doi:10.1007/s11252-016-0553-1, 2016.

Peters, W., Jacobson, A. R., Sweeny, C., Andrews, A. E., Conway, T. J., Masarie, K., Miller, J. B., Bruhwiler, L. M. P., Pétron, G., Hircsh, A. I., Worthy, D. E. J., van der Werf, G. R., Randerson, J. T., Wennberg, P. O., Krol, M. C., and Tans, P. P.: An atmospheric perspective on North American carbon dioxide exchange: CarbonTracker, Proc. Natl. Acad. Sci. USA, 104, 18925–18930, doi:10.1073/pnas.0708986104, 2007.

Pillai, D., Buchwitz, M., Gerbig, C., Koch, T., Reuter, M., Bovensmann, H., Marshall, J., and Burrows, J. P.: Tracking city CO_2 emissions from space using a high-resolution inverse modelling approach: a case study for Berlin, Germany, Atmos. Chem. Phys., 16, 9591–9610, doi:10.5194/acp-16-9591-2016, 2016.

Pugliese, S. C., Murphy, J. G., Vogel, F. R., Moran, M. D., Zhang, J., Zheng, Q., Stroud, C. A., Ren, S., Worthy, D., and Broquet, G.: High-resolution quantification of atmospheric CO_2 mixing ratios in the Greater Toronto Area, Canada, Atmos. Chem. Phys., 18, 3387–3401, doi:10.5194/acp-18-3387-2018, 2018.

Richardson, S. J., Miles, N. L., Davis, K. J., Lauvaux, T., Martins, D. K., Turnbull, J. C., McKain, K., Sweeney, C., and Cambaliza, M. O. L.: Tower measurement network of in-situ CO_2, CH_4, and CO in support of the Indianapolis FLUX (INFLUX) Experiment, Elem. Sci. Anth., 5, 59, doi:10.1525/elementa.140, 2017.

Rigby, M., Toumi, R., Fisher, R., Lowry, D., and Nisbet, E. G.: First continuous measurements of CO_2 mixing ratio in central London using a compact diffusion probe, Atmos. Environ., 42, 8943–8953, doi:10.1016/j.atmosenv.2008.06.040, 2008.

Rosenzwieg, C., Solecki, W., Hammer, S. A., and Mehrotra, S.: Cities lead the way in climate-change action, Nature, 467, 909–911, doi:10.1038/467909a, 2010.

Schneising, O., Heymann, J., Buchwitz, M., Reuter, M., Bovensmann, H., and Burrows, J. P.: Anthropogenic carbon dioxide source areas observed from space: assessment of regional enhancements and trends, Atmos. Chem. Phys., 13, 2445–2454, doi:10.5194/acp-13-2445-2013, 2013.

Schwandner, F. M., Gunson, M. R., Miller, C. E., Carn, S. A., Eldering, A., Krings, T., Verhulst, K. R., Schimel, D. S., Nguyen, H. M., Crisp, D., O'Dell, C. W., Osterman, G. B., Iraci, L. T., and

Podolske, J. R.: Spaceborne detection of localized carbon dioxide sources, Science, 358, 5782, doi:10.1126/science.aam5782, 2017.

Seinfeld, J. H. and Pandis, S. N.: Atmospheric Chemistry and Physics: From Air Pollution to Climate Change, 2nd ed., John Wiley & Sons Inc., Hoboken, NJ, 2006.

Sharma, N., Nayak, R. K., Dadhwal, V. K., Kant, Y., and Ali, M. M.: Diurnal and seasonal variation of measured atmospheric CO_2 at Dehradun during 2009, Int. Arch. Photogramm., 38, 87–90, 2011.

Shusterman, A. A., Teige, V. E., Turner, A. J., Newman, C., Kim, J., and Cohen, R. C.: The BErkeley Atmospheric CO_2 Observation Network: initial evaluation, Atmos. Chem. Phys., 16, 13449–13463, doi:10.5194/acp-16-13449-2016, 2016.

Skamarock, W. C., Klemp, J. B., Dudhia, J., Gill, D. O., Barker, D. M., Duda, M. G., Huang, X.-Y., Wang, W., and Powers, J. G.: A Description of the Advanced Research WRF Version 3, National Center for Atmospheric Research, Boulder, CO, 2008.

Snyder, E. G., Watkins, T. H., Solomon, P. A., Thoma, E. D., Williams, R. W., Hagler, G. S. W., Shelow, D., Hindin, D. A., Kilaru, V. J., and Preuss, P. W.: The changing paradigm of air pollution monitoring, Environ. Sci. Technol., 47, 11369–11377, doi:10.1021/es4022602, 2013.

Stanley, K. M., Grant, A., O'Doherty, S., Young, D., Manning, A. J., Stavert, A. R., Spain, T. G., Salameh, P. K., Harth, C. M., Simmonds, P. G., Sturges, W. T., Oram, D. E., and Derwent, R. G.: Greenhouse gas measurements from a UK network of tall towers: technical description and first results, Atmos. Meas. Tech., 11, 1437–1458, doi:10.5194/amt-11-1437-2018, 2018.

Staufer, J., Broquet, G., Bréon, F. M., Puygrenier, V., Chevallier, F., Xuref-Rémy, I., Dieudonné, E., Lopez, M., Schmidt, M., Ramonet, M., Perrussel, O., Lac, C., Wu, L., Ciais, P.: The first 1-year-long estimate of Paris region fossil fuel CO_2 emissions based on atmospheric inversion, Atmos. Chem. Phys., 16, 14703–14726, doi:10.5194/acp-16-14703-2016, 2016.

Stuiver, M. and Quay, P. D.: Atmospheric ^{14}C changes resulting from fossil fuel CO_2 release and cosmic ray flux variability, Earth Planet. Sci. Lett., 53, 349–362, doi:10.1016/0012-821X(81)90040-6, 1981.

Super, I., Denier van der Gon, H. A. C., Visschedijk, A. J. H., Moerman, M. M., Chen, H., van der Molen, M. K., and Peters W.: Interpreting continuous in-situ observations of carbon dioxide and carbon monoxide in the urban port area of Rotterdam, Atmos. Pollut. Res., 8, 174–187, doi:10.1016/j.apr.2016.08.008, 2017a.

Super, I., Denier van der Gon, H. A. C., van der Molen, M. K., Sterk, H. A. M., Hensen, A., and Peters, W.: A multi-model approach to monitor emissions of CO_2 and CO from an urban–industrial complex, Atmos. Chem. Phys., 17, 13297–13316, doi:10.5194/acp-17-13297-2017, 2017b.

Thompson, R. L., Manning, A. C., Gloor, E., Schultz, U., Seifert, T., Hänsel, F., Jordan, A., and Heimann, M.: In-situ measurements of oxygen, carbon monoxide and greenhouse gases from Ochsenkopf tall tower in Germany, Atmos. Meas. Tech., 2, 573–591, doi:10.5194/amt-2-573-2009, 2009.

Turnbull, J. C., Sweeney, C., Karion, A., Newberger, T., Lehman, S. J., Tans, P. P., Davis, K. J., Lauvaux, T., Miles, N. L., Richardson, S. J., Cambaliza, M. O., Shepson, P. B., Gurney, K., Patarasuk, R., and Razlivanov, I.: Toward quantification and source sector identification of fossil fuel CO_2 emissions from an urban area: results from the INFLUX Experiment, J. Geophys. Res.–Atmos., 120, 292–312, doi:10.1002/2014JD022555, 2015.

Turner, A. J., and Jacob, D. J.: Balancing aggregation and smoothing errors in inverse models, Atmos. Chem. Phys., 15, 7039–7048, doi:10.5194/acp-15-7039-2015, 2015.

Turner, A. J., Shusterman, A. A., McDonald, B. C., Teige, V., Harley, R. A., and Cohen. R. C.: Network design for quantifying urban CO_2 emissions: assessing trade-offs between precision and network density, Atmos. Chem. Phys., 16, 13465–13475, doi:10.5194/acp-16-13465-2016, 2016.

United Nations, Human Settlement Programme: Hot Cities: Battle-Ground for Climate Change, 2011.

United Nations, Department of Economic and Social Affairs, Population Division: World Urbanization Prospects: The 2014 Revision, Highlights, 2014.

United Nations, Framework Convention on Climate Change: Adoption of the Paris Agreement, 21st Conference of the Parties, Paris, 2015.

United Nations Framework Convention on Climate Change Intended Nationally Determined Contributions: http://unfccc.int/focus/indc_portal/items/8766.php/, last access: 4 June 2016.

United States Environmental Protection Agency, 2017 and Later Model Year Light-Duty Vehicle Greenhouse Gas Emissions and Corporate Average Fuel Economy Standards, Washington, D.C., 2012.

United States Environmental Protection Agency, Notice of Violation to Volkswagen Group of America, Inc.: Washington, D.C., 2015.

Valin, L. C., Russell, A. R., Hudman, R. C., and Cohen, R. C.: Effects of model resolution on the interpretation of satellite NO_2 observations, Atmos. Chem. Phys., 11, 11647–11655, doi:10.5194/acp-11-11647-2011, 2011.

van Leeuwen, C. Improved operation of the Vaisala Carbocap GMP343 for the school CO2-web. Manuscript in preparation, 2010.

Verhulst, K. R., Karion, A., Kim, J., Salameh, P. K., Keeling, R. F., Newman, S., Miller, J., Sloop, C., Pongetti, T., Rao, P., Wong, C., Hopkins, F. M., Yadav, V., Weiss, R. F., Duren, R. M., and

Miller, C. E.: Carbon dioxide and methane measurements from the Los Angeles Megacity Carbon Project – Part 1: calibration, urban enhancements, and uncertainty estimates, Atmos. Chem. Phys., 17, 8313–8341, doi:10.5194/acp-17-8313-2017, 2017.

Wang, P., Zhou, W., Niu, Z., Cheng, P., Wu, S., Xiong, X., Lu, X., and Du, H.: Emission characteristics of atmospheric carbon dioxide in Xi'an, China based on the measurements of CO_2 concentration, $\Delta^{14}C$ and $\delta^{13}C$, Sci. Total Environ., 619–620, 1163–1169, doi:10.1016/j.scitotenv.2017.11.125, 2018.

Worthy, D. E. J., Platt, A., Kessler, R., Ernst, M., Braga, R., and Racki, S.: The Canadian atmospheric carbon dioxide measurement program: measurement procedures, data quality and accuracy, in: Report of the 11th WMO/IAEA Meeting of Experts on Carbon Dioxide Concentration and Related Tracer Measurement Techniques, Tokyo, Japan, 25–28 September 2001, 112–128, 2003.

Wu, K., Lauvaux, T., Davis, K. J., Deng, A., Lopez Coto, I., Gurney, K. R., and Patarasuk, R.: Joint inverse estimation of fossil fuel and biogenic CO_2 fluxes in an urban environment: an observing system simulation experiment to assess the impact of multiple uncertainties, Elem. Sci. Anth., 6, 17, doi:10.1525/elementa.138, 2018.

Wu, L., Broquet, G., Ciais, P., Bellassen, V., Vogel, F., Chevallier, F., Xueref-Remy, I., and Wang, Y.: What would dense atmospheric observation networks bring to the quantification of city CO_2 emissions?, Atmos. Chem. Phys., 16, 7743–7771, doi:10.5194/acp-16-7743-2016, 2016.

Wunch, D. G., Toon, G. C., Blavier, J.-F. L., Washenfelder, R. A., Notholt, J., Connor, B. J., Griffith, D. W. T., Sherlock, V., and Wennberg, P. O.: The total carbon column observing network, Philos. Trans. R. Soc. A, 369, 2087–2112, doi:10.1098/rsta.2010.0240, 2011.

Yadav, V., Michalak, A. M., Ray, J., and Shiga, Y. P.: A statistical approach for isolating fossil fuel emissions in atmospheric inverse problems, J. Geophys. Res.–Atmos., 121, 12490–12504, doi:10.1002/2016JD025642, 2016.

Yanowitz, J., McCormick, R. L., and Graboski, M. S.: In-use emissions from heavy-duty diesel vehicles, Environ. Sci. Technol., 34, 729–740, doi:10.1021/es990903w, 2000.

Yokota, T., Yoshida, Y., Eguchi, N., Ota, Y., Tanaka, T., Watanabe, H., and Maksyutov, S.: Global concentrations of CO_2 and CH_4 retrieved from GOSAT: first preliminary results, Sola, 5, 160–163, doi:/10.2151/sola.2009-041, 2009.

Zhao, C. L. and Tans, P. P.: Estimating uncertainty of the WMO mole fraction scale for carbon dioxide in air, J. Geophys. Res.–Atmos., 111, 1–10, doi:10.1029/2005JD006003, 2006.

Zhu, Y., Kuhn, T., Mayo, P., and Hinds, W. C.: Comparison of daytime and nighttime concentration profiles and size distributions of ultrafine particles near a major highway, Environ. Sci. Technol., 40, 2531–2536, doi:10.1021/es0516514, 2006.